A MECHANICAL MODEL OF VASCULAR ENDOTHELIUM

by

ROBERT L. SATCHER, JR.

S.B., Massachusetts Institute of Technology, Cambridge, MA, U.S.A. (1986)

Submitted to the Department of Chemical Engineering
in Partial Fulfillment of the Requirement
for the Degree of

DOCTOR OF PHILOSOPHY IN CHEMICAL ENGINEERING

at the

MASSACHUSETTS INSTITUTE OF TECHNOLOGY

February, 1993

Signature of Author _____
Department of Chemical Engineering
December 30, 1992

Certified by _____
C. Forbes Dewey, Jr., Professor of Mechanical Engineering

Certified by _____
Michael A. Gimbrone, Jr., Professor of Pathology
Harvard Medical School

Certified by _____
Clark K. Colton, Professor of Chemical Engineering

Accepted by _____
Robert E. Cohen, Chairman
Committee on Graduate Student

A MECHANICAL MODEL OF VASUCLAR ENDOTHELIUM

Robert L. Satcher, Jr.

ABSTRACT

Hemodynamic forces play an important role in the regulation of vascular tone, the remodelling of blood vessels, and the localized development of atherosclerosis near bifurcations and curvatures in the arterial tree. These effects are mediated by the vascular endothelium, which forms a continuous monolayer covering the innermost aspect of arteries.

In vitro studies have shown that endothelium responds to shear stress. In the case of laminar flow, the cells align and elongate in the direction of the principal flow axis. Prominent changes occur in the intracellular arrangement of F-actin--stress fibers are constructed which are also oriented with the flow axis. In contrast, changes in microtubules and intermediate filaments are not as dramatic. The mechanism by which forces produce these effects has remained unclear in part, because the mechanics of endothelium is poorly understood. This thesis is one of few attempts to construct a model for the mechanism of adjustment in response to shear stress.

The actin network and regions of intercellular contact were studied by exposing bovine aortic endothelial cells (BAEC) to specified flow conditions using a modified cone-and-plate flow apparatus. Forces on a monolayer of cells were characterized by computing the flow over a surface with similar geometry. Laminar flow caused shear stress gradients across individual cells (~35% of average shear stress) which might be expected to distrupt intercelluluar junctions in cells which have not been previously conditioned with flow. Once aligned, however, the gradients are reduced (~20% of average).

Confocal microscopy showed that stress fibers in unoriented baec are found almost exclusively in basal regions. Intercellular junctions are distrupted by laminar flow, implying that this may be a stiumuls for observed changes in cell morphology. In cells conditioned with flow, stress fibers appear in apical regions, including above the nucleus. Staining patterns for the actin binding protein, α-actinin, suggest that stress fibers are attaching to the apical membrane. Confocal microscopy, however, did not have the resolution to allow for study of the cytoskeleton in further detail.

Electron microscopy revealed that the cortical cytoskeleton is a filamentous cross-linked network which is predominantly composed of f-actin. It appears to attach directly to the apical membrane, therby transmitting forces to the underlying network and attachment points. The apical network is enhanced in response to shear stress by the construction of additional filaments and stress fibers. Our findings strongly implicate the cytoskeleton as the load bearing element inside of the cell. Therefore, we analyzed the mechanical properties of the network in order to quantitatively assess this possibility. Modelling the actin network as an open cell foam, we obtained estimates of the elastic moduli. These predictions were in excellent agreement with experimental measurements with cytoplasm and F-actin solutions. Stress fibers would serve to increase the overall network modulus, and thus decrease the deformability of the cells. Moreover, they serve as stress concentration markers within the network--their redistribution when the cells experience shear stress may indicate where resultant stress becomes concentrated within the cell. Thus, the actin network seems to be an important component of the cellular adjustment to shear stress.

December 30, 1992, 3:00-5:00 pm, Room 66-360

Thesis Supervisors: C. Forbes Dewey, Jr., Prof. of Mechanical Engineeering
M. A. Gimbrone, Jr., Prof. of Pathology (Harvard Med.)
C. K. Colton, Prof. of Chemical Engineering

ACKNOWLEDGEMENTS

There is a cast of thousands that must be acknowledged for playing roles in my being able to complete this thesis. But before this I wish to thank God for this experience, and giving me the ability to complete the task and learn something in the process.

My deepest gratitude is to my advisors: Prof. C. Forbes Dewey, Jr., of MIT, and Prof. Michael A. Gimbrone, Jr., of Harvard Medical School and Brigham and Women's Hospital. They introduced me to this area of research and have been supportive throughout. I realize that I have been fortunate in landing in such a positive and encouraging environment for my graduate studies. I am grateful for their guidance and genuine concern for my personal and professional growth.

I would like to thank the members of my thesis committee, Prof. Clark K. Colton, Prof. William M. Deen, and Dr. Mark Johnson, for stimulating discussions, lively committee meetings, and continued support and guidance.

One of the most pleasant aspects of this work was the diversity of people and laboratories with whom we collaborated to complete the work. Most of the work was done in 3 laboratories. At MIT, the Fluid Mechanics laboratory; at Brigham and Women's Hospital, the Vascular Research Division, and the Division of Experimental Medicine. I wish to thank Richard Fenner for his technical expertise and guidance; and of course, many good jokes, lively discussions, and excursions on his sail boat. It would have been a less enriching experience without Donna Wilker at MIT. I thank her for her assistance, and more importantly her friendship and encouragement, and reminding me not to forget to eat, sleep, and stay up on my politics. I am grateful to many of my labmates; but especially Natacha DePaola-Garcia, Jian Shen, and Patrick Erk (the east coast mafia, as we are now referred to at conferences). I also wish to thank the FML crew: Wilson Hu, Mariano Garfinkel, Manuel Cruz, James Shen, MacMurray Whale, Chunghai Wang, Dave Otis, and Edwin Osawa, for making my stay a truly memorable one.

I wish to thank Bill Atkinson for his instruction in endothelial cell culture, and taking me under his wing during my years in the lab at BWH. Without your patience, I would have never made it! I also wish to thank Myron Cybulsky for teaching many of the staining techniques that have been an essential part of my thesis. And I must thank Kay for conversations en Francais, and Vanessa for goo-gobs of endothelial cells. I thank the good folks of Whitehead Institute; in particular Mark Chafel for teaching me how to use a confocal microscope.

I am deeply grateful to Dr. John H. Hartwig, who has become an unofficial advisor. He introduced me to electron microscopy, and has provided

encouragement while expecting the best from me (although I have never done EM work before). Many thanks to Rebecca, Michelle, and Andrea; all of whom took me through the finer points of electron microscopy, and provided some livelier moments in lab.

Finally, I must thank my friends in the MIT and HMS community, without whom I never would have remained sane. The MIT posse: Steve Isabelle, Jim Oliver, Darryl Pines, Vince McNeil, Pamela Shelton and Derrick Cameron; the Chem-E gang: Cathy, Paula, and Susan; and of course, the BGSA crew: LaCries and Sandra; and Dr. Clarence Williams for many an encouraging word and interesting insight. At HMS I must thank my friends, Robin Lee, Howard Francis, BK Edmund, Colin Stultz, Jamela Kenea, and D'Juanna White, for immeasurable support. I thank the Rev. Henderson and Dr. Deborah Brome for being a family away from home. And of course my roomates and friends, Robert Jones, Dexter Haywood, and John Hyman, for putting up with my wierd hours and at times less than tidy habits.

Finally, and most importantly, this thesis is dedicated to my family: Dr. Robert L. Satcher, Sr. (dad), Mrs. Marian H. Satcher (mom), Rodney, Robin, and Serena (thanks for all the meals--and for being there). I could not ask for a more wonderful and loving family. My parents have provided me with encouragment and guidance and love that has never wavered. By following their example, I know that all is possible.

TABLE OF CONTENTS

Chapter One

INTRODUCTION

Cardiovascular disease is the leading cause of death in the U.S. and Western Europe. The underlying problem in the majority of these deaths is atherosclerosis, a disease of large and medium size arteries [DHEW, 1981]. Pathologic change associated with this disease has been recognized since the 19th century or earlier, as evidenced by early attempts to explain its etiology [Fuster et. al., 1992]. von Rokitansky suggested a mechanism in 1852, which was later embellished by Duguid in 1946 [von Rokitansky, 1852; Duguid, 1946]. Known as the "incrustation hypothesis", the theory stated that fibrin deposition causes intimal thickening, with secondary lipid accumulation and organization of fibroblasts. The other well known theory, the "lipid hypothesis", was published by Virchow in 1856 [Virchow, 1856]. He proposed that accumulation in the arterial wall represents a shift in the balance from removal to deposition of lipids. The incorporated lipid forms complexes with mucopolysaccarhides, eventually creating plaques. Virchow also appreciated the importance of the vascular lining for maintainence of blood fluidity. It was the basis for his now famous triad of predisposing factors for pathologic thrombosis.

The plasma coagulation system is inactive when in contact with the vascular lining. Until recently, this was thought to be a passive property of the endothelial cells, which form the innermost aspect of blood vessels. They were described as a "cellophane" wrapping on the inside of arteries [Gimbrone, 1987]. However, with the discovery that endothelial cells synthesize prostacyclin, the

most potent natural inhibitor of platelet aggregation, a more active role was established [Weskler et. al., 1986]. It became apparent that the vascular endothelial lining, the body's "blood-compatible container", is the locus of a multifactorial hemostatic-thrombotic balance involving both antithrombotic and prothrombotic influences [Gimbrone, 1986].

Atherosclerosis has been a difficult disease to investigate because relevant changes occur over a lifespan. In addition, there are multiple etiologies and sequelae, so that plaque formation and vaso-occlusive disease do not always occur [Ross, 1986]. The final consequence depends on genetic as well as environmental factors.

With current understanding there is agreement, however, that injury to or perhaps more accurately, dysfunction of the endothelium, is a critical and necessary event in the pathogenesis of atherosclerosis. This injury or dysfunction can result from various physiologic stimuli (viral, chemical, or hemodynamic) [Gimbrone, 1986]. The prevailing view of atherogenesis is represented in the "response-to-injury" hypothesis [Ross et. al., 1976], which is summarized in what follows.

Endothelial injury is the initial event in the disease process. Subsequent developments depend on the method of injury, which can be classified in two major catagories [Ross, 1986]:

1. Dysfunction of cells without morphologic changes. Atherosclerosis develops slowly over many years by a cascade of events. Functional

alterations of the endothelium lead to accumulation of lipids and monocytes. Macrophages release toxic products causing platelets to adhere. Subsequent growth factor release by endothelial cells, macrophages, and platelets, causes migration and proliferation of smooth muscle cells. This process may contribute to formation of fibrointimal or lipid lesions, which distort the artery wall. The stretched overlying endothelium is more susceptible to denudation.

2. Endothelial denudation by direct damage or manipulation, such as in patients undergoing heart transplantation, saphenous vein bypass grafting, or percutaneous transluminal coronary angioplasty. This puts the arterial interstitium in direct contact with blood, increasing the risk for a vaso-occlusive event.

Once exposed, intimal and medial elements activate the plasma coagulation system leading to thrombosis. Small thrombi can become organized, contributing to the growth of an atherosclerotic plaque. Large thrombi can be occlusive, causing (for instance) acute coronary syndromes and ischemic events in the brain [Ross, 1986].

In recent years, the focus of research efforts has narrowed, so that efforts are directed towards determining aspects of endothelial biology which are inducible. Many surface and metabolic properties of endothelial cells change in response to environmental stimuli. Thus, the cells can potentially undergo reversible phenotypic modulation to a nonadaptive but functional state. The net result

could be loss of nonthrombogenicity, a local thrombotic event, or a more chronic, systemic thrombotic tendency as a precursor of disease [Gimbrone, 1987].

Hemodynamic shear stress is a prominent candidate for induction of endothelial cell dysfunction [Ross, 1986; Gimbrone, 1987; Fuster et. al., 1992]. Atherosclerosis is a focal disease--plaques form in localized areas, leaving other regions of the same artery unaffected [Montenegro, 1968; Schwartz, 1972]. Moreover, this disease pattern is unchanged for supopulations who have other specific risk factors [Wissler, 1990]. Lesions tend to form in regions of disturbed flow at bifurcations, branchings, curves, or expansions/contractions in the arterial tree [Spain, 1966] (see Figure 1.1). At these locations, the flow field includes features such as vortices, flow reversals, and stagnation points, which change the direction and duration of shear stress on the vessel walls [Karino et. al., 1980; Ku et. al., 1983]. Shear stresses which are orders of magnitude higher than physiologic levels are required to denude normal endothelium [Fry, 1968]. Thus the first events leading to atherosclerosis occur in the presence of an intact endothelial monolayer [Davies et. al., 1976]. A maladaptive state could be the result of chronic exposure to disturbed flow patterns. A better understanding of the endothelial cell response to environmental stimuli would clarify mechanisms of vascular disease. This thesis is an effort to determine some details of how endothelial cells are affected by hemodynamic influences.

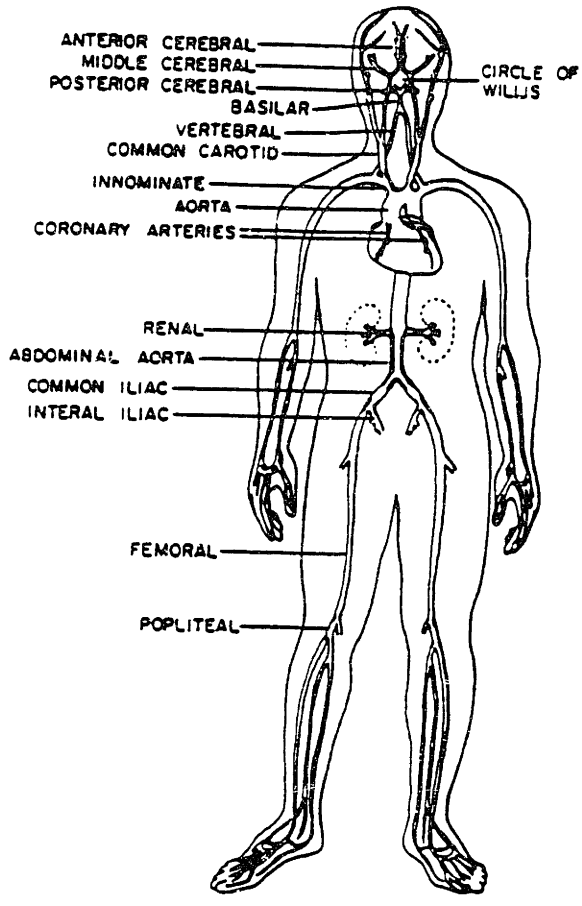

Figure 1.1: Pattern of atherosclerotic disease in man [Spain, 1966]. Regions of arterial branching and sharp curves, such is the abdominal aorta, carotid arteries, coronary arteries, iliacs, and femorals, are favored sites for the development of atherosclerosis.

1. HEMODYNAMICS

The vascular endothelium is the simple epithelium that lines the cardiovascular system (Figure 1.2). It consists of a cellular monolayer which rests on a complicated matrix of cells and intercellular material. Intact endothelium provides a selectively permeable barrier to the passage of macromolecules from the bloodspace to the extravascular space [Gimbrone, 1986]. Endothelial cells are subjected to fluid generated forces on one side, and anchored to the underlying substrate at the opposite aspect. Forces perpendicular to the wall are caused by pressure, and are transmitted to the underlying structures in the blood vessel wall [Fry, 1972; Dewey, 1976]. Forces parallel to the wall are caused by shear stress, and are absorbed by the endothelial cells themselves. The endothelium must resist shearing forces in order to maintain continuity of the monolayer and serve as a selectively permeable barrier between blood and tissue.

Identifying flow patterns associated with atherosclerotic lesions has been difficult [Karino et. al., 1980; Ku et. al., 1983]. Arterial flow is a complex phenomenon determined by interaction of a non-Newtonian fluid (blood) with a compliant and geometrically varying conduit (arteries), driven with a pulsatile pressure force. Flow in large and medium size arteries where lesions develop is predominantly laminar. In the normal vascular tree, turbulent flow exists only in the aorta at increased volumetric flow rates, such as with exercise; and in bursts during peak systole [Nerem et. al., 1972]. Turbulence can also occur in abnormal states such as with diseased vessel occlusion; or with anastamoses [Davies et. al., 1986]. Atherosclerotic lesions develop in the aorta; however, fatalaties result

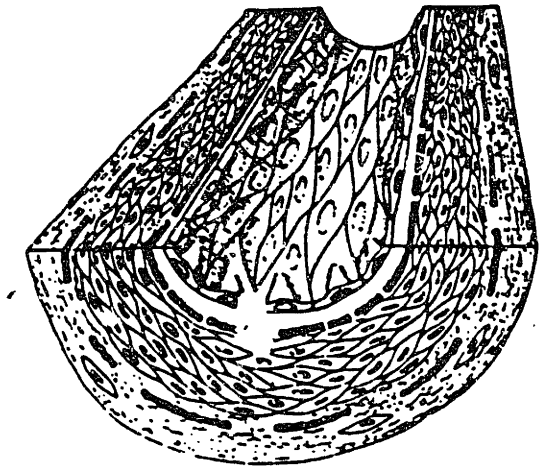

Figure 1.2: The arterial wall. Vascular endothelium is the monolayer of cells at the innermost aspect [Ross, 1986].

from occluded smaller vessels such as the carotids and coronaries. In these medium sized vessels, the flow is laminar.

Flow patterns in susceptible vessels have been studied by both experimental and numerical methods. Important features identified by this work include flow separations in branching arteries with helical patterns of secondary laminar flow within the separation zone. Perturbed flow regions have been visualized by Dewey, 1979, Friedman et. al., 1980, Giddens, et. al., 1983, Ku et. al., 1985, Karino et. al., 1983, and others, in transparent models and casts of vessels; and via flow studies of preserved post-mortem human arteries [Karino et. al., 1983]. In recent years, the availability of efficient algorithms and faster computers has enabled numerical studies of complex flows. Full computational simulations have been used to investigate effects of non-Newtonian fluid properties, varying geometry, and vessel compliance [Ku et. al., 1986; Davis, 1990].

Flow separation normally occurs near the outer wall opposite to a flow divider. The inner wall is typically exposed to non-perturbed and unidirectional laminar flow. Atherosclerotic plaques usually develop on the outside wall, in the region of predicted flow separation (Figure 1.3). Here, the shear stress is varying temporally and spatially. There are zones of flow reversal, stagnation, and reattachment of flow. In the region of flow reversal, shear stress can be as high as in non-perturbed regions [DePaola, 1991]. Downstream from this, there is a stagnation point where the shear stress goes to zero. Since flow is pulsatile, this region moves back and forth during the cardiac cycle. Beyond this the flow reattaches and the shear stress soon returns to average non-perturbed levels.

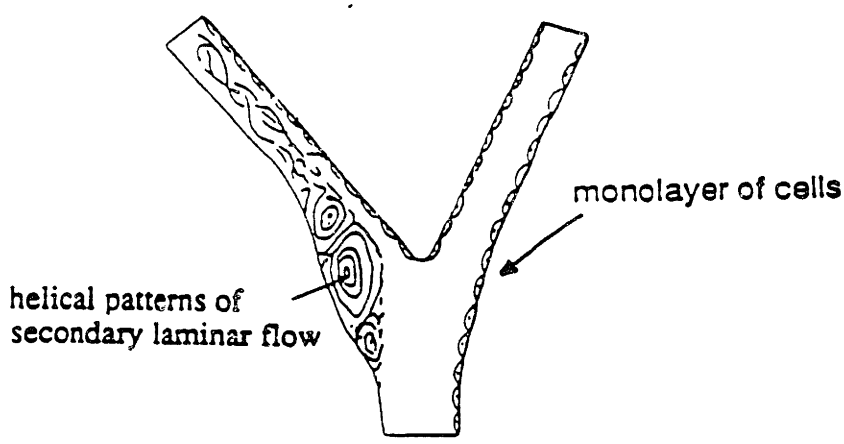

[adapted from Dewey, Adv.Exp.Med.Biol, 115: 55, 1979]

Figure 1.3: A schematic of a bifurcation in an artery. The flow separates at the outside wall, but remains attached along the inner wall. Atherosclerotic plaques usually develop in the outside wall.

Thus, perturbed flow regions are characterized by increased shear stress gradients [DePaola, 1991], and correlate with plaque formation. A direct causal relationship has not been established; however, spatial gradients in force may be an important agent for producing focal endothelial dysfunction [DePaola et. al., 1992].

DePaola et. al., 1992, performed the only *in vitro* study with perturbed flow. The modified cone-and-plate apparatus was fitted with rings on which a small ramp was attached, which produces a downstream region of flow separation and recirculation. Cultured endothelial cells exposed to this flow display morphology similar to endothelium on the outer wall opposite flow dividers *in vivo*. Moreover, cell turnover is increased in the region where there are shear stress gradients. Data from turbulent flow experiments also point to shear stress gradients as the element which triggers responses that may be important in the pathogenesis of atherosclerosis [Davies et. al., 1986].

2. ENDOTHELIAL CELLS

Endothelial cells have been extensively studied in recent years. Once thought to be simplistic entities, it is now realized that they comprise a highly complex biological system. Individual cells are incorporated into a monolayer composed of millions of cells, exhibiting different characteristics depending on the presence or absence of flow. Studying the cells with shear stress has been facilitated by the availability of various apparati which enable specification of the flow environment.

In vitro culture of endothelial cells allowed for the study of how endothelial cells adjust in response to laminar, turbulent, and disturbed flow conditions. Such experiments established that endothelial cells respond dramatically to shear stress [Dewey et. al., 1981; Davies et. al., 1986; DePaola et. al., 1992]. Both the structure and function of the monolayer is affected by these mechanical factors (see Figure 1.4); however, the specific mechanisms mediating these cellular responses have not been identified.

In a series of experiments, Dewey and colleagues examined the dynamic response of endothelium to shear stress using a modified cone-and-plate apparatus. By varying the angular velocity of the cone, it was possible to produce well defined and reproducible shear stress in various flow regimes. Confluent cultured bovine endothelial cell monolayers were subjected to shear stress in steady laminar flow, disturbed laminar flow, or turbulent flow. The results are summarized below:

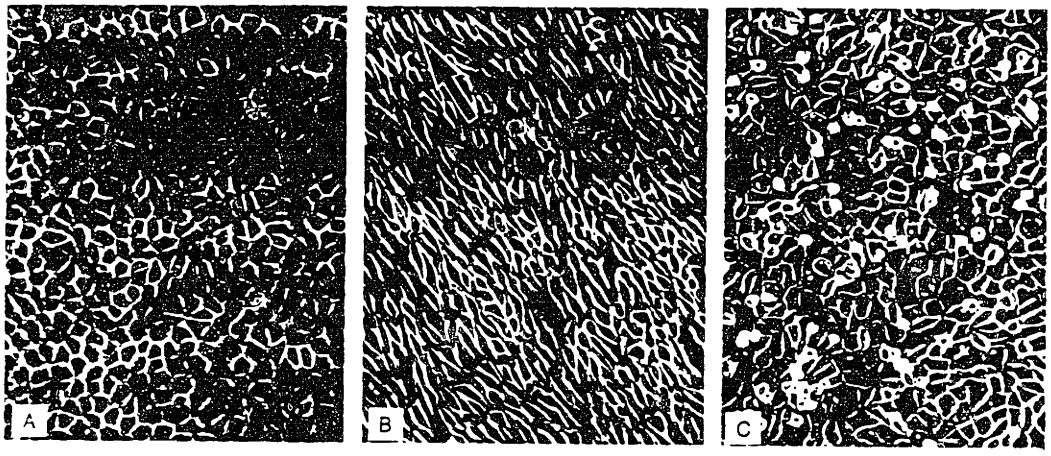

Figure 1.4: Fluid flow affects vascular endothelium *in vitro* [Davies et. al., 1986]. With no flow, cells exhibit a "cobblestone" morphology (a); laminar flow causes cells to align in the flow direction, as indicated by arrow (b); turbulent flow induces cell division (c).

1. Laminar flow - a time dependent (>24 hours) and shear magnitude dependent (>8 dynes/cm^2) response was observed. The endothelial cells aligned and elongated in the direction of flow, the degree of elongation increasing with shear stress maginitude. The cytoskeleton was altered so that stress fibers became prominent and aligned, suggesting that they play a role in anchoring the cell to substrate [Dewey et. al., 1981].

2. Turbulent flow - turbulent flow resulted in greatly enhanced cell turnover rate compared to cells exposed to laminar flow or static culture conditions. This response was detected at average shear stress values (2-3 dynes/cm^2) which are less than those needed to align cells in laminar flow. However, the cells did not align. *In vivo*, cell division is enhanced in regions predisposed to development of focal atherosclerotic lesions [Davies et. al., 1986].

3. Disturbed flow - a characteristic of disturbed laminar flow is the presence of vortices. Cells were aligned where flow was steady and attached. In the region where flow reattached and there was a stagnation point (where shear stress is zero and spatial gradients are largest) cells had an enlarged cobblestone morphology and an increased rate of turnover. Upstream in the region of reverse flow, local shear stress magnitudes became comparable with bulk flow values. Cells in these areas were elongated and oriented [DePaola et. al., 1992].

Experimental observations are supported by *in situ* and *in vivo* morphological studies [Flaherty et. al., 1972; Silkworth et. al., 1975; Nerem et. al., 1981]. The

normal morphology of large vessel endothelial cells *in vivo* is an elongated shape whose axis is aligned with the major flow direction. Cells at flow dividers, where there are predicted regions of recirculation and large spatial gradients in wall shear stress, have the cobblestone morphology observed in cultures *in vitro* [Kim et. al., 1989; Yoshida et. al., 1990].

Laminar shear stress has been shown to cause additional changes in the biological processes of cultured cells. These include: increased secretion of tissue plasminogen activator (tPA) [Frangos et. al., 1985]; upregulation of the PDGF (platelet derived growth factor) gene [Resnick et. al., 1992]; decreased adherence of platelets and monocytes; inhibition of cell division [Davies et. al., 1986; Shen, 1992]; increased endocytosis of low density lipoprotein [Davies et. al., 1984]; intercellular calcium release [Shen et. al., 1992]; and K^+ currents [Oleson et. al., 1988]. Dynamic experiments demonstrated that abrupt changes in the magnitude of shear stress cause elevated rates of pinocytosis and bursts of prostacyclin (PGI_2) [Frangos et. al., 1986; Davies et. al., 1984].

The detailed events which constitute the cellular response to shear stress have not been deciphered. Certain aspects of the early response have been studied. Shen et. al., 1992, showed that intracellular calcium is released and an oscillating signal is created in response to shear stress. Sachs, 1987, looked for stretch receptors in the endothelial membrane which are postulated transducers of intracellular currents in response to mechanical perturbation. However, the hypothetical structures have not been observed. The cytoskeleton is thought to play a role since stress fibers become prominent in oriented cells. But the details

of these and further cytoskeletal changes have not been explored, so that theories to date have been based on a restricted set of observations. Without more information about cell structure, it is impossible to envision a model for the mechanism of shear stress response which unifies experimental observations.

It has been shown that certain genes are turned on/off or up/down -regulated when endothelial cells experience shear stress [Resnick et. al., 1992]. This regulation presumably allows the cells to accomplish their requisite functions in an environment which includes constant stress due to fluid flow, pressure fluctuations, and transient wall movements because of vasoconstriction or vasodilation. The pressure forces, though of much greater magnitude, are essentially absorbed by underlying wall constitutents (i.e. matrix and smooth muscle). Arterial pressure changes during the cardiac cycle cause transient stretching of the artery and a corresponding stretching of the intima to which the endothelium is attached. Shear stress is the only mechanical force which is directly absorbed by the cells. The responses with immediate pathophysiological implications are those which alter endothelial interactions with blood cells (monocytes and platelets) and blood vessel smooth muscle cells; or which adversely affect endothelial function as a non-thrombogenic, selectively permeable barrier. By determining the normal adjustments in gene regulation, it will be possible to recognize an abnormal response in a cell which is for instance, exposed to disturbed flow patterns. In addition, abnormal responses to other important influences, such as altered levels of blood-borne immunological mediators, lipoproteins, and cholesterol, can be detected.

The difficulty with studying endothelial biology is due to the complexity of cells in general. There are many genes known (and unknown) that could be part of the cellular response to shear. Where to look is at best a calculated gamble. Current studies focus on genes for secreted factors such as PGDF, PGI_2, etc., which influence cells (lymphocytes, leukocytes, platelets, and smooth muscle) playing a role in atherogenesis. But there is a finite possibility that a crucial secreted or non-secreted factor, and thus gene or genes have not yet been discovered.

The approach of this thesis is rooted in the recognition that endothelial cells live and function in an unique mechanical environment. And most importantly, that lesion formation in atherosclerosis correlates with curves and bifurcations in arteries, where there are specific flow patterns and forces experienced by the cells. This serves as a pointer--a place to begin to decipher the complex changes occurring in the cell. If correct, the strategy could expedite determination of the genes and proteins which a cell must adjust in order to function "normally" in a flow environment. Moreover, studying the mechanical properties of the cell reveals aspects of cell function and monolayer dynamics which have not been previously examined.

3. OBJECTIVES

Studying the mechanical characteristics of endothelial cells provides a systemmatic method for analyzing the pathogenesis of atherosclerosis. We are able to identify entities within the cell which are possibly involved with and/or affected by changes in shear stress. Modelling complements and confirms laboratory observations. It is hoped that the relevant *early* changes can be identified by creating and using models to focus on involved cellular constituents.

The mechanism by which endothelial cells transmit forces, and what stress is experienced by the nucleus, cell membrane, cytoskeleton, and other constituents, remains undefined. There have been few mechanical models of endothelial cells. Theret et al., 1988, did micropipette aspiration measurements on oriented and nonoriented cells. They observed that oriented cells were more resistant to deformation when aspirated, and retained an elongated shape. A half space model was created which ascribed the increased mechanical stiffness to changes in bulk cortical cell properties. Fung et. al., 1992, have described a mechanical model of the endothelium which examines two limiting possibilities:

1. the cytoplasm has fluid-like character, so that the cell membrane absorbs mechanical stresses via tensile deformation.

2. the cytoplam has solid-like character and is involved in dissipating forces on the cell resulting from shear stress.

These models have serious limitations. Little is known about the internal structure of endothelial cells. Thus the mechanism of force transmission, which is

probably a crucial parameter governing cell behavior, is presumed.

In this thesis, we examine the mechanical anatomy of the cell, i.e. which organelles function to transmit forces to the underlying substrate. The results suggest a probable model for the mechanical properties of the cells. We can then propose a mechanism for the transduction of luminal shear stress to intracellular signal. In the process, we learn more about details of shear induced changes in the cytoskeleton, structural proteins involved with cell-cell attachments, cell-substrate adhesions, and basal-luminal distributions of these proteins.

Chapter Two

SHEAR STRESS DISTRIBUTION ON ARTERIAL ENDOTHELIUM: A COMPUTATIONAL MODEL

1. INTRODUCTION

The vascular endothelium is the simple epithelium that lines the cardiovascular system. It consists of a cellular monolayer which rests on a complicated matrix of cells and intercellular material. Intact endothelium provides a selectively permeable barrier to the passage of macromolecules from the bloodspace to the extravascular space. Moreover, the vascular endothelium bears the shear stress imparted by blood flow. The structure and function of the monolayer is affected by these mechanical factors (see Fig. 1.4) [Davies et. al., 1986; DePaola et. al., 1991; Dewey et. al., 1981; Fry, 1968; Gimbrone, 1986; Sato et. al., 1986; Shen et. al., 1992]; however, the specific mechanisms mediating these cellular responses have not been identified.

A detailed description of the flow is needed. An endothelial cell *in vivo* witnesses flow which passes in rhythmic waves. The cells are only 1-2 μm thick and 20-50 μm in the circumferential and axial dimensions. They are primarily affected by detailed flow behavior very near the wall. In this region, the fluid velocity profile is nearly linear, although the magnitude of the average velocity may vary by a factor of four or more from systole to diastole, and from point to point on the microscopically rough surface. Because of the small size of endothelial cells, flow at any instant may be considered quasi-steady near the wall, as described by the local linear shear flow.

One of the most difficult problems in fluid mechanics is studying flow details near a rough surface. The disturbed wall region is typically buried inside a boundary layer or is difficult to access in experiments. Additional complications include: tiny dimensions (typically microns), wall probe interference effects, and the intrinsic difficulty of accurately measuring wall shear stress. Previous studies demonstrate that numerical solutions of the Navier-Stokes equations yield accurate predictions of flow characteristics in such circumstances [Caponi et. al., 1982; DePaola et. al., 1989; Fischer et. al., 1990; Folie et. al., 1989; Hara et. al., 1990; Kiya et. al., 1975; Lyme, 1971]. We are using computational methods to study flow near arterial endothelium, whose surface is modelled as a wavy wall.

Endothelial cells withstand fluid forces and maintain intercellular connections in a confluent layer which is only one cell thick in arteries and veins. Preserving the integrity of intercellular junctions is critical for the monolayer to serve its function as a selectively permeable barrier between blood and tissue [Caro et. al., 1985; Jo et. al., 1991; Weinbaum et. al., 1985]. When a quiescent monolayer of cells is exposed to flow, the cells can potentially align and elongate in the flow direction, altering the bulk mechanical characteristics of the cell, and modulating physiological responses *in vitro* [Davies et. al., 1986; DePaola et. al., 1991; Dewey et. al., 1981; Wechezak et. al., 1989; White et. al., 1983]. The nature of this response depends on whether the flow is laminar, disturbed, or turbulent (see Fig. 1.4). Exposure to shearing forces also causes dramatic changes in the cytoskeleton. The actin network is rearranged from dense peripheral bands to form prominent stress fibers [Matsudaira, 1991; Wechezak et. al., 1989; White et. al., 1983]. Stress fibers are normally found in the basal aspect of cells which have

not experienced shear stress. In such cells, they are arranged in random directions and appear to interconnect regions of adherence of the plasma membrane to the substrate (focal contacts). In aligned cells, stress fibers are parallel to the direction of flow; and appear to attach to the apical membrane [Schnittler et. al., 1989]. These stress fibers may prevent endothelium from hydrodynamic injury and/or detachment by tethering the apical membrane and stabilizing intercellular junctions. Others have made observations which support this possibility:

- aligned cells appear to be "stiffer" than non-aligned cells [Jamney et. al., 1991; Sato et. al., 1986].
- there is increased ATP utilization in cells exposed to shear stress, presumably in part due to contracting stress fibers [Schnittler et. al., 1989].
- the permeability of a monolayer with no previous exposure to shear stress is transiently and acutely increased in response to flow [Davies et. al., 1986; Jo et. al., 1991].

DNA synthesis is altered in cells by exposure to flow affecting gene expression, and apparently producing a different phenotype. Few (if any) other cells in the body experience shearing forces of similar magnitude on only one side. Thus, it is difficult to identify analagous cellular models for comparison. An unrelated phenotypic modulation has been observed in microvessel endothelial cells in response to chemical factors [Lipton et. al., 1991]. Similar transdifferentiation studies suggest that extracellular environment, the cytoplasm, and nucleus, interact to confer the gene expression exhibited by cells [Ingber, 1990; Lipton et.

al., 1991].

In order to understand how shear stress produces such profound effects in endothelial cells, the detailed distribution of forces on a cell and monolayer of cells must first be known. In early studies, investigators did not consider cell shape. The average shearing force imparted by bulk fluid flow was considered determinant: high shear stress caused direct desquamation, and low shear stress caused concentration polarization effects at the wall [Caro et. al., 1985; Fox et. al., 1966]. Subsequent studies suggest that disturbed flow patterns (such as are found near branchings in arteries) are more closely associated with possible pathological processes [Fry, 1976]. The flow field in such regions is characterized by high shear stress gradients [DePaola et. al., 1992]. Theoretical and experimental work has demonstrated the importance of local geometry, corresponding to cell shape in our problem, in affecting the flow field near a surface [Caro et. al., 1971]. In cases where the surface geometry scaling is much smaller than bulk flow conduit geometry, the stress distribution depends on the local flow field induced by the object [Bussolari, 1983; Hyman et. al., 1972]. For a wavy surface, the relevant flow field is contained in a small region near the wall that scales with the wavelength of the surface variation.

The wavy wall problem has been studied in two dimensions by others [Benjamin, 1959; Caponi et. al., 1982; Hara et. al., 1990; Hyman, 1972; Kiya et. al., 1975; Lyme, 1971]. Such computations were used for studying wave growth under the influence of wind (beach processes). Theoretical solutions for steady flows at large hydraulic Reynold's number (Re) over small-amplitude wavy

surfaces were obtained [Benjamin, 1959; Kiya et. al., 1975]. Similar calculations have been performed for low Re oscillatory flows over wavy surfaces [Hara et. al, 1990; Hyman, 1972; Lyme, 1971]. The theory for our problem follows from these latter works.

Recent studies include numerical treatments of low Re flows over objects in shear flows. In one study, finite elements are used to estimate forces acting on a thrombus [Folie et. al., 1989]. We apply linear theory to predict the local flow field over a coordinate surface which models an endothelial cell monolayer [see *APPENDIX*] [Bussolari, 1983]. A comparison is made with results from spectral element numerical calculations in order to define the range of geometric parameters for which linear theory is applicable.

2. COMPUTATIONAL METHODS

A model surface was chosen which represents the cell monolayer (see Fig. 2.1). The fluid flow near this surface is characterized by a vanishing Reynold's number [Re~O(10^{-4})] so that momentum transfer is dominated by viscous forces. The pertinent governing equations are for an incompressible, constant-property, steady-state fluid, leading to a so-called Stokes calculation. Conservation of momentum and mass can be written as (respectively):

$$\frac{1}{Re}\nabla^2\bar{u} = \nabla p \tag{1}$$

$$\nabla\bar{u} = 0 \tag{2}$$

The unknowns are the vector velocity $\bar{u}$ and the pressure p. The single parameter appearing is the Reynold's number, $Re = \sigma\hat{\eta}^2/\nu$, where σ is the shear rate in the linear shear flow far from the surface, and $\hat{\eta}$ is the surface undulation amplitude (characteristic length scale of the problem). The kinematic viscosity of the fluid is $\nu \equiv \mu/\rho$, where ρ is the fluid density and μ is the fluid viscosity. The equations are parabolic so velocity boundary conditions must be provided on all sides of the computational domain. The complete theoretical solution is included in the *APPENDIX* [Bussolari, 1983].

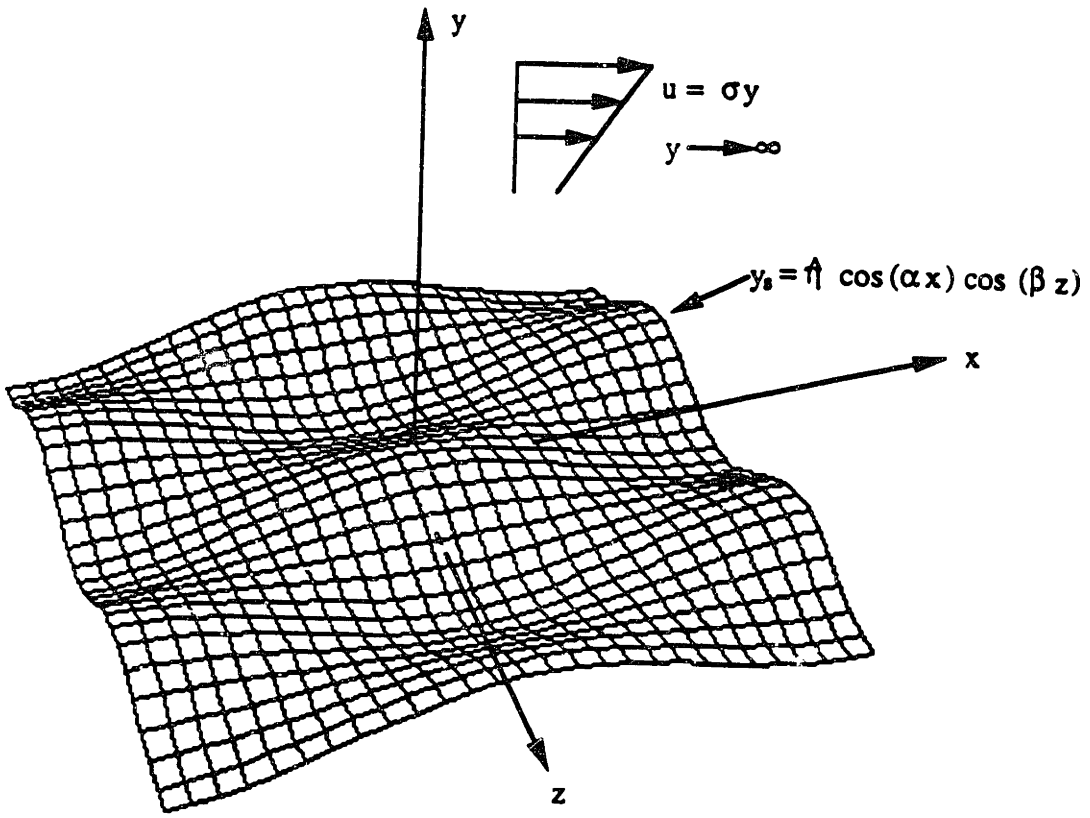

Figure 2.1: Cell surface model.

Our calculations simulate conditions in an artery very near the vessel wall at any instant in time. The upper boundary can be represented as a shear flow at infinite distance from the surface. However, the computational code did not explicitly provide for boundary conditions at infinity. Instead we specified the upper boundary to be a rigid surface which is moved far enough away (at least 4 times the cell surface modulation amplitude) so that wall effects are no longer important. The velocity at the upper surface is fixed at the value corresponding to a linear shear flow field. The cell surface is the lower boundary of the domain. It is rigid and extends infinitely in x and z. Thus, the solution (which is periodic) is determined by solving for one full period of the cell model surface in the relevant directions (x and z). Boundary conditions are expressed below:

$$|\bar{u}|_{y\to\infty} = \sigma y \quad \text{(shear flow at large distance)}$$

$$|\bar{u}|_{y=y_s} = 0 \quad \text{(zero velocity at wall)}$$

where σ is the undisturbed shear rate far away from the wall. A shear rate of σ = 800 s^{-1} was used for all calculations. Unsteady motion dynamics for physiologic frequencies are such that a quasi-steady approximation can be made ($\alpha = h\sqrt{\omega/\nu} = 0.1$ to 0.001).

The computational code NEKTON was used for numerical solution of the problem [Fischer et. al., 1990; Maday et. al., 1989; Ronquist et. al. 1987]. This code is robust and efficient, and was easily modified to generate the model cell surface as the lower boundary of the computational domain. NEKTON has powerful pre- and post- processing packages for mesh generation and visualization of results. The code runs on a wide variety of computers (from workstations to supercomputers). Thus, computational experiments can be performed on smaller machines, while production runs can be directed to the most efficient computers available [DePaola et. al., 1989; Dewey et. al., 1989]. Only three-dimensional steady state Stokes results are presented in this paper (quasi-steady approximation), although NEKTON supports both unsteady and three-dimensional incompressible fluid calculations for the full Navier-Stokes equations.

The spectral element method for partial differential equations is the basis for spatial discretization. Spectral elements combine high-order (spectral) accuracy with the geometrical flexibility of low order finite-element methods. The computational domain is divided into K non-degenerate macro-quadrangles (spectral elements). In our problem, three-dimensional domains were broken up into "bricks", in which the two horizontal parallel faces are nondegenerate quadrangles [DePaola et. al., 1989; Dewey et. al., 1989; Maday et. al., 1989].

The data, geometry, and solution, are approximated by high-order polynomial expansions within each macro-element. A local Cartesian mesh is constructed within each element which corresponds to NxNxN tensor-product

Gauss-Lobatto Legendre collocation points. The Gauss-Lobatto points are clustered near elemental boundaries, an arrangement which gives an accurate approximation and favorable interpolation and quadrature properties. Dependent variables are expanded in terms of $(N-1)^{th}$ order polynomial Lagrangian interpolants (through the Gauss-Lobatto Legendre collocation points) [DePaola et. al., 1989; Dewey et. al., 1989; Fischer et. al., 1990].

Spatially discrete equations are generated by inserting assumed forms of dependent variables into the governing equations, and requiring that the residual vanish in some integral and weighted sense. The computed numerical variables correspond to values occurring at the collocation points of the mesh. Convergence is obtained by increasing the number of macro-elements (K) or the order of the interpolants (N) in the elements. The error decreases algebraically (like K^{-N}) as K is increased; and exponentially for smooth solutions (like $e^{-\alpha N}$) as N is increased [DePaola et. al., 1989; Dewey et. al., 1989].

For our computations, two domains in x and z, and one in y (total of 4) were adequate to resolve the details of the flow. Increased accuracy (in the spectral sense) was achieved by increasing the polynomial degree. The present calculations used values of N between 7 and 11. Calculations were performed on a Concurrent 6450 computer.

3. RESULTS

An analytical solution for linearized flow over a wavy wall is given in the *APPENDIX* [Bussolari, 1983]. If the amplitude of the sinusoidal boundary modulation is small relative to the wavelength, the boundary condition at the cell model surface , y_s, can be linearized. The function which defines the surface is:

$$y_s = \hat{\eta}\cos(\alpha x)\cos(\beta z) \tag{3}$$

where y_s is the displacement from the mean surface height and $\hat{\eta}$ is the amplitude of surface oscillation. The streamwise and transverse wavenumbers α and β are given by,

$$\alpha=\frac{2\pi}{\lambda_x} \; ; \; \beta=\frac{2\pi}{\lambda_z} \tag{4}$$

where λ_x and λ_z are the surface undulation wavelengths. The resulting dimensionless shear stress and pressure force distributions on the model endothelial surface are:

$$\tau^*_{yx} = 1 + 2\pi\frac{2+q^2}{\sqrt{1+q^2}}\frac{\hat{\eta}}{\lambda_x}\cos(\alpha x)\cos(\beta z) \tag{5}$$

$$\tau_{yz}^{*} = -2\pi \frac{q}{\sqrt{1+q^2}} \frac{\hat{\eta}}{\lambda_x} \sin(\alpha x)\sin(\beta z) \tag{6}$$

$$p^{*} = -4\pi \frac{\hat{\eta}}{\lambda_x} \sin(\alpha x)\cos(\beta z) \tag{7}$$

where,

$$q = \frac{\lambda_x}{\lambda_z} = \frac{\beta}{\alpha} = \frac{\text{length}}{\text{width}} \tag{8}$$

$$\tau_{yx}^{*} = \frac{\tau_{yx}}{\mu\sigma};\ \tau_{yz}^{*} = \frac{\tau_{yz}}{\mu\sigma};\ p^{*} = \frac{p}{\mu\sigma} \tag{9}$$

τ_{yx}^{*} is the normalized surface shear stress in the x-direction; and τ_{yz}^{*} is the normalized surface shear stress in the z-direction. The term $\mu\sigma$ is the mean wall shear stress imposed by flow far (i.e. many times the cell height) from the endothelial surface. The solution predicts:

1. The surface shear stress in the x-direction consists of the sum of the average shear stress imposed by flow and a spatially varying stress perturbation due to cell shape. The magnitude of the shear stress perturbation depends

on q and $\hat{\eta}/\lambda_x$. As $\hat{\eta}/\lambda_x$ (dimensionless surface amplitude) increases, the perturbation increases linearly. For q>>1 it is proportional to q. τ^*_{yx} is in phase with surface variations in x and z--it is maximum at the highest point on the cell surface, and minimum at the lowest point on the surface.

2. The presence of surface waviness introduces a lateral shear stress perturbation which is linear with $\hat{\eta}/\lambda_x$. It is caused by the transverse flow away from surface peaks and toward surface valleys. As q becomes large (>>1), there is no dependence on q. τ^*_{yz} is 90° out of phase with the surface waviness in the streamwise and transverse directions. It is maximum or minimum at points of maximum surface slope.

3. The pressure perturbation is linear with $\hat{\eta}/\lambda_x$, but does not depend on q. It is asymmetric along the cell longitudinal axis, tending to increase the pressure on the proximal side and reduce it on the distal side. The pressure is 90° out of phase with the surface variations in the direction of flow. Pressure is maximum or minimum at points of maximum slope in the flow direction.

Numerical and analytical computations were compared for 5 surface geometries: length/width ratios of q =0, 0.25, 1, 4, and ∞ (see Fig. 3). Eight amplitudes ($\hat{\eta}$ = 1, 2, 4, 8, 12, 20, 30, and 40μm) were evaluated for each geometry. The resulting

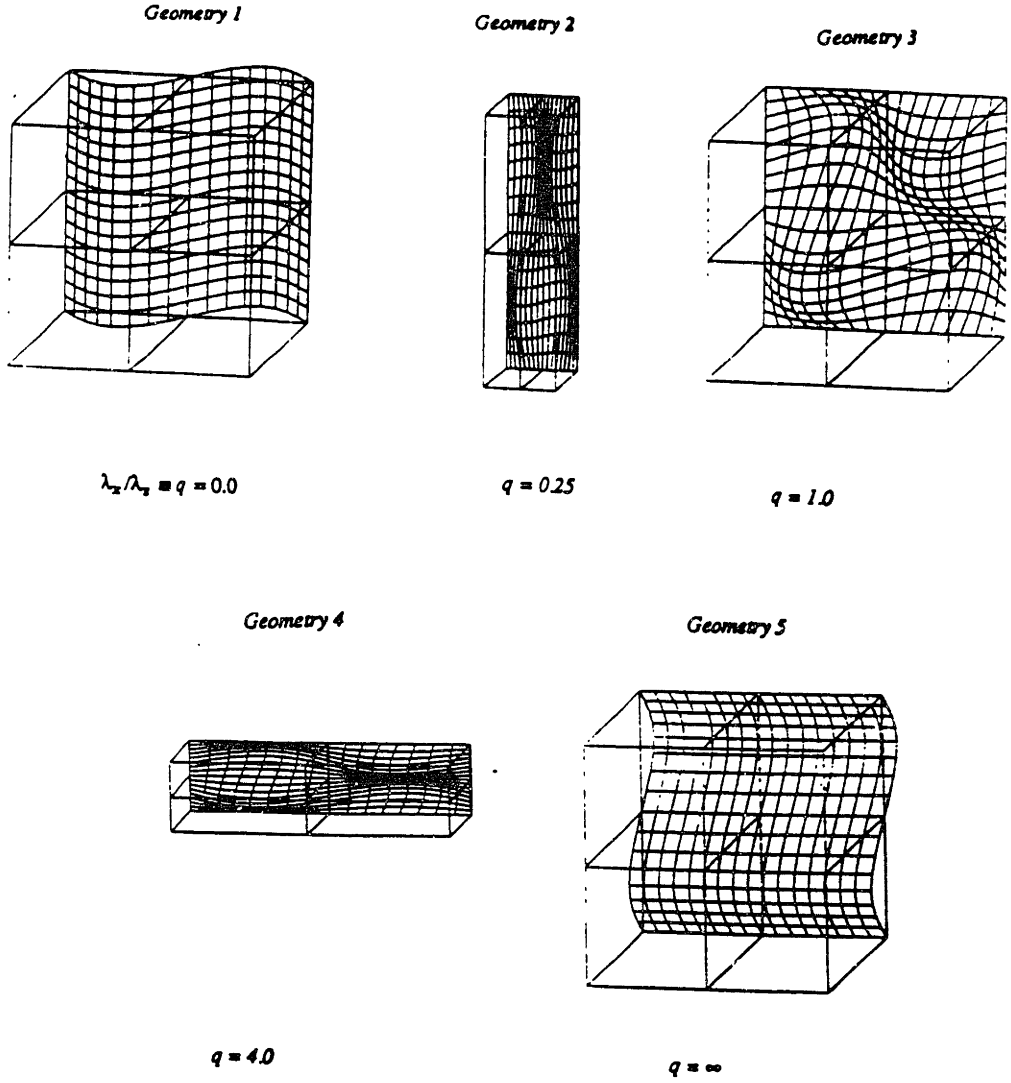

Figure 2.2: Surface geometries.

range for the height/length ratio [$0 \le \hat{\eta}/\lambda_x \le 4/3$] includes values which violate the condition $\hat{\eta}/\lambda_x \ll 1$. Physiologic values of length/width ratio for large vessel endothelial cells typically range from 0.25 to 4.0 [Bussolari, 1983]. For healthy (non-atherosclerotic) arteries, cell heights (corresponding to surface amplitude) are usually 1-4 μm, yielding values $\hat{\eta}/\lambda_x$ in the range 0.02-0.2.

For a limited range, numerical results and linear theory predictions agree (not illustrated). Both numerical and theoretical methods predict that the wall shear stress τ^*_{yx} is maximum at the highest points of the coordinate surface, and minimum at the lowest points. The pressure distribution is 90° out of phase in the direction of flow, and the wall shear stress and pressure distributions are periodic.

Numerical *magnitudes* no longer agree with linear theory after the onset of separated flow. Figs. 2.3a and 2.3b compare pressure distribution profiles for q=1 as $\hat{\eta}/\lambda_x$ is increased from 0.025 (Fig. 2.3a), to 0.1 (Fig. 2.3b) (NOTE: for plotting purposes, the orgin was shifted by 90° so that the peak in the pressure profile occurs at the orgin). The linear solution no longer closely follows numerical predictions as the dimensionless surface amplitude becomes of order O(0.1), where recirculations appear in the flow field.

Maximum ($\tau^*_{yx,max}$) and minimum ($\tau^*_{yx,min}$) shear stress magnitudes for both numerical and analytical solutions are plotted in Figs. 2.4a and 2.5a for a range of parameter values. Groups of points corresponding to a particular geometry (fixed length/width value) fall along the same line when shear stress and pressure are plotted vs. surface amplitude (Figs. 2.4-2.6). The maximum wall shear

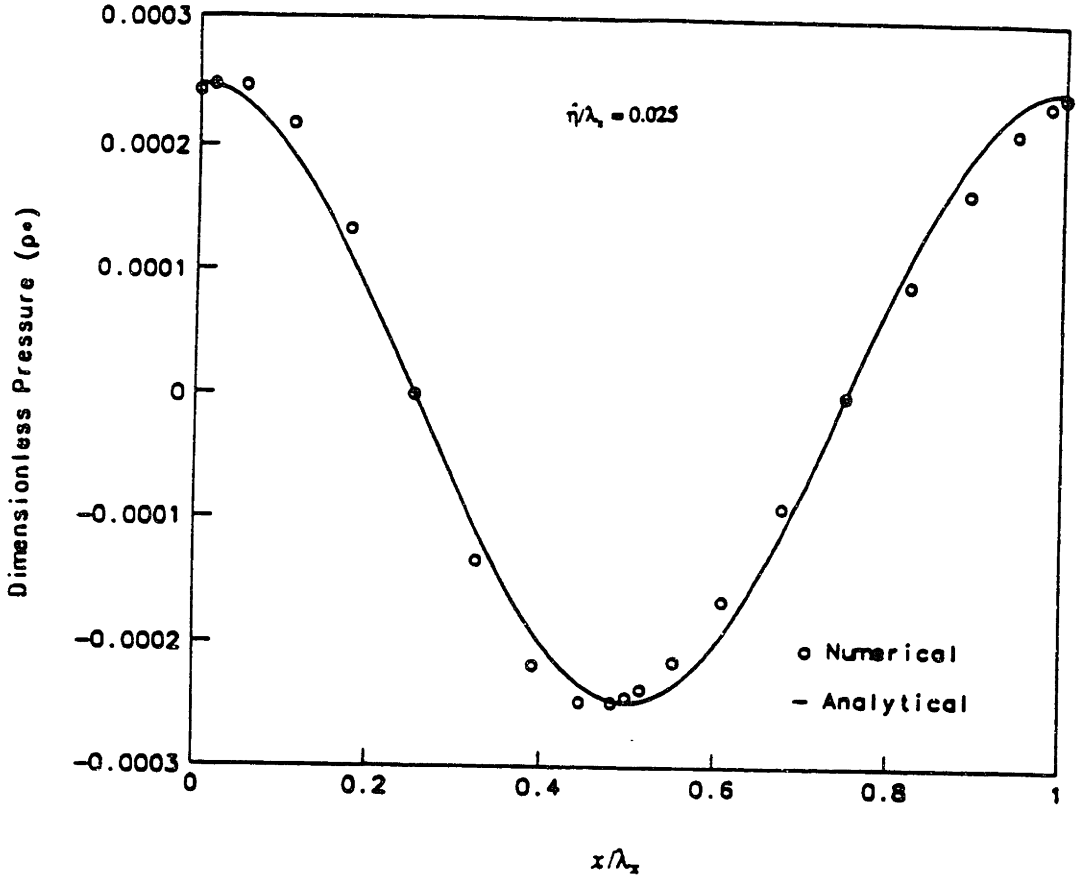

Figure 2.3a: Surface pressure distribution profile for the case of q=1; $\hat{\eta}/\lambda_x = 0.025$.

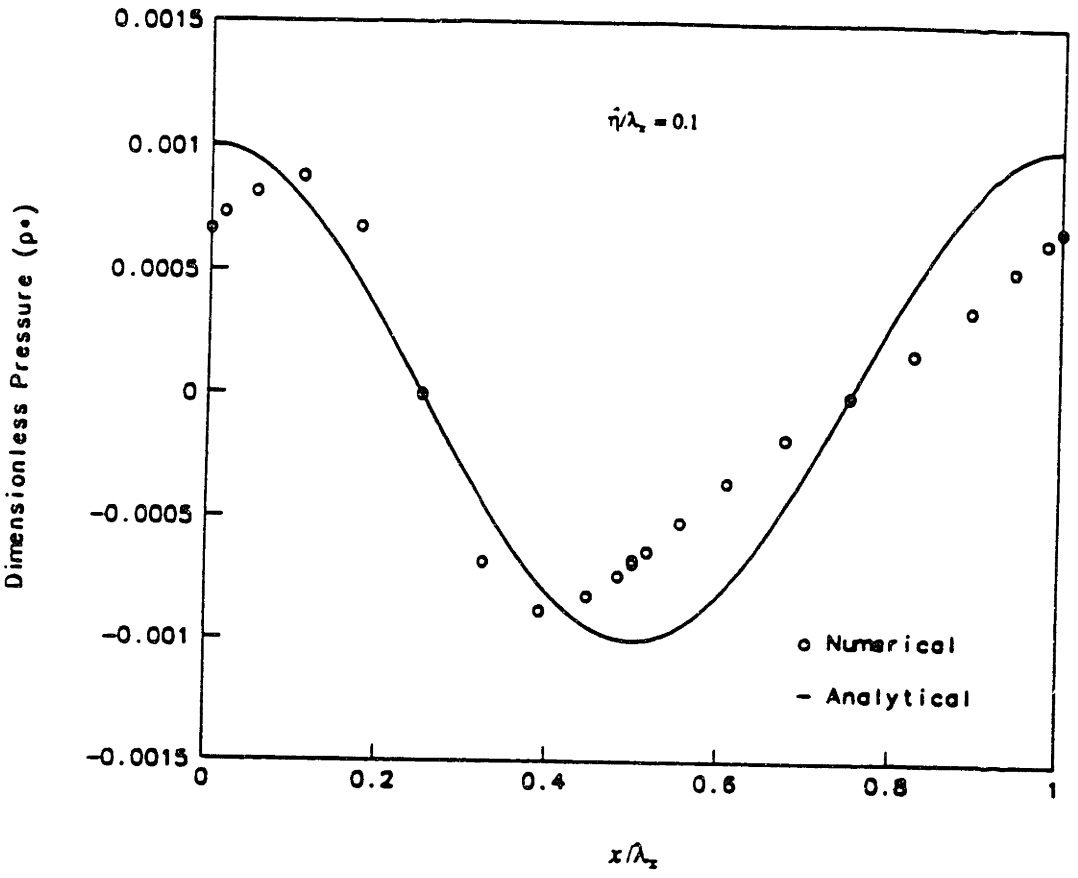

Figure 2.3b: Surface pressure distribution profile for the case of q=1; $\hat{\eta}/\lambda_x = 0.1$.

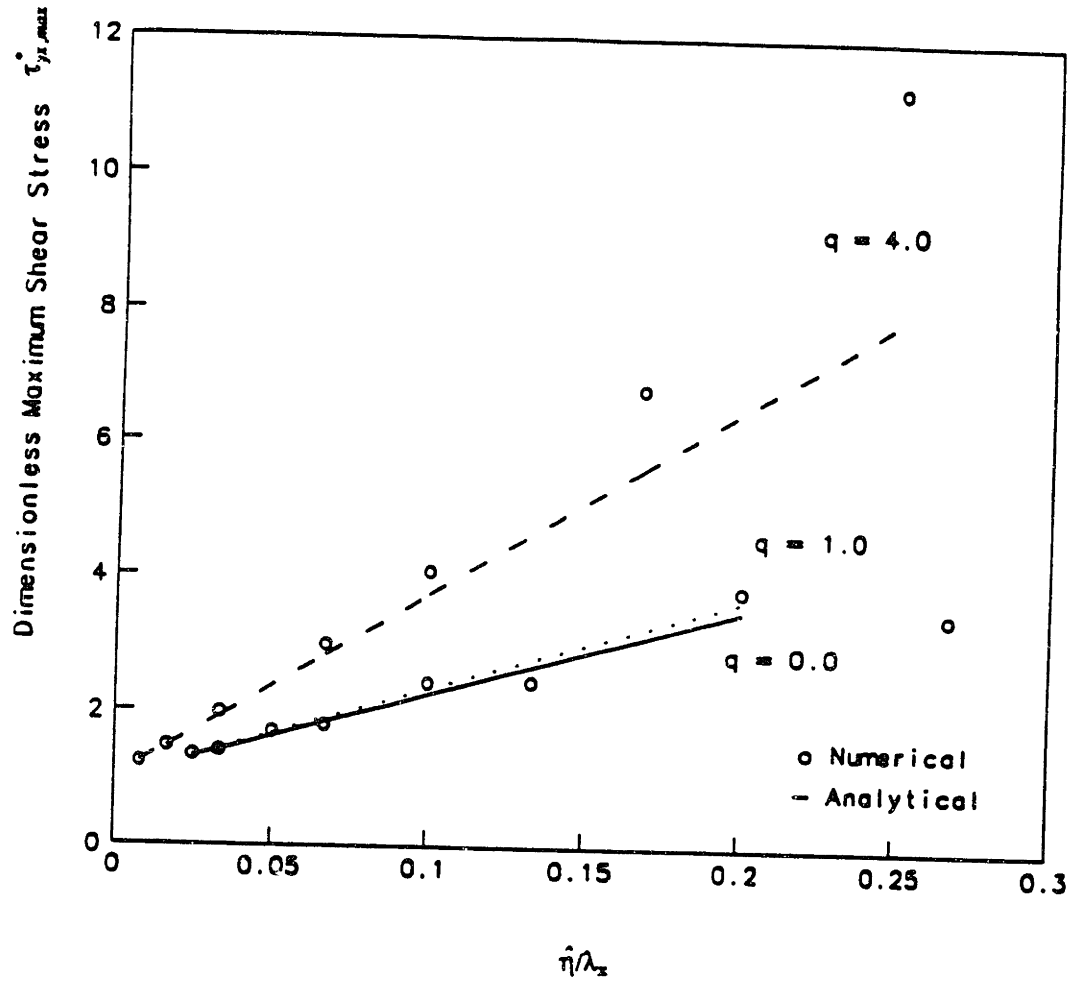

Figure 2.4a: Dimensionless maximum shear stress vs. height/length for numerical and analytical solutions.

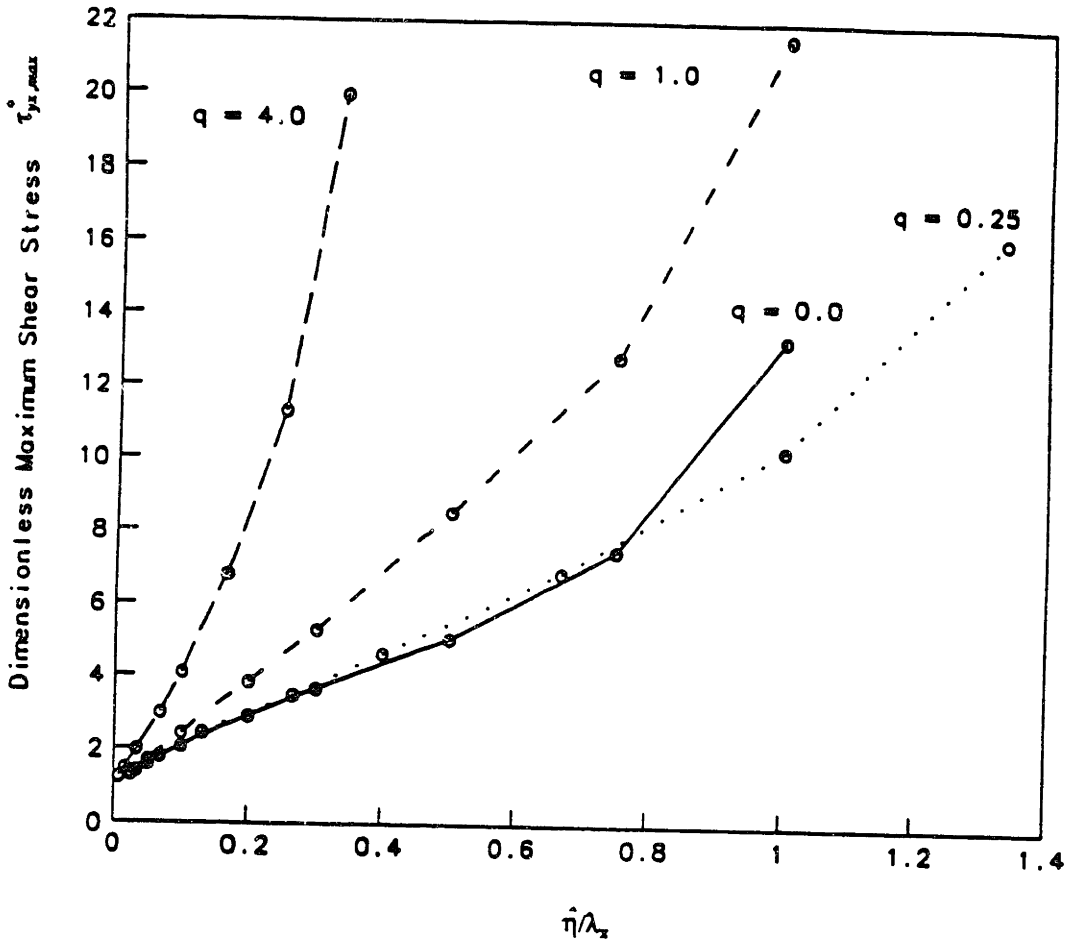

Figure 2.4b: Dimensionless maximum shear stress vs. height/length for numerical solution.

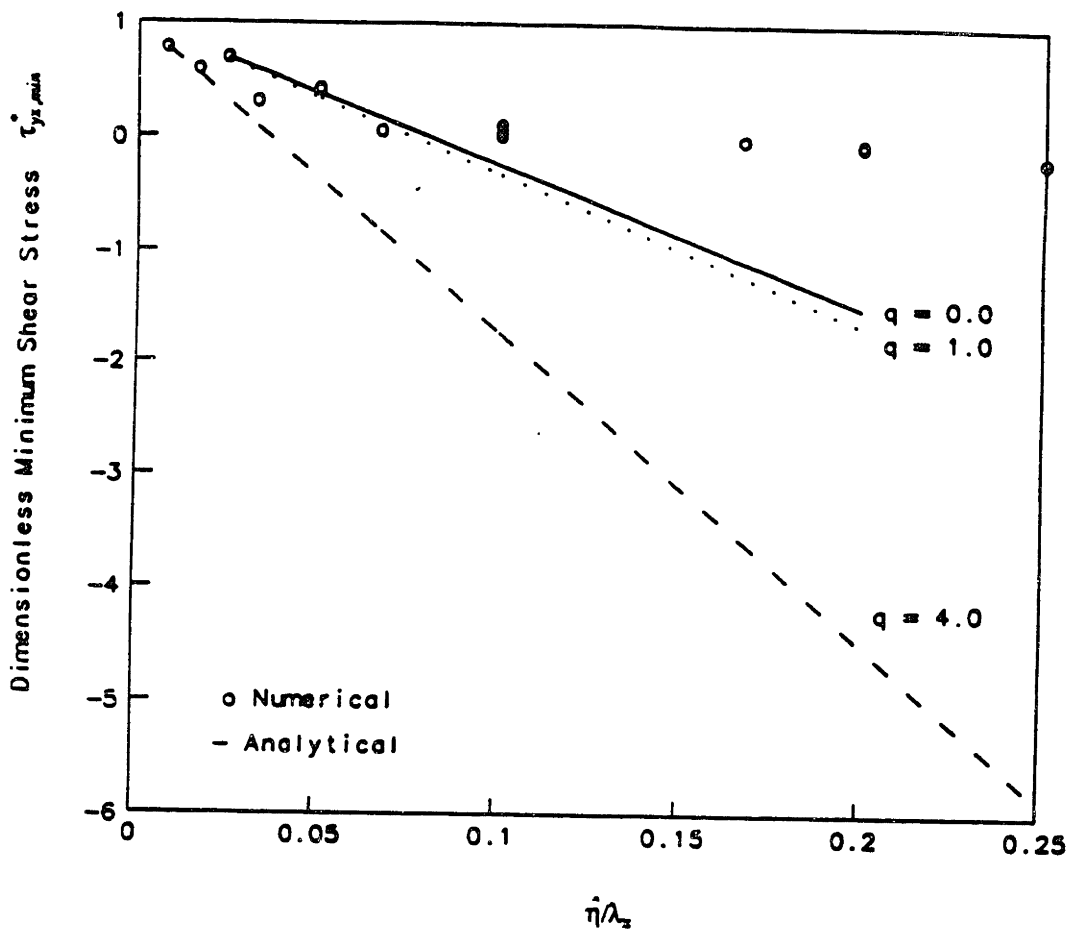

Figure 2.5a: Dimensionless minimum shear stress vs. height/length for numerical and analytical solutions.

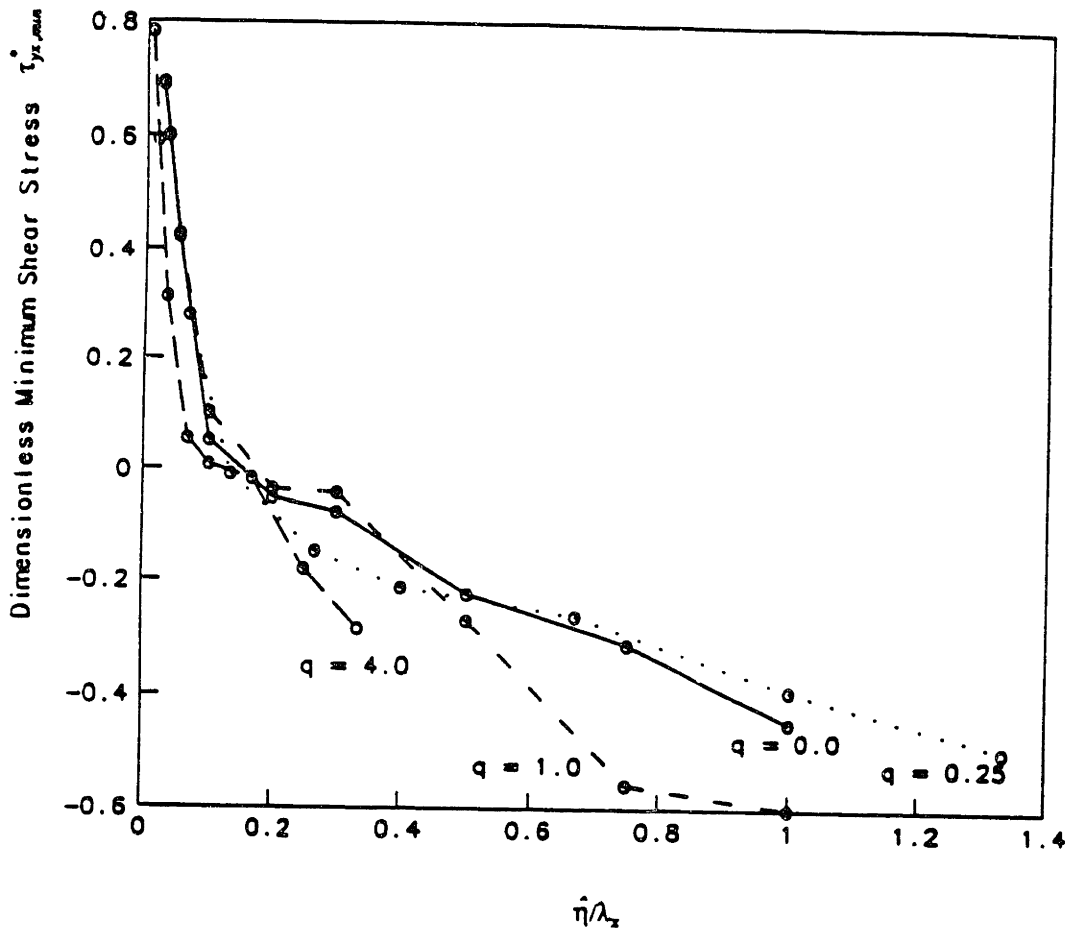

Figure 2.5b: Dimensionless minimum shear stress vs. height/length for numerical solution.

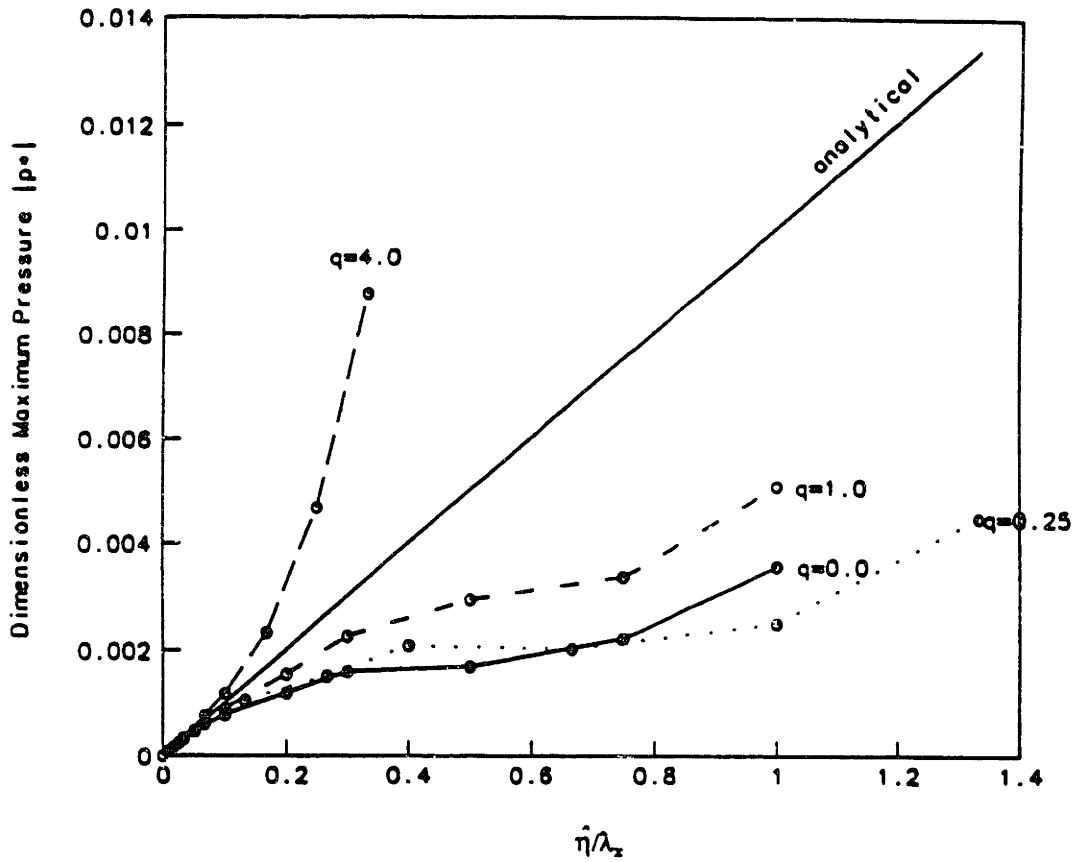

Figure 2.6: Dimensionless maximum pressure magnitude vs. height/length for numerical and analytical solutions.

predictions are in better agreement with linear theory than the minimum wall shear values. As shown in Fig. 2.4a, the maximum wall shear values increase almost linearly for $\hat{\eta}/\lambda_x < 0.2$. The slopes agree initially, but diverge as the amplitude increases. This effect becomes more pronounced for higher q values. Fig. 2.4b is a plot of the numerical maximum shear stress data. As the dimensionless amplitude is increased well beyond 0.2, nonlinear behavior prevails. For minimum wall shear, the analytical solution predicts a linear decrease with increasing $\hat{\eta}/\lambda_x$ (Fig. 2.5a). But for $\hat{\eta}/\lambda_x > 0.1$, the numerical ($\tau^*_{yx,min}$) values become independent of q and weakly dependent on the dimensionless amplitude. These differences are attributable to the formation of regions of reverse flow.

Linear theory fails to predict reverse flow. It only accounts for flow accelarations and decelerations due to expansion or contraction of the flow domain. Describing the relevant processes which cause recirculation would require using higher order terms in the analytical model. The numerical solution predicts and resolves flow reversals as the dimensionless amplitude is increased. As shown in Fig. 2.7, streamline plots indicate that vortices form in the valleys of the cell model surface. Recirculation regions occur when there is surface variation in the primary flow direction (i.e. for *Geometries 1-4*).

We did not resolve the exact amplitude where recirculation begins; however, the range which contains the critical amplitude is recorded in the table in Fig. 2.7. The critical dimensionless surface amplitude is of order O(0.1), and it defines 2 regions:

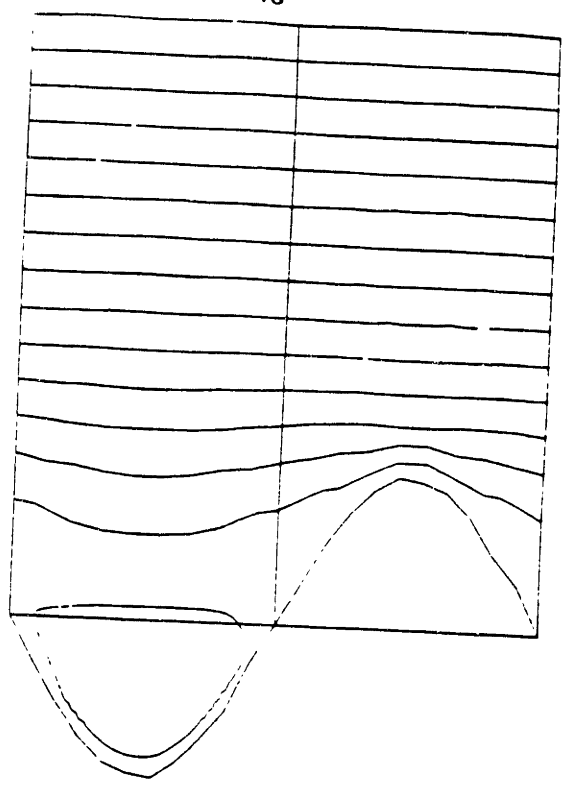

Vortices Appear		
Geometry	Crit. ampl. range	q
Geometry 1	0.10-0.20	0.00*
Geometry 2	0.07-0.13	0.25
Geometry 3	0.10-0.20	1.00
Geometry 4	0.10-0.16	4.00
Geometry 5	**	∞**

*Transverse ribs
**Vortices do not appear: streamwise ribs

Figure 2.7: Streamline plot for the case of q=1; $\frac{\hat{\eta}}{\lambda_x} = 0.5$; showing region of recirculation. Fluid flow is from left to right. The table indicates the values of the critical dimensionless surface amplitude for each geometry.

1. For $\hat{\eta}/\lambda_x < (\hat{\eta}/\lambda_x)_{crit}$, the numerical values are in good agreement with linear theory.

2. For $\hat{\eta}/\lambda_x > (\hat{\eta}/\lambda_x)_{crit}$, the values diverge. The physical processes can no longer be represented by a linear perturbation. Higher order terms are needed for a more accurate theoretical treatment.

The analytical solution for surface pressure predicts a linear dependence on $\hat{\eta}/\lambda_x$, and no dependence on q. The numerical result exhibits dependence on q; namely, the slope increases with q (Fig. 2.6). In contrast, the symmetrical *form* of the numerical solution agrees with linear theory. The average surface pressure must be zero so that there is no net flow in the direction normal to the top boundary. The periodicity of the problem provides an additional condition, constraining the maximum surface pressure to be of equal magnitude and opposite sign to the minimum surface pressure. With *Geometry 5*, the pressure field is zero everywhere (for both numerical and analytical results) since there is no surface variation in the flow direction.

4. DISCUSSION

The flow fields predicted by the numerical and analytical solutions are qualitatively similar. The wall shear stress and pressure distributions vary periodically at the wavy wall surface. However, the results from the two methods diverge as the amplitude of the surface waviness increases. Flow vortices appear as the key assumption of linear theory is violated [namely, $\hat{\eta}/\lambda_x \ll 1$ -- see Appendix], where the critical dimensionless amplitude is of order O(0.1). Departure from linear theory predictions can be observed by comparing surface pressure distributions (Figs. 4a and 4b). There is:

- a departure from linear growth of peak-to-peak pressure.
- variation in the phase of pressure distribution.
- contributions from higher harmonics of the pressure distribution.
- dependence on the length/width ratio (parameter q).

Others have obtained similar results with linear theory [Benjamin, 1959; Caponi et. al., 1982; Hyman, 1972]. Linear theory does not predict the formation of recirculation regions, since the physical phenomena responsible for vortex flow are nonlinear processes. Adverse pressure gradients arise in the regions between surface peaks, inducing a reverse flow when the fluid momentum can no longer overcome the pressure gradient. As recirculation regions form in geometries of low aspect ratio (q), the pressure profile predicted by linear theory is relaxed. The momentum of the flow that would be lost in the pressure recovery region (trough)

is preserved as the flow separates. In geometries of higher q, the vortices are smaller due to the transport of momentum around the sides of the peaks into the low pressure region and thus the "shadowing effect" of the vortices is reduced. The flow passing over the smaller vortices impinges on the proximal sides of the surface peaks, resulting in higher peak pressures near the points of maximum slope.

At the highest surface points, the wall shear stress grows almost linearly with increasing surface amplitude as predicted by linear theory. Flow acceleration occurs along streamlines towards the peaks due to the constraint provided by the continuity equation. These processes are different than those producing flow separation in the lower surface regions.

Nonuniform shear stress gradients of significant magnitude across a cell surface could be of potential importance for explaining flow-induced morphological changes. The forces which result from a cell-to-cell variation on the order of the perturbation shear stress are sufficient to disturb protein-protein interactions. Bell, 1978, has determined that a noncovalent interaction is disrupted by a critical force of 10^{-5} dyne. The difference in shear force on 2 adjacent cells in laminar flow can be of order 10^{-4} dyne, which corresponds to 10 protein-protein interactions. Experimental studies of others indicate that a force of ~1 dyne (10^5 protein-protein interactions) can detach a cell from a monolayer [Hubbe, 1981]. Thus, the imbalanced forces produced by surface variations are potentially large enough to disturb small numbers of a cell's protein-protein noncovalent associations with other cells, but cannot detach the cells. An endothelial monolayer will

have more geometric variability than our model; consequently, the resulting shear stress gradients could exceed those predicted for the model surface. A sequential disruption of a large number of bonds holding a monolayer together could lead to alterations in cell morphology. However, we believe that the substantial morphological changes that are observed in the presence of flow are progressive changes requiring internal synthesis and rearrangement of actin filaments. This is discussed more fully in Chapter 4.

The predicted forces acting on the aligned monolayer are reduced in comparison to nonaligned endothelium. For a surface approximating a nonaligned monolayer, the perturbation shear stress can be as large as 34% of the average shear stress imposed by the primary flow (Figure 2.8). This decreases to 20% for aligned monolayers since the height/length ratio is reduced (essentially, the surface is less "bumpy"). Perhaps the monolayer is able to achieve stability by reconfiguring the actin filament system so that stress fibers attach to the apical membrane. Nonaligned cells do not have stress fibers in the proper arrangement to experience this stabilizing effect (Figure 2.9).

Modelling the distribution of forces on cells also aids in understanding the role of shear stress in the pathophysiology of atherosclerosis. Endothelium exposed to large shear stress *gradients* displays dramatic changes in cell shape, density, and rate of division [DePaola et. al., 1991; Fry, 1968]. Our analysis predicts that shear stress gradients associated with laminar flow are smaller in magnitude than disturbed or turbulent flow. Consequently, the observed endothelial response to laminar flow is marked (cells elongate in the flow

A

Cells	Length/width	Height/length	$[\tau_{max} - \tau_{av}]/\tau_{av}$	
			Analytical	Numerical
Nonaligned	1.0	0.025	0.33	0.35
Aligned	3.5	0.0083	0.20	0.20

B

Critical force per bond = 10^{-5} *dyne/bond*

Exptl. cell detachment ~ O(1 dyne/cell) = 10^{5} *bonds/c*

# of bonds needed to resist.....		
Cells	8 dynes/cm^2	Pulling
Non-aligned	10	~*O*(10)
Aligned	<10?	~*O*(10)

cell adhesion strength >> imposed forces via shear stress

Figure 2.8: Estimates of (a) forces on monolayer with shear stress; and (b) adhesive forces for a cell in a monolayer.

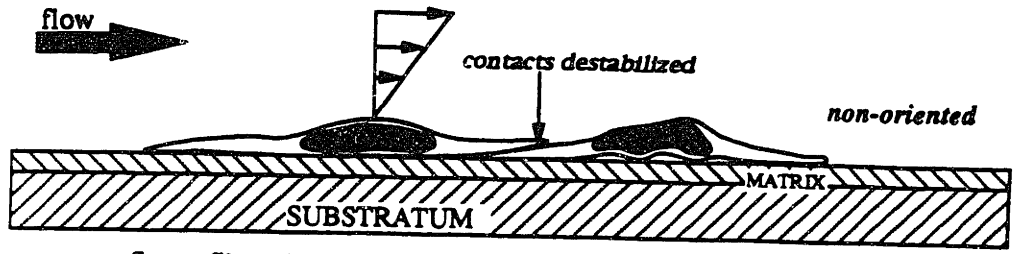

Stress fibers in non-oriented cells are found almost exclusively in the basal regions of cells. With this arrangement, the cell-cell attachments are unstable in the presence of shear stress associated with laminar flow.

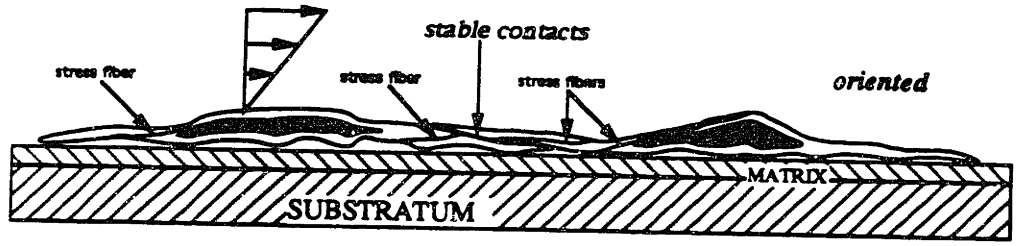

Stress fibers attach apically, basally, and to cell-cell junctions in oriented cells. This provides structural stability for the monolayer in the presence of shear stress associated with laminar fluid flow.

Figure 2.9: Hypothesis for endothelial adjustment to laminar shear stress.

direction), but differs from disturbed flow in that there is little change in cell division and density [Davies et. al., 1986; DePaola et. al., 1991; Dewey et. al., 1981]. Loss of contact with neighboring cells has been shown to induce migration and cell shape changes [Davies et. al., 1986; Wechezak et. al., 1989]. Thus the larger forces associated with disturbed flow may exceed the cells' adaptive capabilities, resulting in pathological behavior. Observed responses include: increased cell division, changes in cell density, altered arachidonate metabolism, growth factor and cytokine production, surface adhesive properties, coagulation and fibrinolytic activities and altered permeability to macromolecules and lipoproteins [Gimbrone, 1989; Gimbrone, 1986; Gimbrone et. al., 1990].

Chapter Three

SHEAR STRESS INDUCES ADJUSTMENTS IN F-ACTIN ORGANIZATION AND INTERCELLULAR JUNCTIONS

1. INTRODUCTION

The vascular endothelium is a monolayer of cells which lines arteries and veins. It serves many roles including regulation of the passage of molecules between bloodstream and tissue, and provides a non-thrombogenic interface with blood. Following exposure to shear stress *in vitro*, cultured bovine aortic endothelial cells undergo a dramatic morphological transformation from a polygonal shape to an elongated shape (Figure 1.4) [Dewey et. al., 1981]. Simultaneous changes must occur in the cytoskeleton which produce cellular elongation. In this chapter, confocal microscopy was used to identify adjustments in F-actin organization and intracellular junctions induced by shear stress.

Endothelium is subjected to forces imparted by the blood on one side only. Fluid forces perpendicular to the wall are caused by pressure, and are transmitted to the underlying structures in the blood vessel wall. Those parallel to the wall are caused by shear stress, and are absorbed by the endothelial cells themselves. Average physiological fluid shear stress in arteries is from 2 to 40 dynes/cm^2 for the resting human. Peak physcological levels may reach 100 dynes/cm^2 [Ling et. al., 1968]. The endothelium resists disruption by shearing forces while maintaining continuity of the monolayer and serving as a selectively permeable barrier between blood and tissue [Caro et. al., 1971; Jo et. al., 1991; Weinbaum et. al., 1985; Davies et. al., 1986]. The cytoskeleton of the endothelial cell is thought to provide mechanical integrity to resist these stresses, although the precise load

bearing mechanism is unknown.

The idea that shear stress could directly influence endothelial integrity was first developed by Fry and colleagues [1968]. *In vitro* culture of endothelial cells has allowed for the study of how endothelial cells adjust when flow conditions change. Endothelial responses to flow include changes in: cytoskeletal organization, intracellular Ca^{++} currents, K^{+} channel status, endocytosis, tissue plasminogen activator synthesis, gene transcription, and histamine synthesis [Fry, 1968; Gimbrone, 1986; Dewey et. al., 1981; Shen et. al., 1992; Franke et. al., 1984; Schnittler et. al., 1989; Deforrest et. al., 1978; Diamond et. al., 1984; Olesen et. al., 1988]. Adjustments occur acutely (seconds, as with Ca^{++} currents), in an intermediate time period (2-3 hours, as with pinocytosis and DNA synthesis), and chronically (24 hours for gross morphological changes) [Dewey et. al., 1983; Davies et. al., 1984]. Previous studies have explored macroscopic morphological adjustments. The shape of endothelial cells correlates with anticipated flow patterns in arteries [Nerem et. al., 1981; Reidy et. al., 1980]. Endothelial cells grown *in vitro* have been observed to change from the cobblestone morphology to the elongated shape when exposed to laminar shear stresses above a magnitude of 5 dynes/cm^2 for 24-28 hours [Dewey et. al., 1981]. The correlation between shape and flow conditions suggests that the morphological changes are part of an adaptive response, but the details of this change are unknown beyond observations with light microscopy. The cytoskeleton, which produces these changes, has not been adequately studied to identify its role in these adjustments.

Investigators have suggested a role for shape in predicting the functional state of endothelium [Ingber, 1990]. The elongated shape may indicate that a cell is "well adjusted" to the flow conditions. Polygonal shape may be displayed by cells which are ready to divide or migrate--changes associated with endothelial injury or dysfunction. When endothelial cells orient, modifications are made in microtubules and intermediate filaments [Gotlieb et. al., 1991]; but the most dramatic (and most studied) adjustments are in actin. F-actin is important for control of cell adhesion, migration, cell permeability, and maintainence of cell shape [Dewey et. al., 1981; Franke et. al., 1984; Schnittler et. al., 1989; Kim et. al., 1989; Langille et. al., 1991; Gotlieb et. al., 1991; DePaola et. al., 1992; Wechezak et. al., 1989; White et. al., 1983; Sato et. al., 1986]. *In situ*, F-actin is generally present in nonoriented cells as an orthogonal network in the cell periphery and grouped as bundles (stress fibers) in the central regions of cells [Kim et. al., 1989]. Actin is reorganized when cells orient, so that more stress fibers are found in the central region, and they tend to be aligned with the flow direction [Dewey et. al., 1981; Franke et. al., 1984; White et. al., 1983]. Large vessel endothelial cells have a similar actin morphology *in vivo* [Langille et. al., 1991]. Our objective is to determine how these stress fibers form (when cells align in response to shear stress).

Ultrastructural studies have been limited to techniques which use 2-D specimens. Thus, important questions remain concerning the detailed 3-D structural modifications in the cytoskeleton and the mechanisms which produce these changes when cells orient. We used confocal microscopy: 1. to define 3-D structure and to determine adjustments in the actin network and associated

structural proteins of cells exposed to laminar shear stress; and, 2. to examine changes in cell-cell adhesion in response to laminar and turbulent shear stress. Significant changes occur in the organization of actin in apical and basal cell regions, and in the distribution of α-actinin, an actin cross-linking protein. Cell-cell junctions are disturbed when monolayers experience either laminar or turbulent flow, suggesting that destabilization of intercellular junctions is a stimulus for further structural adjustments.

2. METHODS

2.1 Materials

Dulbecco's Modified Eagle Medium (DMEM), Dulbecco's Phosphate Buffered Saline (DPBS), and RPMI, were purchased from GIBCO (Grand Island, NY). Calf serum, glutamine, penicillin and streptomycin, were purchased from Whitaker Bioproducts (Walkersville, MD).

2.2 Cell Culture

Bovine aortic endothelial cells (BAEC) were isolated and cultured as previously described.[7] Briefly, cells from a single strain (11 BAEC) between passages 15-30 were subcultured in DMEM supplemented with 10% calf serum, 2 mM L-glutamine, and 100 U/ml each of penicillin and streptomycin. For experimental work, cells were seeded on 15 mm diameter glass coverslips (Bellco Glass), and used after achieving confluence.

2.3 Experimental Apparatus

To generate defined flow over endothelial monolayers grown *in vitro*, we used a modified cone-and-plate flow chamber (Figure 3.0). This apparatus was originally developed in our laboratory ~10 years ago [Bussolari, 1983] and recently modified [DePaola, 1991]. The system can produce a wide range of shear stress, including both laminar and turbulent flows. The flow characteristics of fluid between the rotating and stationary plate depend on a local dimensionless parameter [Sdougos et. al., 1984]:

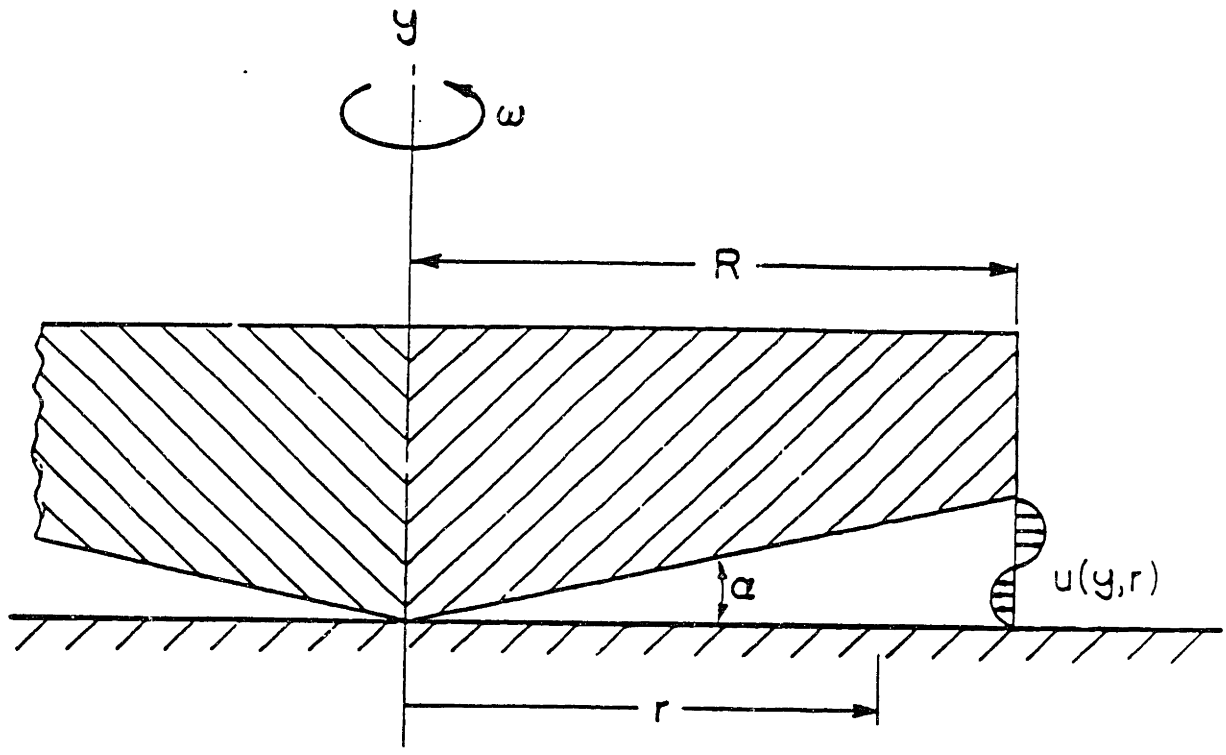

Figure 3.0: Schematic of cone-and-plate flow apparatus [Bussolari, 1983].

a.

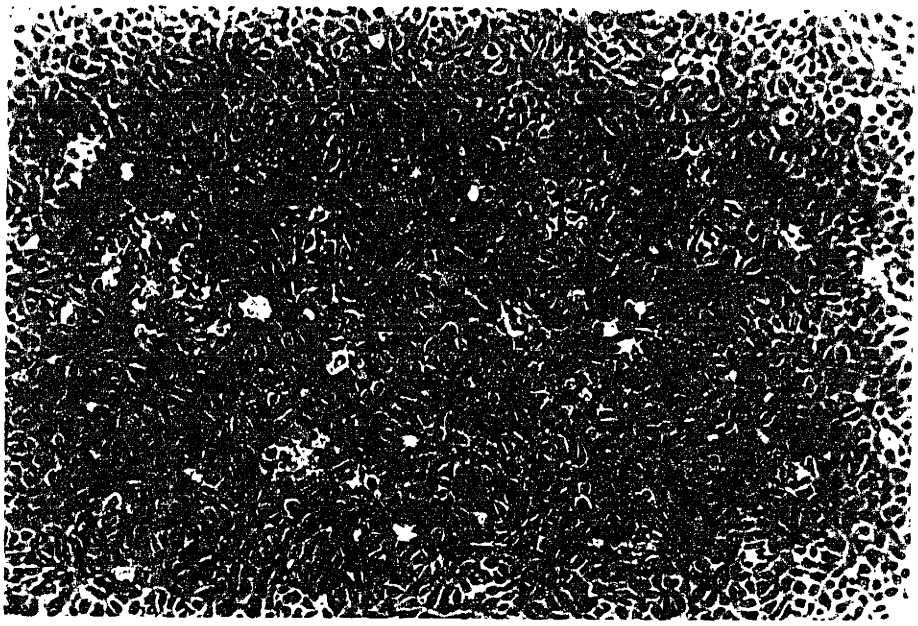

b.

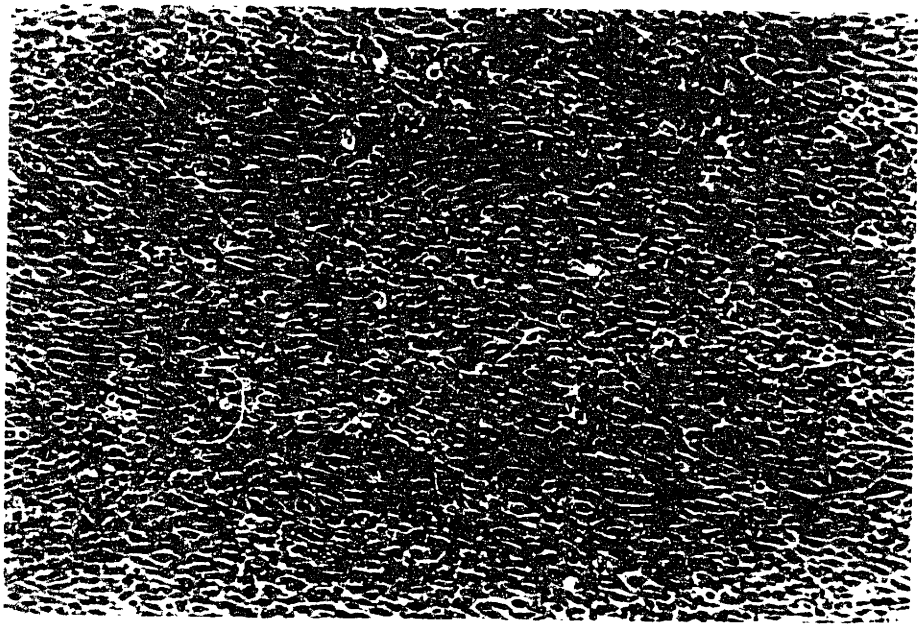

Figure 3.1: Bovine aortic endothelial cells grown without flow (a); or aligned with 10 dynes/cm^2 (b).

$$\bar{R} = \frac{r^2 \omega \alpha^2}{12\nu}$$

where r is the radial distance from the apex of the cone, ω is the angular velocity of the cone, α is the cone angle in radians, and ν is the kinematic viscosity of the fluid. $\bar{R}$ is analagous to the Reynold's number and measures the ratio of centrifugal to viscous forces acting on the rotating fluid. At low rotational speed and small cone angle ($\bar{R} \ll 1$) the centrifugal force is insignificant in comparison to viscous forces, and the fluid velocity is purely azimuthal with a linear gradient in the vertical direction. The surface shear stress is:

$$\tau = (\mu \frac{\partial v}{\partial y})_{y=0} = \mu \frac{v_0}{h} = \mu \frac{\omega r}{r \tan\alpha}$$

where μ is the fluid viscosity, y is the coordinate normal to the plate, and v_0 is the velocity at radius r.

At small cone angle, $\tan\alpha \sim \alpha$, so that shear stress can be estimated by:

$$\tau \simeq \frac{\mu\omega}{\alpha}$$

As $\bar{R}$ increases to O(1), the fluid near the cone experiences increasing centrifugal force that promotes radial fluid motion (secondary flow). As $\bar{R}$ exceeds 4, the

local flow becomes fully turbulent. The wall shear stress for $\bar{R}$ can be estimated using the following semi-empirical expression [Sdougos et. al., 1984]:

$$\tau = 1 + 2.58\frac{\bar{R}^{3/2}}{3.5+\bar{R}} - \frac{\bar{R}^{5/2}}{(3.5+\bar{R})^2}$$

In our experiments, the flow was either laminar ($\bar{R} \ll 1$) or fully turbulent ($\bar{R} \geq 4$). Laminar flow was produced using a 0.5^{o} cone; turbulent flow was obtained using a 3^{o} cone. The construction details of the system have been described by DePaola [1992] and Bussolari [1983]. The plate holds 12 test rings. Glass coverslips are glued to these rings which fit into recesses in the plate. The cone is rotated by a modified milling machine.

The cone and plate are contained inside a plexiglass chamber so that the environment can be precisely controlled during experiments. The temperature of plate and atmosphere is maintained at 37^{o}C and a 5% CO_2/95% air mixture continuously replinishes the box. Biological compatibility of the apparatus has been previously verified--cells are viable under both conditions of flow and no flow.

Baec were oriented in laminar flow for all cases with shear stress of 10 dynes/cm^2 for 36 hours. This yielded well aligned cells (Figure 3.1). For turbulence experiments, the specifications were: 2.5 dynes/cm^2 for 16 hours.

2.4 Antibodies

Monoclonal mouse antibody (mAb) to α-actinin was purchased from Sigma Chemical Co. (St. Louis, MO). Rabbit polyclonal and mouse monoclonal antibodies to endoCAM were generously provided by Dr. Steven Albelda (The Wistar Institute, Philadelphia, PA). Mouse mAb to vinculin was obtained from Chemicon International (El Segundo, CA). FITC and rhodamine labelled goat anti-mouse and anti-rabbit antibodies were purchased from Caltag Laboratories (South San Francisco, CA).

2.5 Fluorescence Studies

For immunofluorescence microscopy, cells were grown on glass coverslips as previously described. The protocol for immunostaining below is a modification of that used by Dejana, et. al., 1988. Coverslip attached cells were fixed for 10 minutes with 3% paraformaldehyde/2% sucrose in PBS, pH 7.6, warmed to 37°C. Oriented cells were briefly inspected with phase contrast to check that the monolayers had not been visibly damaged in the cone-and-plate apparatus. They were then fixed while the glass coverslip was still attached to the metal ring from the cone-and-plate apparatus, so as to minimize the time between stopping flow and fixing the cells. Oriented cells will return to the cobblestone morphology over several hours once flow is suspended. Thus, procedures were followed so that a maximum of 15 minutes time elapsed from removing the oriented cells from the cone-and-plate and fixing. The glass coverslip was finally separated from the ring upon completion of the immunostaining procedure.

The cells were next permeabilized with ice cold 0.1% Triton X-100, 20mM Hepes, 300 mM sucrose, 50 mM NaCl, 3 mM $MgCl_2$, pH 7.4, for 3 minutes, and rinsed with DPBS/1% FBS (except when staining with anti-endoCAM, in which case this step was omitted). For indirect immunofluorescence experiments, the primary antibody at IgG concentrations ranging between 10 and 30 μg/ml (diluted as appropriate in DPBS/1% FBS) was layered on fixed and permeabilized cells and incubated in a 37°C humid chamber for 30 min. After rinsing thoroughly with 5 washes of DPBS/1% fetal bovine serum (FBS), coverslips were incubated with the appropriate rhodamine- or fluorescein-tagged secondary antibody for 30 min. at 37°C. To show F-actin, 2 μg/ml rhodamine or FITC-labelled phalloidin (Molecular Probes, Eugene, OR) was included with the secondary antibody. Coverslips were mounted on glass slides in 50% glycerol-50% PBS for viewing.

To image the cell membrane, fixed cells (without permeabilizing) were labelled with the fluorescent lipophilic carbocyanine membrane probes, DiO (1,1'-dihexadecyloxacarbocyanine perchlorate) and DiI (1,1'-dioctacecyl-3,3,3',3'-tetramethylindocarbocyanine perchlorate) (Molecular Probes, Eugene, OR). Nuclei were viewed with propridium iodide (Molecular Probes) which binds to DNA in fixed cells.

Observations were carried out with a BIORAD MRC-500 laser scanning confocal microscope. The scanner is capable of co-excitation at 2 different wavelengths, with co-detection at 2 wavelengths, so that it was possible to view and compare 2 distributions of labelled proteins in the same field of cells simultaneously. Excitation and emission spectra for the fluorochromes fluorescein and

rhodamine are shown in Figure 3.2. These fluorochromes have some overlap of emission bands, but the emission peaks are well separated so that with the appropriate optical filters, signal detection with little background cross-signal is achieved. The MRC-500 gave best results with this set of fluorochromes. Thus, the other fluorochromes were selected with the criterion that they have similar spectra to either rhodamine or fluorescein. DiI has a rhodamine-like spectrum. DiO and propridium iodide have fluorescein-like spectra.

Serial optical sections of the monolayers were recorded by focussing on the tops of cells, then stepping through the cells in regular, fixed increments. The microscope is fitted with a precision motor for vertical movements, so that reproducible steps of 0.1 μm are possible. Endothelial cells are typically 1-2 μm thick when oriented, and 2-3 μm thick with the non-oriented or cobblestone morphology. The optical resolution of the microscope was ~0.3 μm. Thus, optical sections were in most cases spaced 0.9 μm apart to distinguish between apical and basal features.

Digital images of cell fields were stored on 3.5 inch high-density floppy diskettes. Photographs of cell fields were taken with Kodak-Ektachrome (160T-35 mm) tungsten film.

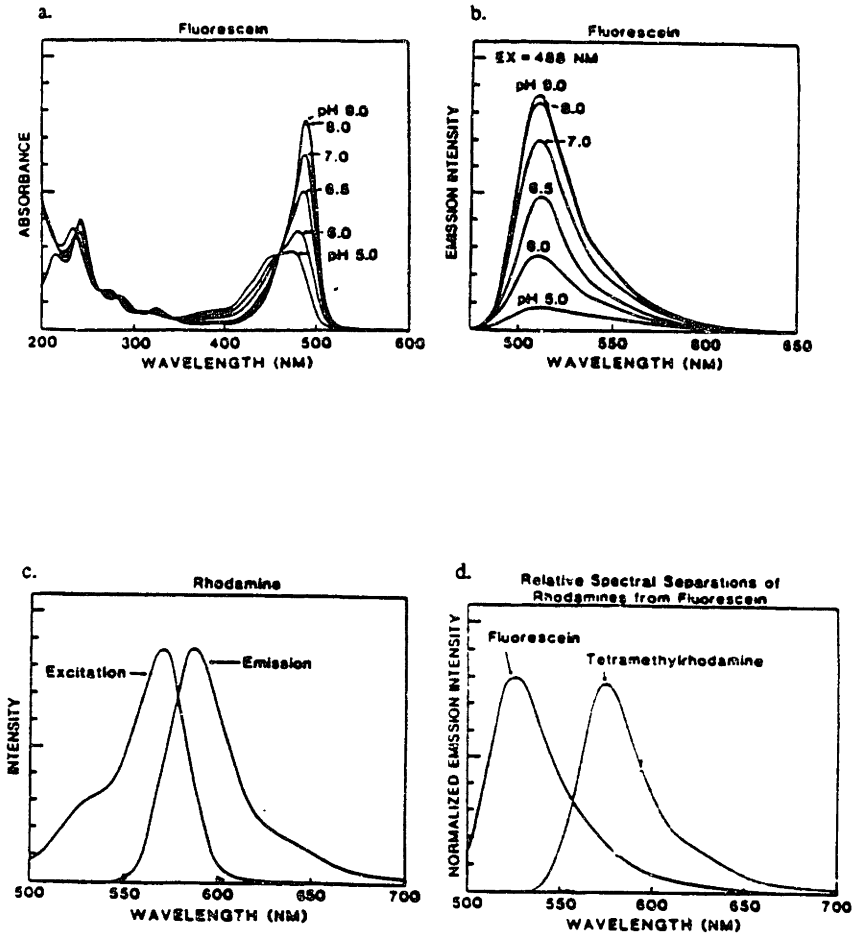

Figure 3.2: (a) Excitation and (b) emission spectra of fluorescein; (c) rhodamine excitation and emmission; and (d) rhodamine and fluorescein emmission on common plot for comparison [Haugland, 1989]. Fluorescein emmission spectrum overlaps the rhodamine peak; thus, some fluorescein background signal was seen when detecting rhodamine in a doubly labelled sample.

3. RESULTS

At confluence with static conditions, cultured endothelial cells have a "fried egg" shape (see Figure 3.3.1) with a flat periphery and bulging nucleus. Typical dimensions for a non-oriented cells of polygonal shape are 2-3 μm thick above the nucleus and 40 μm in transverse dimension. Following alignment, the cells adapt torpedo-like profiles and the nuclear bulge is less pronounced. Oriented cells are usually 1-2 μm thick, 40-80 μm long, and 10-20 μm wide. Figure 3.3.2 is a series of non-oriented BAEC fixed (without permeabilization) and stained with the membrane binding probe DiI. Series optical sections are spaced 0.9 μm apart; the monolayer is crossed (top to bottom) within 3 sections, corresponding to 1.8 ± 0.9 μm. Cells are thickest over the nucleus and thinnest in peripheral regions. In Figure 3.3.2a, staining of the "domes" of cells identifies membrane overlying the nucleus. In Figure 3.3.2b, "holes" in regions of staining correspond to locations of nuclei. Figure 3.3.2c is in the basal aspect of cells. Impressions of the nuclei of some cells below the plane of the basal cell membrane indicates that these nuclei bulge into the membrane.

Shear stress affects the cytoskeleton. In oriented cells, stress fibers become prominent and align with the flow axis (Figure 3.4.1). Changes in the other major cytoskeletal fibrous components are less impressive. Microtubules maintain their previous organization, consisting of a perinuclear arrangement and convergence of fibers at the microtubule organizing center (MTOC) near the nucleus (Figure 3.4.2). Intermediate filaments (vimentin) are also arranged

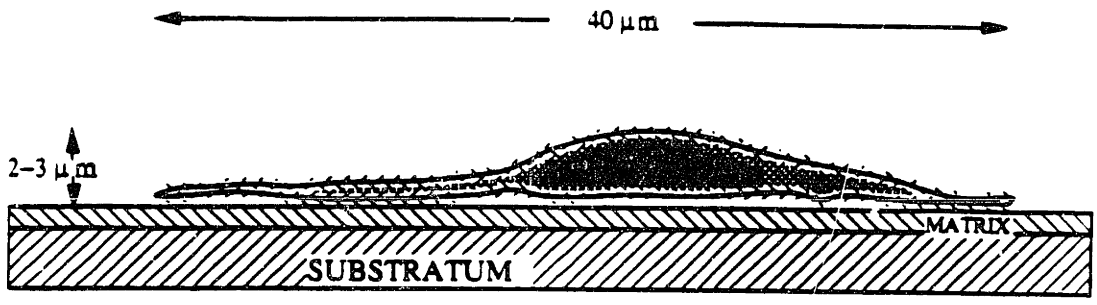

Figure 3.3.1: Schematic of endothelial cell. Cells have a "fried egg" appearance, where the bulge in the cell is above the nucleus.

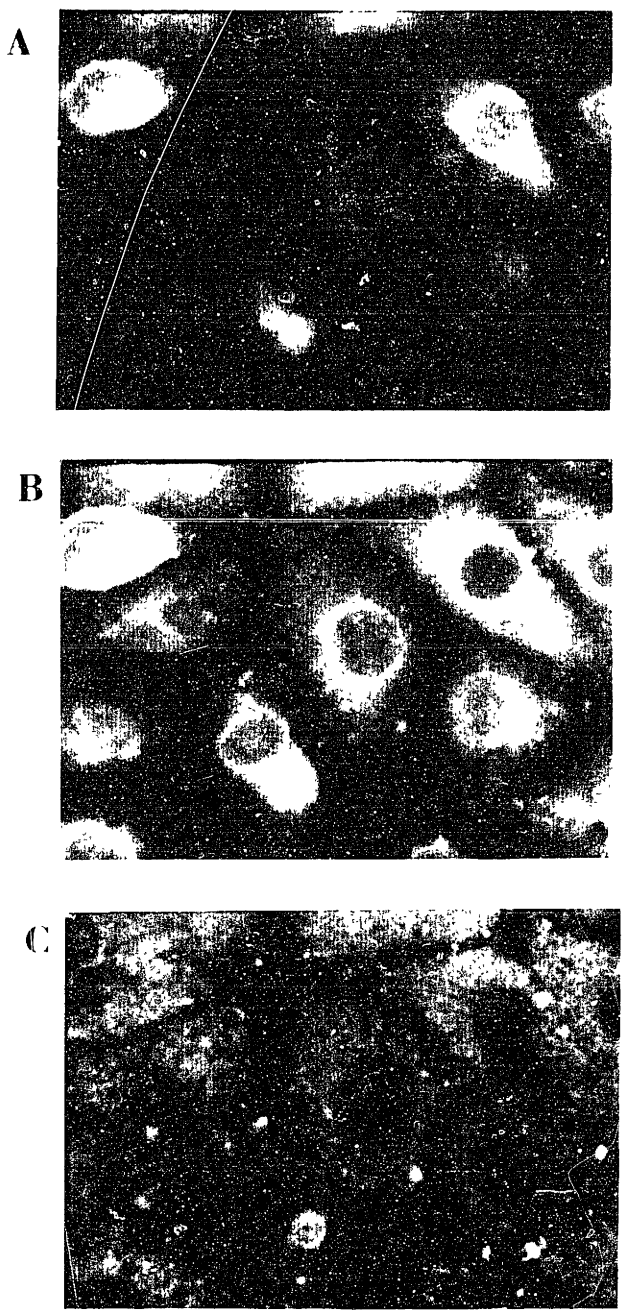

Figure 3.3.2: Series of confocal images of cell membrane from a non-oriented monolayer of BAEC. The panels proceed from (a) to (c) basal for the same field of cells, in 0.9 μm steps.

a.

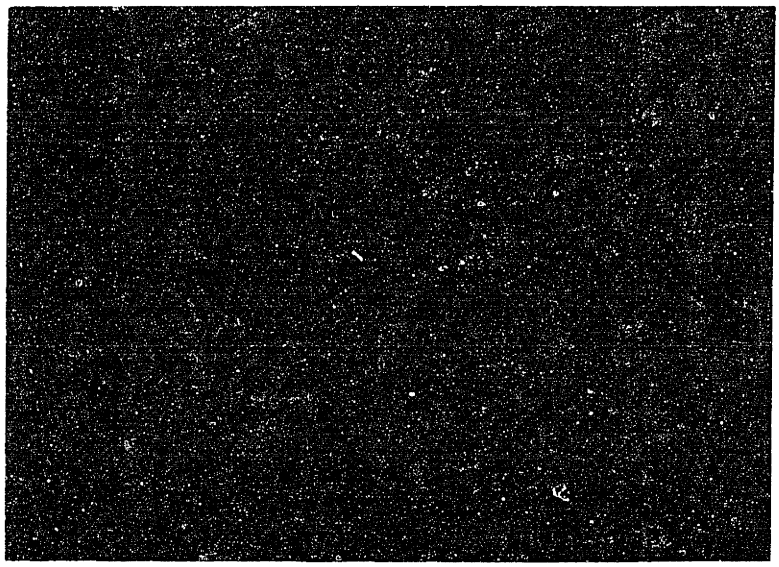

b.

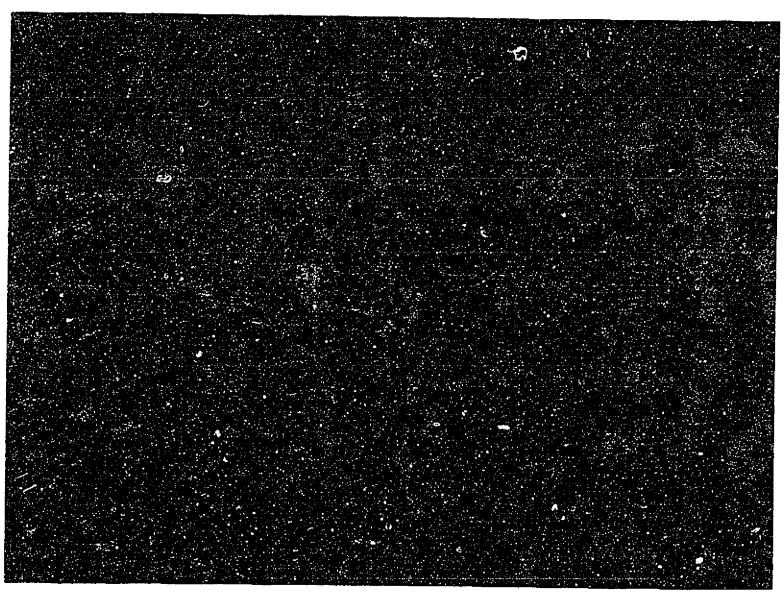

Figure 3.4.1: F-actin in nonoriented endothelial cells (a); and oriented cells (b). In oriented cells, stress fibers are prominent and centrally located. Magnification 32X.

a.

b.

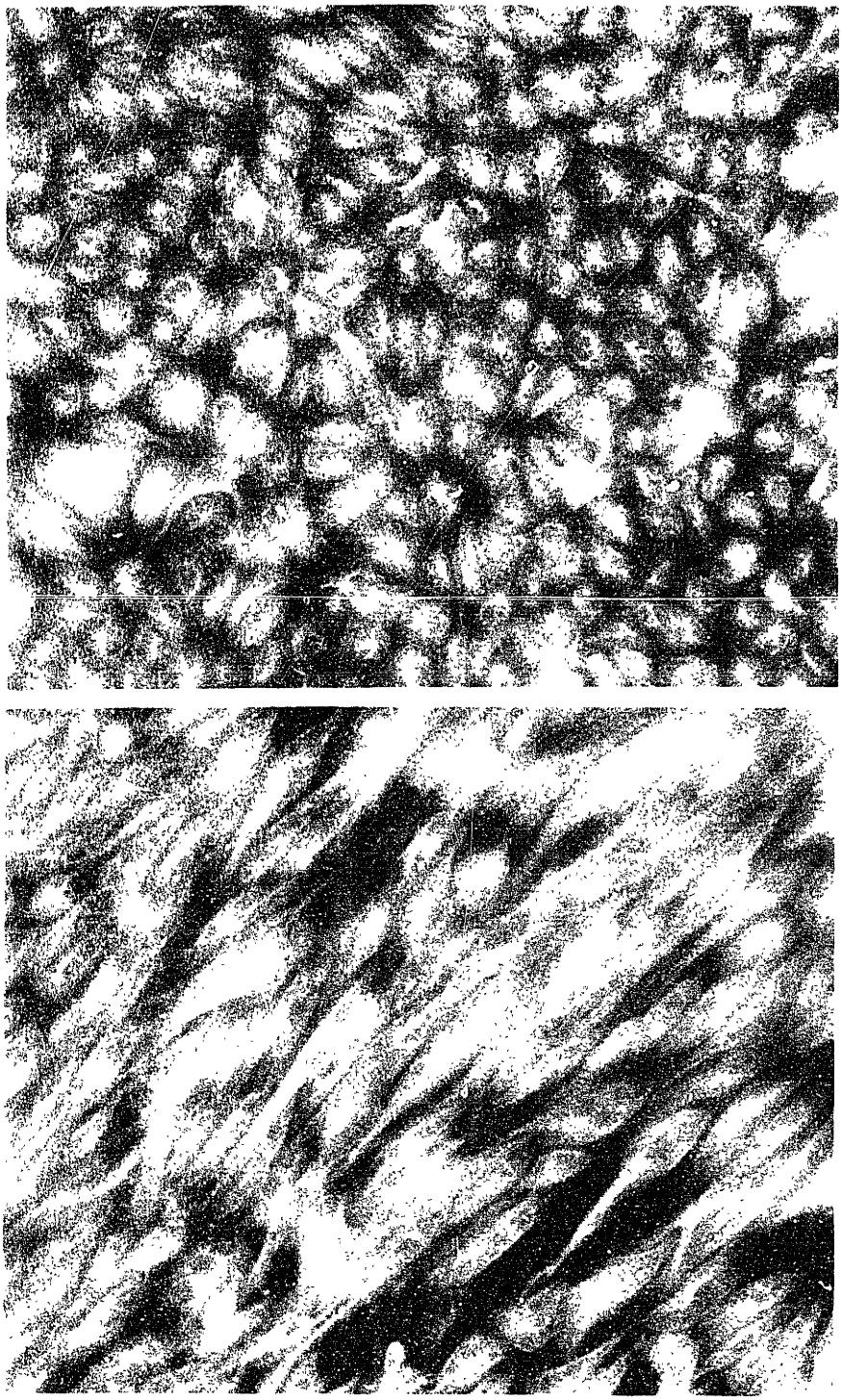

Figure 3.4.2: Microtubules in nonoriented endothelial cells (a); and oriented cells (b). Magnification 62.5X.

around the nucleus, with no significant change when cells orient (data not shown). These findings are consistent with others [Gotlieb et. al., 1991], and imply that actin is important for adjustments to shear stress.

Actin filaments are present with distinct patterns in both non-oriented and oriented cells. In non-oriented cells, stress fibers are located in the basal aspect (see Figure 3.5) around and beneath the nucleus (Figure 3.6). Stress fibers are also prominent just inside the cell periphery. A hazy pattern is also present, which is most clearly observed in the apical plane over the nuclei of several cells. This is probably actin fibers within the cortical network, whose precise organization cannot be resolved with confocal imaging. Stress fibers within a particular cell region are arranged in a predominant direction, giving an apparent orientation. However, the direction of orientation varies from region to region, so that at a lower power of magnification, the overall stress fiber pattern appears random (Figure 3.4.1).

In oriented cells, the actin filament arrangement is markedly altered (Figure 3.7). Stress fibers are now visible in top as well as bottom regions. Because the cell periphery can be extremely thin (<0.5 μm), basal stress fibers are detected in the apical image (and vice versa for apical fibers). Therefore, it is difficult to determine the spatial arrangement of a fiber when it spans both regions (as a fiber would appear if it passed from the top to the bottom of a cell). Prominent fibers in the top are most easily observed when the fiber passes above the nucleus (see Figure 3.7). In a previous paper [Satcher et. al., 1992], we proposed that there are points of attachment of these stress fibers to the

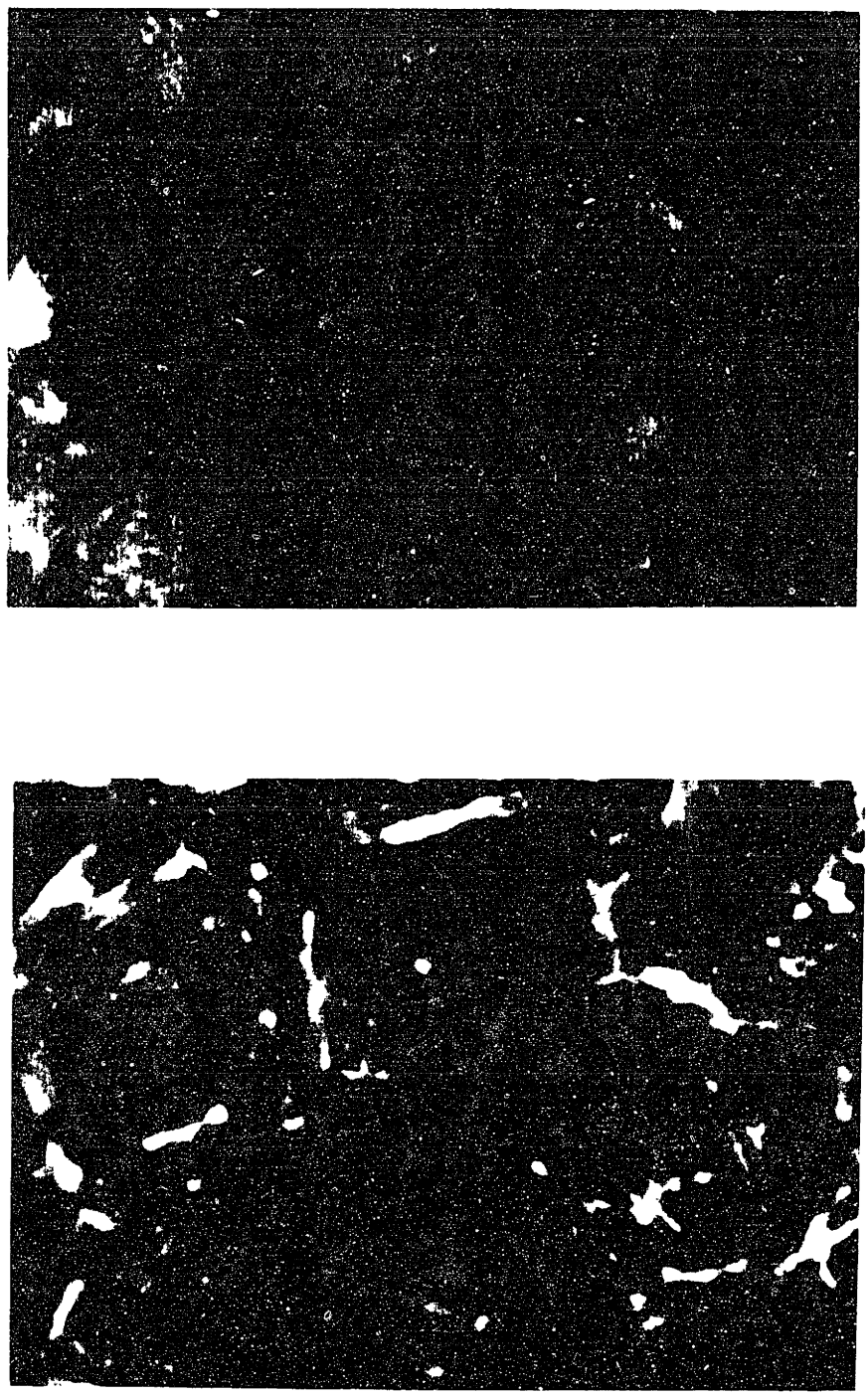

Figure 3.5: Micrograph image of typical F-actin distribution in non-oriented monolayer of BAEC. (a) The apical plane is 1.8 μm above (b) the basal plane. Stress fibers are found in central and peripheral regions in the basal plane.

- nucleus F-actin

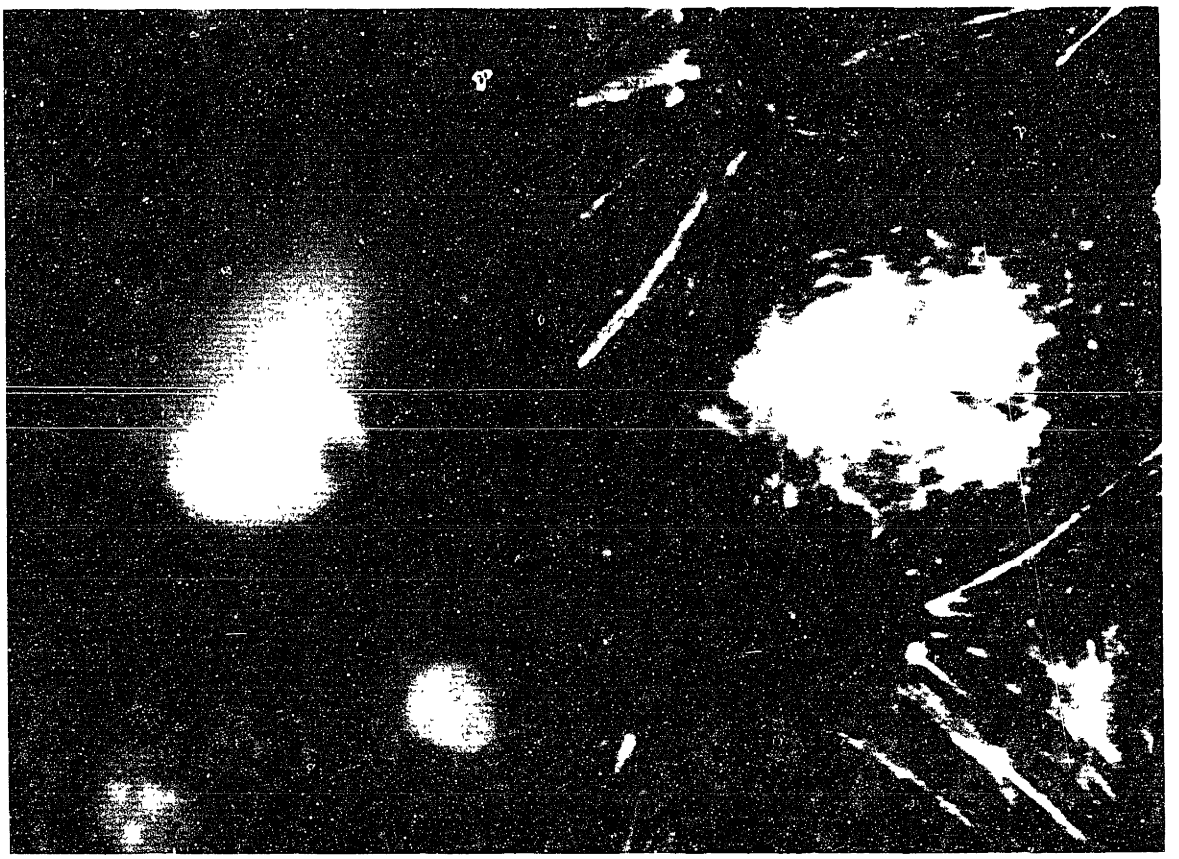

Figure 3.6: Double labelling for nucleus (left) and F-actin (right) in basal plane of non-oriented cells. Stress fibers are visible under the nuclei.

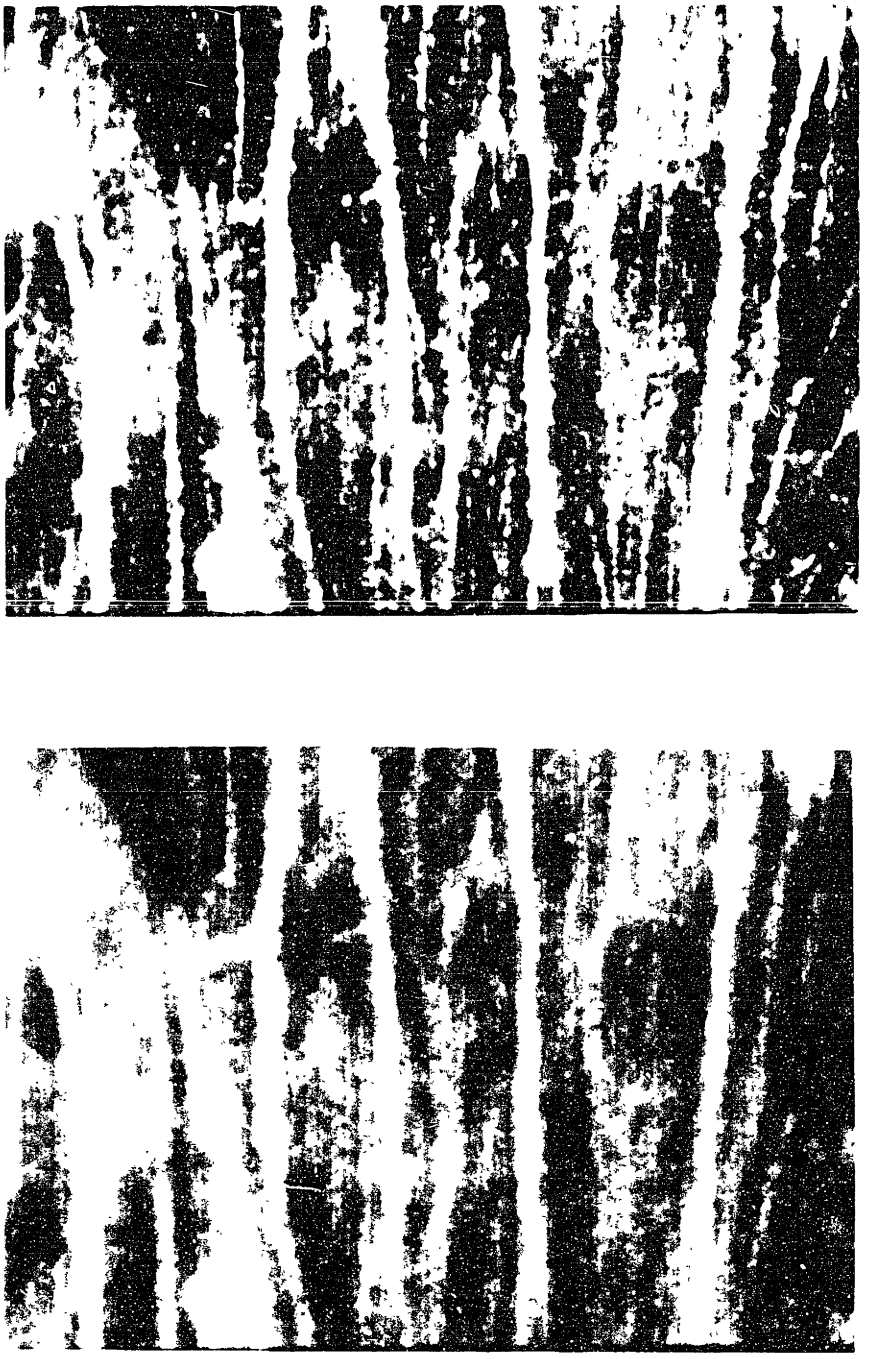

Figure 3.7: Typical F-actin distribution in oriented cells. (a) The apical plane is 0.9 μm above (b) the basal plane. Long aligned stress fibers are visible in both apical and basal planes; while little peripheral F-actin is present.

nucleus F-actin

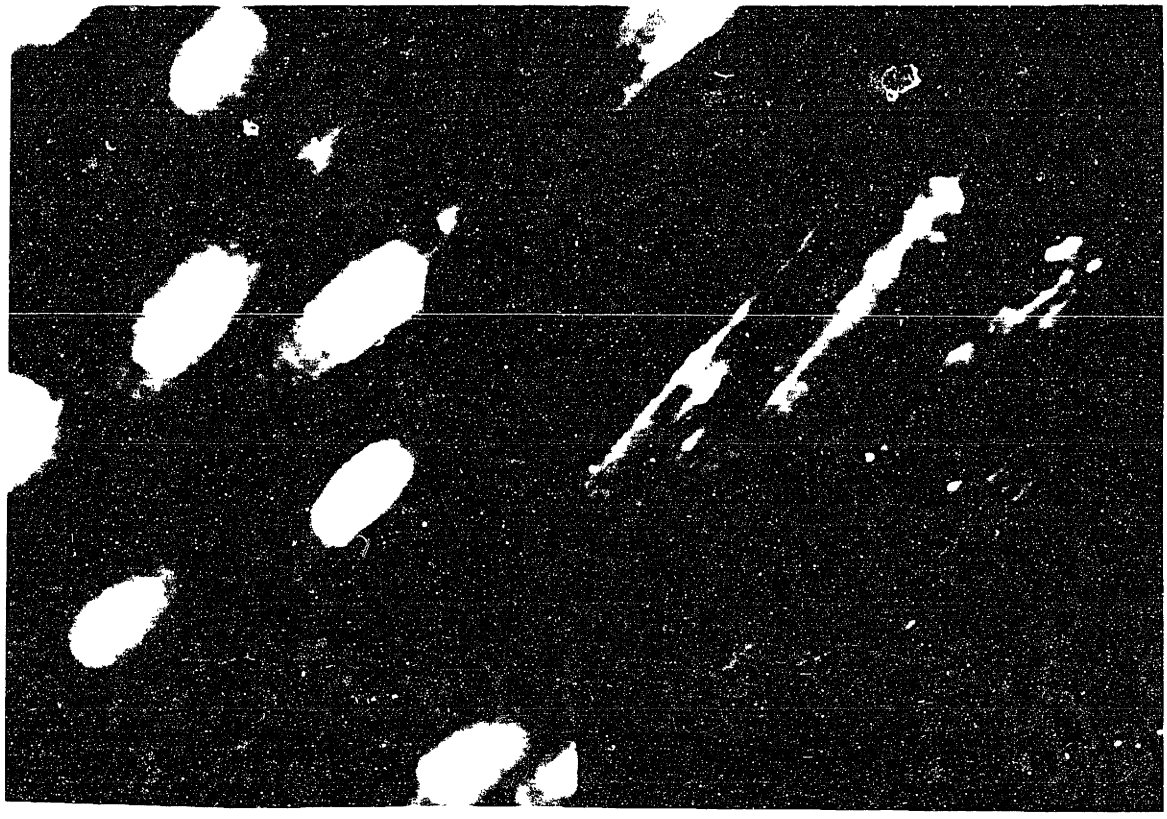

Figure 3.8: Double labelling for nucleus (left) and F-actin (right) in basal plane of oriented cells. Stress fibers are aligned and appear under the nuclei.

apical plasma membrane similar to focal contacts in the basal membrane. By looking for actin accessory proteins used to connect stress fibers to focal contacts (which occur along the adherent surface), we hoped to observe points of stress fiber attachment on the apical membrane (see below).

Stress fibers in oriented cells are not found in circumferential regions. They are predominantly central, passing over and/or under the nucleus (Figures 3.4.2 and 3.8). Those fibers which extend the length of the cell sometimes appear to intersect stress fibers in adjacent cells.

The distributions of vinculin, α-actinin, and the probable intercellular adhesion molecule, endoCAM, were examined by indirect immunofluorescence. Vinculin is incorporated in a protein complex which interconnects stress fibers with the cytoplasmic side of the membrane known as focal contacts or adhesion plaques. These are specialized regions used by the cell to adhere to the substrate (Figure 3.9) [Geiger, 1987; Luna et. al., 1992]. One prediction was that if stress fibers have apical attachments, vinculin could be part of the attachment complex. Vinculin is also present in areas of intercellular contact, presumably as part of the adhesion (or adherens-type) complexes between cells [Geiger, 1987].

In non-oriented cells, immunofluorescence for vinculin localizes to the basal plane of cells (Figure 3.10.1). The 0.1-0.5 μm dots are focal contacts,

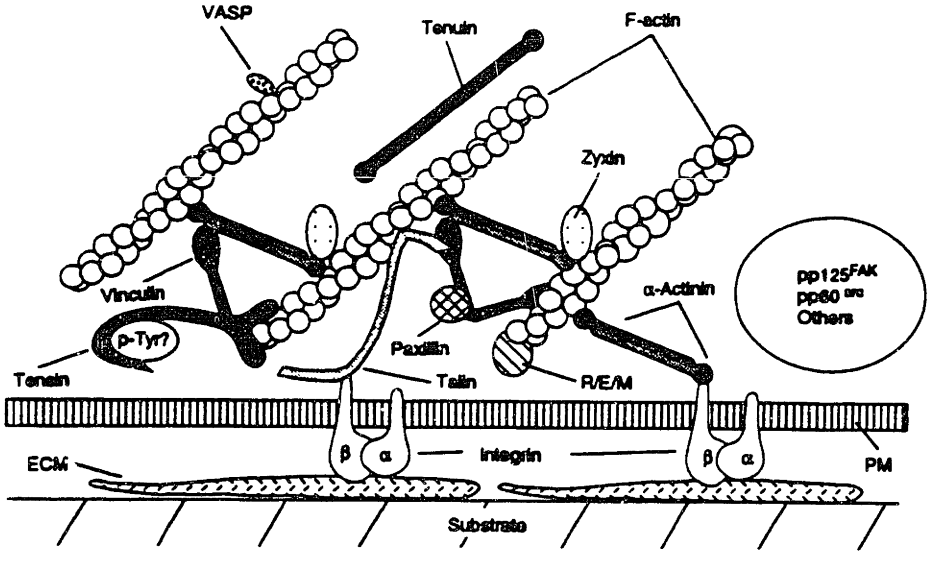

Figure 3.9: Schematic of focal contact [adapted from Luna et. al., 1992]; abbreviations are: ECM-extracellular matrix; PM-plasma membrane; p-Tyr?-unknown phosphotyrosine-containing protein; R/E/M-member of the radixin/ezrin/moesin family; VASP-vasodilator stimulated phospho-protein.

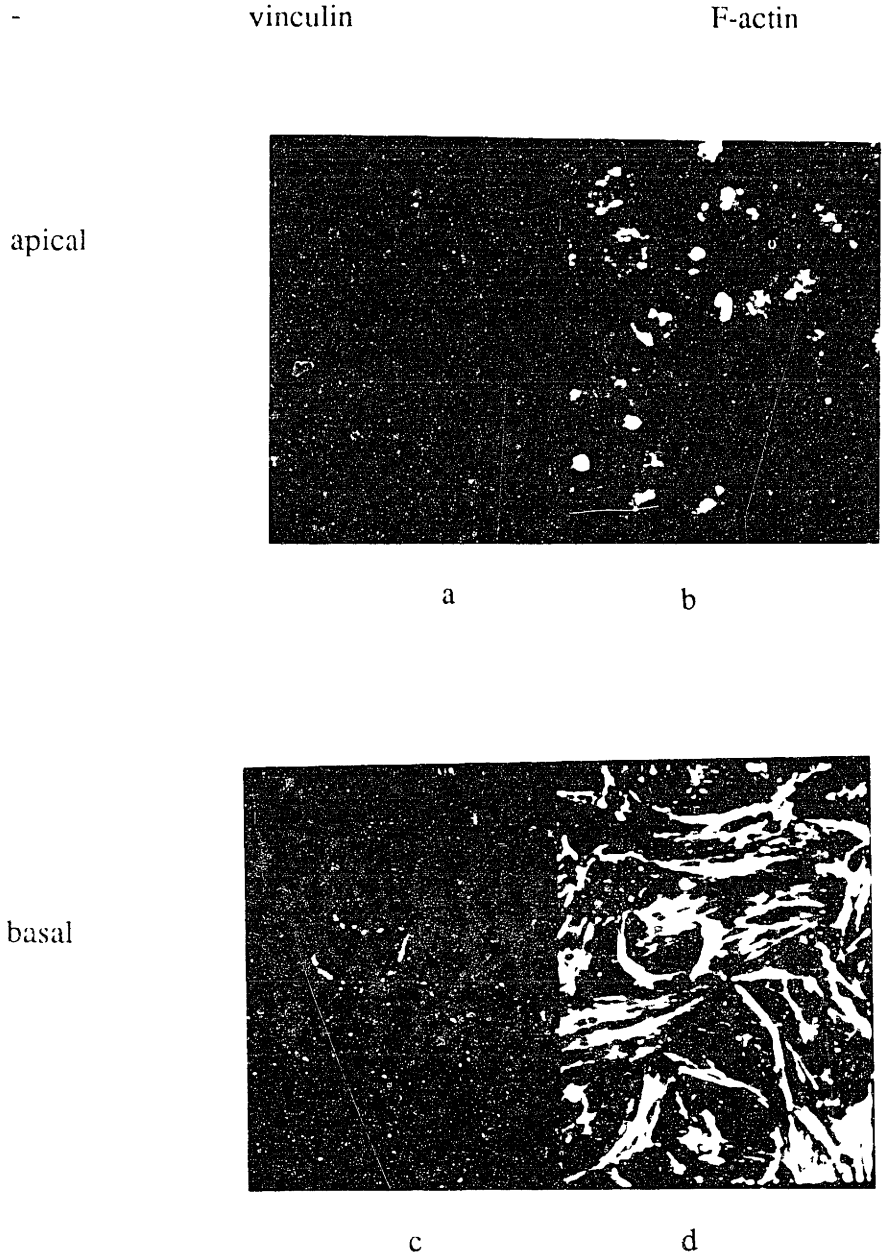

Figure 3.10.1: Double labelling for vinculin (a,c) and F-actin (b,d) in non-oriented cells. (a) & (b) are identical fields in an apical plane. (c) & (d) correspond to (a) & (b) in a basal plane 1.8 μm below. In (c), vinculin labelling is at focal contacts at ends of stress fibers. In apical plane, vinculin staining is diffuse (a).

vinculin F-actin

apical

a b

basal

c d

Figure 3.10.2: Double labelling for vinculin (a,c) and F-actin (b,d) in oriented cells. (a) & (b) are identical fields in an apical plane. (c) & (d) correspond to (a) & (b) in a basal plane 0.9 μm below. In (c) vinculin labelling is at focal contacts at ends of stress fibers. In apical plane (a), staining for vinculin is diffuse.

occurring at the ends of stress fibers. Vinculin is also visible along the cell borders. Diffuse staining in the apical plane could be vinculin which is present in organelles such as the golgi, endoplasmic reticulum, etc.; or that associated with the apical membrane.

Cells oriented for 36 hours have a similar pattern of vinculin staining (Figure 3.10.2). Most is imaged in the basal aspect of the cell, incorporated in focal contacts visible at the ends of prominent, aligned stress fibers. Staining in the apical aspect is diffuse and there is no clear evidence for the involvement of vinculin in attachment of stress fibers. In contrast to non-oriented cells, vinculin staining is absent from regions of intercellular adhesion (no clear borders).

We next located α-actinin, because it is an actin binding protein which crosslinks F-actin in stress fibers and serves as part of the attachment complex linking actin bundles to focal contacts and adhesive intercellular junctions [Baron et. al., 1987; Blanchard et. al., 1989; McKenna et. al., 1986]. Specimens were double labelled for F-actin for comparison. Non-oriented cells stain with distinct patterns which differ from those of oriented cells (Figures 3.11 & 3.12). α-actinin is visible in both the apical and basal regions of the cell (Figure 3.11a & 3.11c). Staining in the basal plane is along stress fibers in the central region and is present peripherally at regions of cell-cell contact.

α-actinin F-actin

apical

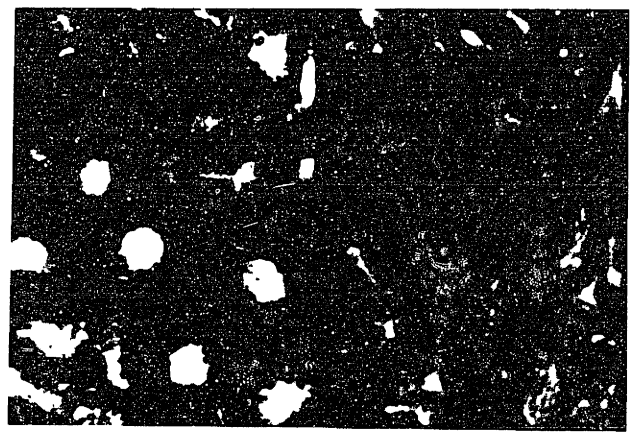

a b

basal

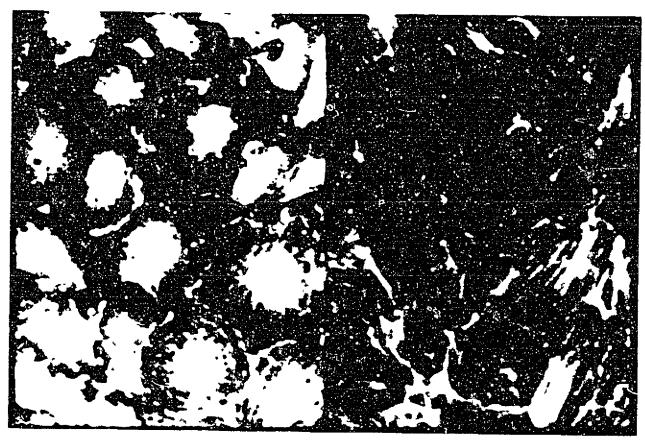

c d

Figure 3.11: Double labelling for α-actinin (a,c) and F-actin (b,d) in non-oriented cells. (a) & (b) are identical fields in an apical plane. (c) & (d) correspond to (a) & (b) in a basal plane 1.8 μm below. In (c) α-actinin is located along stress fibers and cell-cell borders. In apical plane, α-actinin stains diffusely in perinuclear region (a).

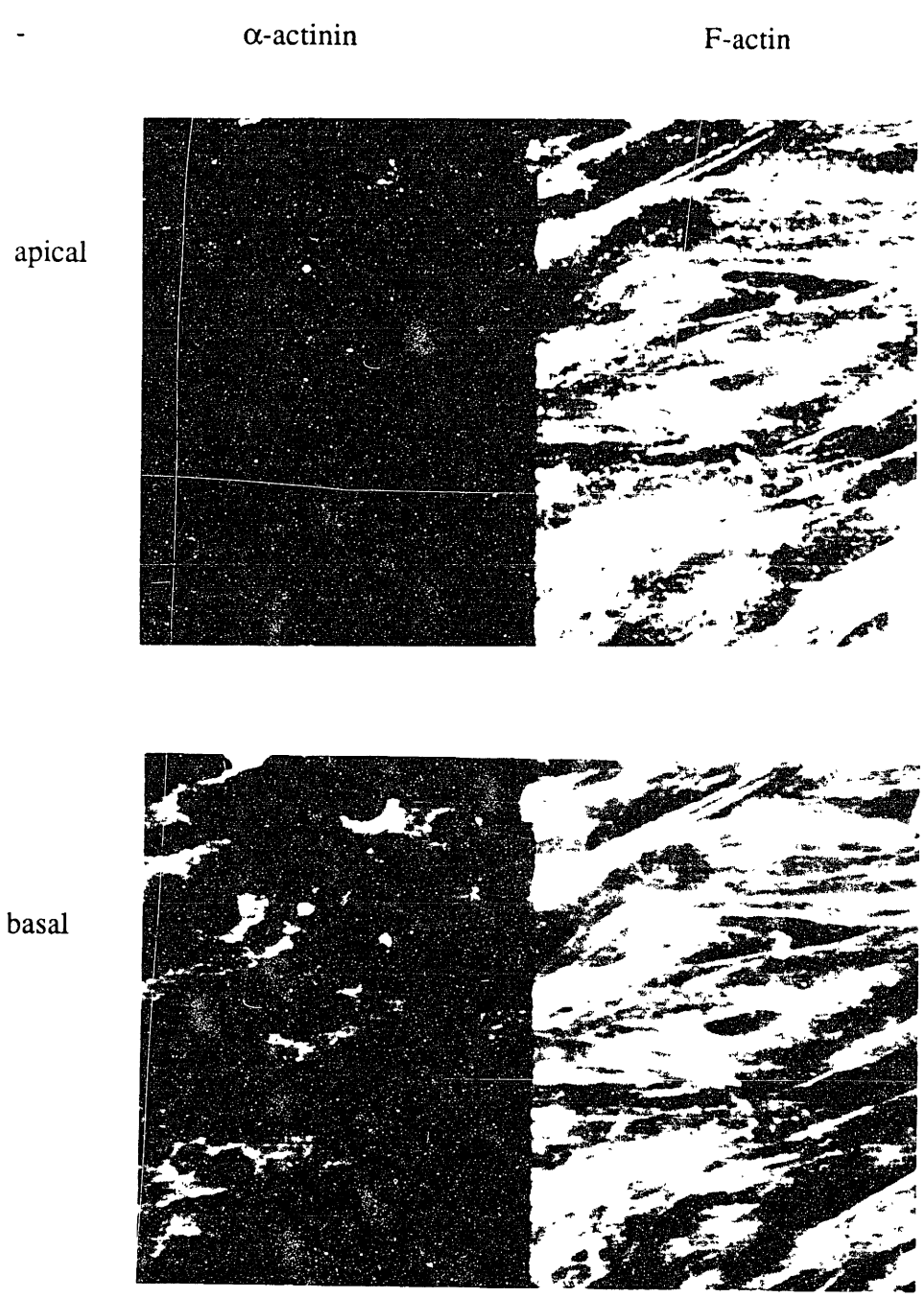

Figure 3.12: Double labelling for α-actinin (a,c) and F-actin (b,d) in oriented cells. (a) & (b) are identical fields in an apical plane. (c) & (d) correspond to (a) & (b) in a basal plane 0.9 μm below. In (c) there is diffuse staining for α-actinin in cortical cytoplasm surrounding nucleus. In apical plane, α-actinin stains in punctate pattern (a).

In oriented cells, punctate α-actinin staining decorates membrane apical regions (Figure 3.12a). Such staining foci are indicative of attachment points for stress fibers on the top membrane. There is no staining above the nucleus--a pattern opposite of that observed in non-oriented cells (Figure 3.11). In the basal regions, the staining is more diffuse.

In order to determine if cell-cell attachments are altered in response to shear stress, we immunolabelled cells for endoCAM, a trans-membrane protein thought to be used by endothelial cells to form intercellular adhesions [Albelda et. al., 1990 & 1991]. In non-oriented cells, staining for endoCAM localizes to the baso-lateral and peri-nuclear regions (Figure 3.13). Cells co-labelled for F-actin were permeabilized with detergent. Cell borders appear in the same planes as actin stress fibers and the dense peripheral band. Punctate staining labels the perinuclear region in both the apical and basal aspects of the cells. This may be due to endoCAM present in organelles.

Cell-cell borders are affected when the cells experience laminar shear stress for 36 hours (Figure 3.14); or turbulent shear stress for 16 hours (Figure 3.15). With cells aligned by exposure to laminar flow, staining in the basal plane is absent from regions of cell-cell contact, with sparse staining in the perinuclear region and cortical cytoplasm. Staining in the apical region is nearly absent.

endoCAM F-actin

apical

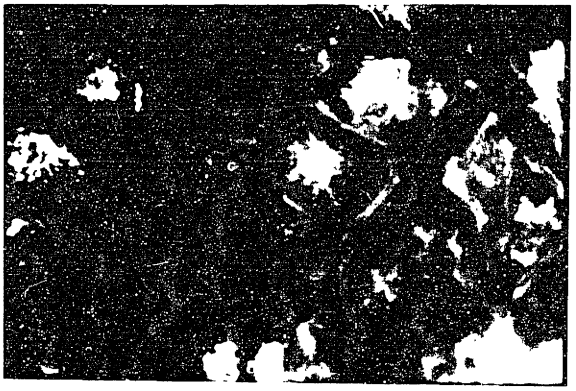

a b

basal

c d

Figure 3.13: Double labelling for endoCAM (a,c) and F-actin (b,d) in non-oriented cells. (a) & (b) are identical fields in an apical plane. (c) & (d) correspond to (a) &(b) in a basal plane 1.8 μm below. endoCAM stains cell-cell borders in basal plane (c).

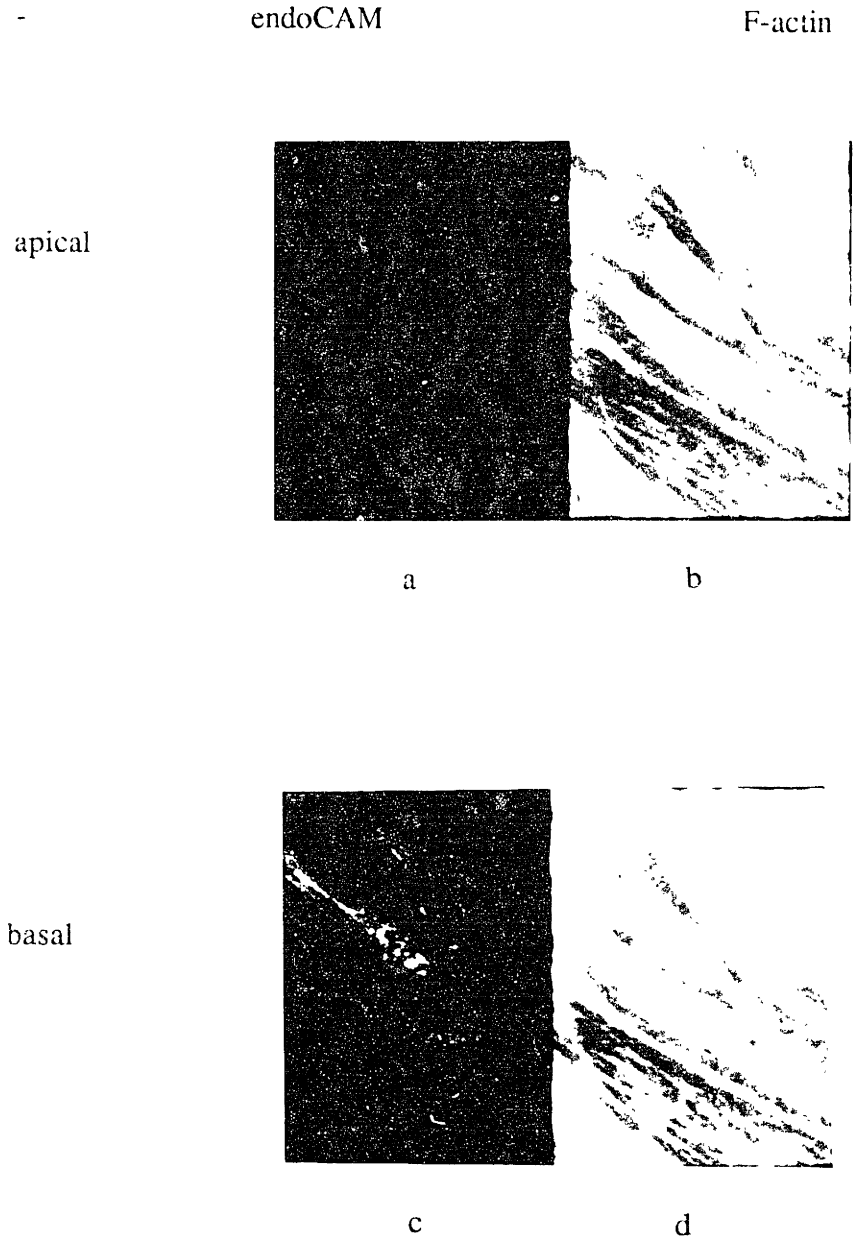

Figure 3.14: Double labelling for endoCAM (a,c) and F-actin (b,d) in oriented cells. (a) & (b) are identical fields in an apical plane. (c) and (d) correspond to (a) & (b) in a basal plane 0.9 µm below. endoCAM is diffuse in basal regions (c); and absent from cell-cell borders.

a

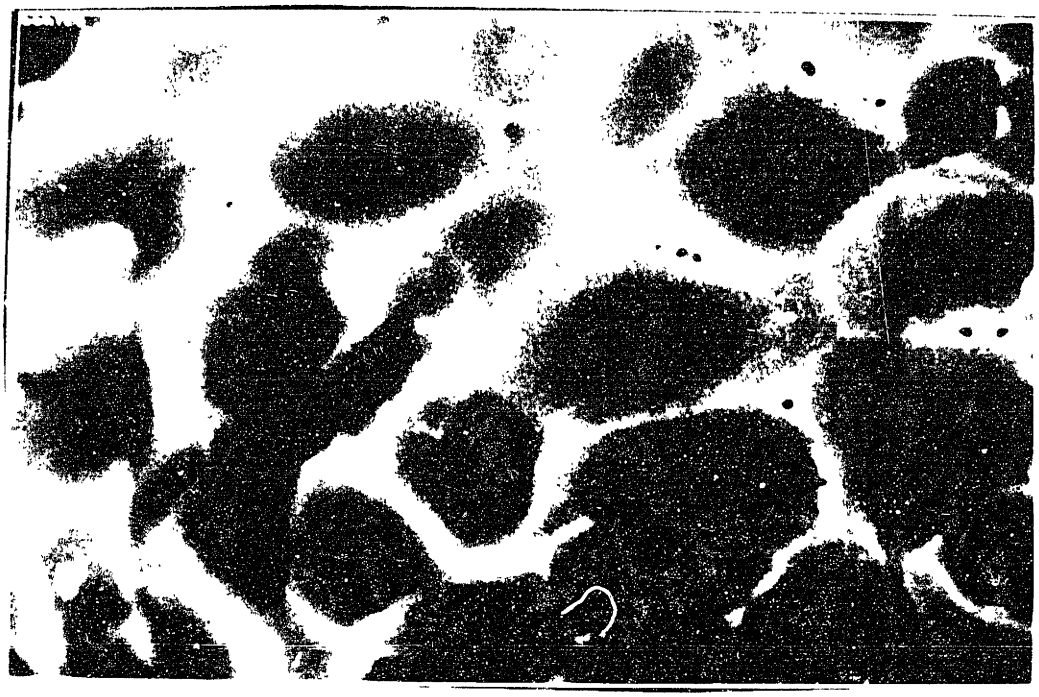

b

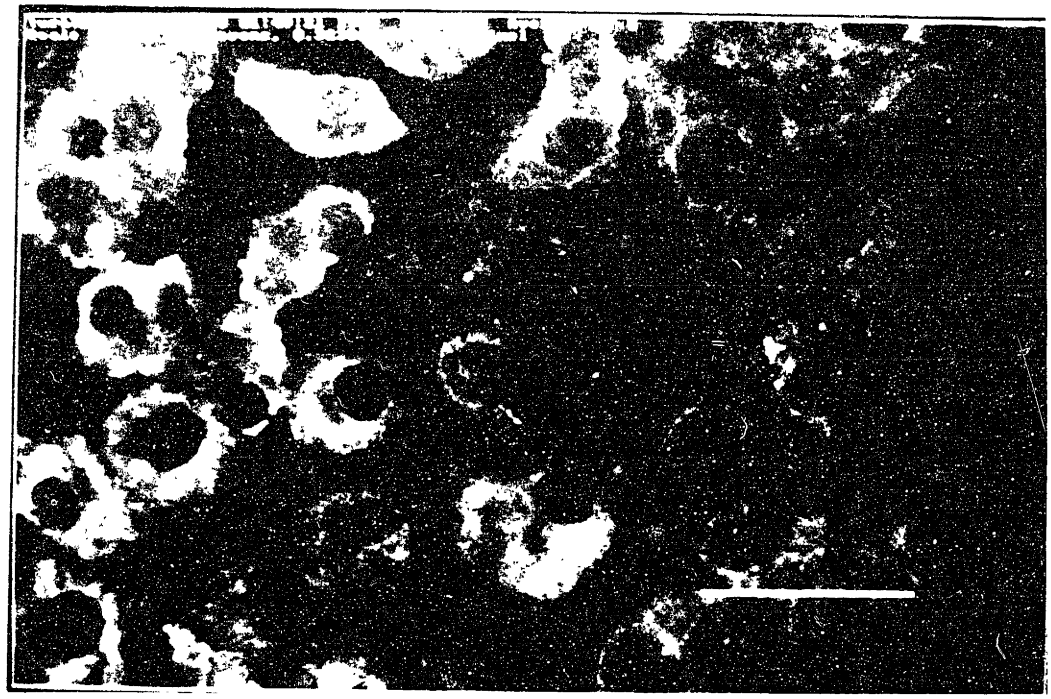

Figure 3.15: Labelling for endoCAM in (a) cells exposed to turbulent flow, and (b) no-flow controls. endoCAM no longer stains borders of cells exposed to turbulence.

Turbulent shear stress at low levels (2-3 dynes/cm^2) for 16 hours causes the cells to retract and divide (Figure 3.15). EndoCAM no longer stains the borders of cells, even if they are in contact with other cells. These cells were not detergent permeabilized, thus there is no intracellular staining as in Figures 3.13 and 3.14. The cell cortical membrane (away from the nucleus) is stained, indicating that the molecule has been redistributed away from cell borders.

4. DISCUSSION

The most prominent change observed by immunofluorescence in the cytoskeletons of endothelial monolayers exposed to laminar shear stress is a reorganization of F-actin. Short, centrally located stress fibers are disassembled or rearranged, so that they become aligned with the main cell axis. Others have also observed this [Dewey et. al., 1981; Franke et. al., 1984; Schnittler et. al., 1989; Langille et. al., 1991; Gotlieb et. al., 1991]; however, in most cases it was assumed that the new stress fibers were located along the adherent surface (as with nonoriented cells). Stress fibers pass both over and under the nucleus. In unpublished work, Gimbrone noted that some stress fibers came into focus over the nucleus using epifluorescence. With confocal microscopy, stress fibers are apparent above the nucleus. In addition, a mesh-like network (the cortical actin network) is visible as diffuse staining in the tops of cells.

Stress fibers are thought to protect the integrity of the endothelial lining when exposed to high levels of shear stress [Dewey, 1988; Schnittler et. al., 1989; Kim et. al., 1989; Langille et. al., 1991; Wechezak et. al., 1989]. Stress fibers in aligned cells may attach to the top membrane, thereby stabilizing the monolayer by transmitting stress to the substrate (as opposed to regions of cell-cell attachment).

Stress fibers insert into cell membranes via complexes called focal contacts. We looked for evidence of such complexes by labelling α-actinin and vinculin. The resulting morphological evidence is inconclusive. α-actinin acts as a F-actin crosslinker [Baron et. al., 1987; Blanchard et. al., 1989; McKenna et. al., 1986].

In nonoriented cells, staining patterns correspond to the arrangement of stress fibers along the cell bottoms. In oriented cells, α-actinin stains the apical membrane with a punctate pattern and a diffuse pattern in basal planes of the cell cortex (Figure 3.12). The spotty apical patterns are suggestive of attachment sites. However, it is unclear whether the ends of apical stress fibers colocalize with these spots. The vertical locations (top vs. bottom) of stress fibers could not be pinpointed in most images, because cortical regions are very thin (<0.5 μm). In addition, much of an endothelial cell's F-actin is contained in the cortical network [Gotlieb et. al., 1991]. Thus, stress fibers are surrounded by diffuse staining which hinders spatial localization without a geographical marker (like the nucleus).

Changes in the cortical actin network have not been previously examined [Schnittler et. al., 1989; Gotlieb et. al., 1991; DePaola et. al., 1992; Wechezak et. al. 1989]. Confocal sectioning enables detection of the cortical actin network and its regulatory proteins, without enough resolution for details. α-actinin is apparently redistributed from F-actin structures in the basal plane of nonoriented monolayers to the cortical network in aligned cells. Increased cross-linking could reinforce the cell cortex against disruptive stresses, essentially making it "stiffer". Rearrangements of this network could, therefore, be as important to the cell for structural integrity as the construction of stress fibers, so there is a need for studies using higher resolution techniques.

Changes in vinculin distribution are less remarkable. Vinculin remains associated with focal adhesions in the basal plane when cells orient. Davies et.

al., 1992, have followed the movement of individual focal adhesions in cells subjected to fluid flow. Cells constantly "pull up" and "place down" focal adhesions when growing in culture. Oriented cells tend to maintain a higher concentration of these adhesions in upstream regions. Our observations confirm the presence of focal adhesions at the ends of stress fibers located along the adherent surface. Apical staining for vinculin is diffuse in oriented cells; thus if stress fibers attach, vinculin is probably not part of the intersection. However, if the low intensity patterns are real, several possiblities exist: 1. there is apical vinculin, but it is solubilized when cells are detergent permeabilized, reducing the quantities which can be visualized with immunofluoresence; or, 2. the concentration and arrangement of apical vinculin complexes could be such that their detection is beyond the resolution of confocal microscopy.

endoCAM is a 130 kD integral membrane protein isolated from bovine aortic endothelial cells [Albelda et. al., 1990]. A similar protein (CD31, PECAM-1) has been found in human umbilical vein endothelial cells. The molecule is associated with regions of cell-cell adhesion, appearing after endothelial monolayers become confluent. Albelda et al., 1991, postulate that a homotypic bond between endoCAM molecules in adjacent cells is the structural building block for adherens type junctions between cells in the monolayer. Presence of the molecule is certainly an indication of confluence, and thus stability of the monolayer.

In cells oriented in laminar flow endoCAM staining is reduced at the cell-cell junctions. (Figures 3.13 & 3.14). At 36 hours, the cells probably have not

reestablished stable cell-cell adhesions, so that the molecule cannot be detected. Perhaps at later times adhesions that stain for endoCAM will reappear. With turbulent shear stress, endoCAM staining is similarly altered. Dewey has proposed that disruption of cell-cell attachment regions is an early consequence of exposure to turbulence. At 16 hours, some cells have rounded up and are dividing (Figure 3.15). There is no staining at cell borders, although diffuse staining is present on the cortical membrane. This indicates that molecule is present in the cell membreane, even as the cells round up to divide. Contrary to expectations, cells which are still in contact with neighboring cells also do not stain at borders. Thus, the entire monolayer is affected in such a way that cell-cell attachment regions are disrupted. These changes in endoCAM staining are consistent with the hypothesis that destabilization of cell-cell contacts is part of the events which initiate the cascade of endothelial adjustments to shear stress. Langille et. al., 1991, indicate that one of the earliest observable events is the appearance of two distinct bands of F-actin in two adjacent cells, where there had previously been a large, apparently contiguous band at the border. This could represent rearrangement of actin triggered by destabilization of cell-cell junctions as they orient.

Stress fibers occassionally appear to intersect with circumferential fibers. If cells orient, the result is an apparent continuity of stress fibers between adjacent cells. Gotlieb et. al., 1991, proposed that stress fibers in aligned cells form a contiguous intercellular network. However, it remains possible that fiber systems are organized separately (within individual cells). Higher resolution techniques are required to determine monolayer stress fiber organization with accuracy.

The following is a hypothesis for the mechanism of endothelial alignment:

1. Exposure to laminar shear stress destabilizes cell-cell adhesions. Mathematical modelling of the monolayer surface predicts forces of sufficient magnitude to disrupt cell-cell attachements, but insufficient for detaching cells from the substrate (see Chapter 2). In the non-oriented (or cobblestone) configuration, much of the force on the apical membrane is transmitted to cell-cell attachment regions, increasing the likelihood that they will be disrupted.

2. This stimulates the cells to alter their cytoskeleton. Prior to orienting, F-actin is located in cortical network, and stress fibers in circumferential and central regions along the bottoms of cells. In response to flow, long, axially oriented stress fibers grow from apical nucleation sites, or are stabilized by sites in the bottoms of cells. Actin and associated proteins are also incorporated into the cortical actin network, which may be rearranged (by increased crosslinking for example) so that it makes the cell "stiffer".

3. Cells probably take longer than 36 hours to reestablish stable intercellular junctions with laminar shear stress. But once they are made in aligned cells, cell-cell contacts can be maintained in the presence of continued laminar shear stress.

Others have made observations which are consistent with this hypothesis. Sato et. al., 1986, found that endothelial cells conditioned by shear exhibit decreased deformability. Microfilament disrupting agents increase deformability.

Wechezak et. al., 1989, showed that adhesion of endothelial cells with flow is impaired if cells are treated with the actin-disrupting agent cytochalasin B.

Endothelial cells are apparently unable to adjust to shear stresses associated with turbulent flows and disturbed laminar flows [Davies et. al., 1986; DePaola et. al., 1992]. The forces disrupting cell-cell attachments in these flows are either too unsteady (turbulent) or of a magnitude (due to large spatial shear stress gradients) which may exceed the cells' abilities to compensate via actin rearrangments. Thus, cell-cell attachments are disrupted, stimulating the cells to divide and/or migrate from the affected region.

In summary, confocal microscopy improves spatial resolution of cell morphology by focussing on individual planes within the sample (essentially excluding signal from planes above and below). We were able to accurately resolve patterns of the structural proteins α-actinin, vinculin, endoCAM, and actin, which would not have been possible using convential fluorescence. However, the transverse optical resolution remains limited by the wavelengths of visible light (i.e. 0.2 μm). Fine details of the cortical actin network and apical interactions of stress fibers were beyond the resolution of the confocal microscope.

Chapter Four

THE MORPHOLOGY OF THE CYTOSKELETON IN NONORIENTED AND ORIENTED ENDOTHELIAL CELLS

1. INTRODUCTION

Atherosclerosis is a focal disease. Plaques form in specific regions of large and medium sized arteries, while other regions are without pathological changes [Montenegro et. al., 1968; Schwartz et. al., 1972]. This suggests a role for hemodynamics in the pathogenesis of the disease. *In vitro* and *in vivo* studies have demonstrated that hemodynamics affect the form and function of endothelial cells [Dewey et. al., 1981; Gimbrone, 1986; Nerem et. al., 1990]. The shape and orientation are primarily determined by local blood flow patterns [Flaherty et. al., 1972; Silkworth et. al., 1975; Levesque et. al., 1986; Nerem et. al., 1981]. Cellular functions altered in response to flow related shear stress include cytoskeletal organization [White et. al., 1983], Ca^{++} currents [Shen et. al., 1992], and PDGF gene regulation [Resnick et. al., 1992]. In addition, shear stress can indirectly affect vasomotor tone via endothelial release of EDRF, prostaglandins, and possibly endothelin [Furchgott et. al., 1980; Koller et. al., 1990; Yoshizumi, et. al., 1989; McIntire et. al., 1990]. Chronically, the arterial wall *in vivo* can be remodelled in response to shear stress [Friedman et. al., 1986; Langille et. al., 1986; Langille et. al., 1989; Zarins et. al., 1987].

The cytoskeleton of endothelial cells consists of three major types of cytoplasmic polymers: microfilaments, microtubules, and intermediate filaments; supported by a large cast of associated proteins. These filament systems maintain

cell shape and produce the rapid and chronic shape changes observed in response to shear stress [Dewey et. al. 1981]. Cytoskeletal rearrangments can be mediated by altering polymer concentration, and/or changing ultrastructure by polymer crosslinking. The actin-based cytoskeleton produces locomotion, such as directional migration in wound healing [Ettenson et. al., 1992; Kreis et. al., 1980].

Studies of endothelial cell cytoskeleton have focussed on the easily observable bundles of actin filaments, or stress fibers [White et. al., 1983; Wong et. al., 1983; Gotlieb et. al., 1991]. Little is known about intermediate filaments; however, microtubules have been studied with increased interest in recent years. They appear to be used by the cell to orient itself internally and relative to external stimuli [Gotlieb et. al., 1981, 1983; Kupfer et. al., 1983]. Endothelial cells are one of a handful of cells which exhibit stress fibers *in vivo* [Wong et. al., 1983]. Stress fibers are bundles of F-actin, containing myosin, and other associated proteins. In BAEC, they are thought to reinforce the cytoskeleton and cell against flow related shear stress [Lewis et. al., 1924; White et. al., 1983, 1986]. When cells are subjected to appropriate flow conditions *in vitro* and *in vivo*, the cell constructs centrally located stress fibers which are oriented with the cell axis and flow direction [White et. al., 1983 & 1986]. In contrast, nonoriented cells contain randomly or circumferentially arranged stress fibers along the adherent membrane.

Studies of endothelial cytoskeletal morphology have been limited to 2-D, using light, confocal, interference reflectance, and electron microscopy. The cytoskeletal architecture is determined from planar sections of the cell, thereby hampering the ability to resolve details of the 3-D arrangements of cytoskeletal

fibers. In this study, we have used detergent permeabilization followed by rapid freezing, freeze drying, and metal shadowing, to obtain high resolution images of the cytoskeleton of non-oriented and oriented bovine aortic endothelial cells. This method was first applied to cytoskeletons by Heuser et. al., 1980, and has been used by Hartwig et. al., 1991 to study platelets and macrophages. The method yields sharply defined 3-D views of the actin filament, intermediate filament, and microtubular networks. The actin filament network spatially fills cortical cytoplasm and connects basal and luminal cell membranes, indicating that actin cytoskeleton is a stress bearing structure that could be used by cells to transmit surface forces to basal attachments. F-actin comprises the bulk of the cortical cytoskeleton. Near the nucleus, intermediate filaments, and to a lesser extent, microtubules are present. Stress fibers are found both in the tops and bottoms of oriented cells. In particular, stress fibers pass over cell nuclei, whereas no stress fibers are observed over nuclei of nonriented cells.

2. MATERIALS AND METHODS

2.1 Preparation of Cells

2.1.1 Cell culture

Bovine aortic endothelial cells (BAEC) were used in all studies. The cells were maintained and passaged by methods previously described (Chapter 3). Briefly, monolayers of cells were grown in T-75 tissue cultured flasks in DMEM supplemented with 10% calf serum, 50 U penicillin/streptomycin (50:50), and 1% L-glutamine. Medium was replinished every 2-3 days. Cells were passaged by detaching the monolayer with trypsin-EDTA (5:2).

For alignment experiments and electron microscopy, monolayers were grown on 5 mm diameter glow discharged glass coverslips, which had been previously affixed to stainless steel rings with silicone medical adhesive (see below). All cells were between 10-30 subculture.

2.1.2 Shear stress

Stainless steel rings with affixed 5 mm glass coverslips were seeded with baec. Special rings were constructed which would accept 5-mm diameter round glass coverslips (Figure 4.0). Monolayers usually reached confluence after 3-5 days in culture and were indistinguishable from those grown on tissue culture plastic. At this time, the rings were placed inside a modified cone-and-plate apparatus used to expose cells to shear stress. This apparatus is described in

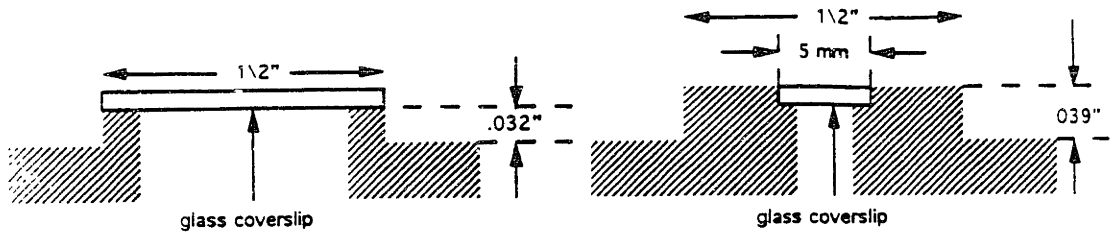

Normal ring with coverslip

Modified ring for EM studies

*Rings fit in standard exchangeable plate shown below

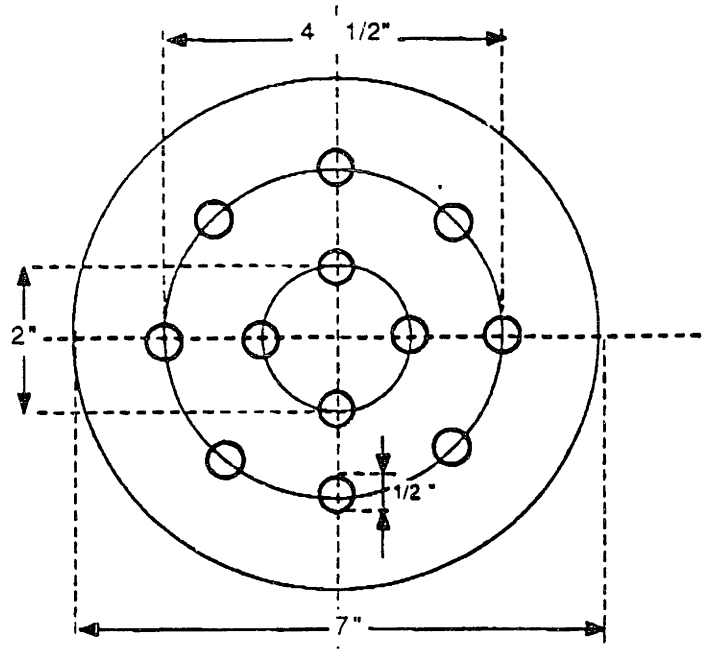

Figure 4.0: Modified ring design.

detail in the previous chapter (see Figure 3.0). For all experiments, the conditions used were: laminar flow, wall shear stress of 10 dynes/cm^2, and 32-36 hours of exposure. Fresh culture medium was provided at 0.5 ml/min. The chamber and plate were kept at 37^{o}C, while maintaining a 95% air/5% CO_2 atmosphere in the device chamber.

Following exposure to shear stress, cells were briefly examined by phase-contrast microscopy to confirm alignment before processing for electron microscopy. Efforts were made such that elapsed time from flow cessation to fixing the cells did not exceed 15 minutes.

2.2 Electron Microscopy

2.2.1 Rapid freezing and freeze-drying

The method for preparing replicas of surfaces and cytoskeletons for electron microscopy has been described in detail by Hartwig et. al., 1991. It can be used with cells that are very thin (<1 μm in thickness). A thin coating of metal is layered on the surface or cytoskeleton to create an electron dense replica. Transmission electron microscopy combined with a tilting specimen holder can then be used to obtain stereoscopic pairs of photographs.

To prepare cytoskeletons, endothelial monolayers were permeabilized for 2 minutes by adding 0.06 M Pipes, 0.025 M Hepes, 0.01 M EGTA, 2 mM $MgCl_2$ (1 X PHEM buffer of Schliwa et. al., 1981), 0.75% Triton X-100, 5 μM phallicidin, and 5.2 nM leupeptin, 1 nM benzamidine, and 12.3 nM aprotinin (protease inhibitors). The cytoskeletons were then fixed for 10 minutes with 1 X PHEM

containing 1% glutaraldehyde and 0.1 μM phallicidin. (Surface replicas were prepared by omitting the detergent extraction step, and immediately fixing for 10 minutes with PHEM/glutaraldehyde.) After several rinses with 1 X PHEM buffer, then distilled H_2O, the cytoskeletons were rapidly frozen on a helium-cooled copper block [Heuser et. al., 1980]; freeze-dried at -80° to -90° C; rotary coated with 1.4 nm of platinum or tantalum-tungsten at an application angle of 45°; and reinforced with 5 nm of carbon at 90°. The metal coating adds ~2 nm in thickness to the surface of objects visualized. This approach yielded intact cytoskeletons of cells arranged in monolayers. The entire thickness of the cell could be visualized in regions away from the nucleus where the endothelial cells are typically thin (~1 μm thickness). In order to visualize the cytoskeleton above the nucleus (where the cell can be as thick as ~5 μm), additional measures were required as described below.

2.2.2 Morphology above the nucleus

In order to observe the cytoskeleton above the nucleus, cells were incubated with 10 μg/ml neocarzinostatin (NCS: generously provided by Dr. Lizzy Kappen and Dr. Irving Goldberg, Dept. of Pharmacology, Harvard Medical School) for 30 minutes at 37°C, prior to extraction. Treatment with NCS presumably cleaved the DNA [Goldberg, 1991; Kappen et. al., 1980], thereby reducing formation of intranuclear aggregates which rendered replicas of the nucleus opaque.

2.2.3 Labelling with myosin S1

Fixed, glass adherent cytoskeletons were incubated with 25 µl of 5 µM rabbit skeletal myosin subfragment 1 (S1) for 10 minutes, washed extensively in 0.15 M NaCl, 10 mM sodium phosphate buffer, pH 7.4 (PBS), and fixed in 1% glutaraldehyde, 0.2% tannic acid, and 10 mM sodium phosphate buffer, pH 7.0 for 10 minutes. Specimens were then rapidly frozen and processed as above.

2.2.4 Labelling cytoskeletons with Abs and anti-primary Ab-coated gold particles

8-nm diameter colloidal gold particles were prepared with tannic acid [Slot et. al., 1985] and coated with affinity purified goat anti-mouse IgG or goat anti-rabbit IgG, all preabsorbed with human IgG. Polyclonal affinity-purified rabbit anti-human vimentin and anti-α tubulin antibodies were obtained from Chemicon International (South San Francisco, CA). To label glass adherent cytoskeletons, residual fixative was blocked with 0.1% sodium borohydride in PHEM buffer for 2 minutes. The cells were then washed extensively in PBS, followed by PBS with 1% bovine serum albumin (BSA), pH 8.2. Coverslips were then covered with 25 µl of primary antibodies at a concentration of 10 µg/ml for 1 hour at 25°C. These were washed three times with PBS/BSA before incubating for 1.5 hours with the appropriate IgG-colloidal gold particles (1:15 dilution of goat anti-rabbit IgG). Finally, coverslips were washed with PBS/BSA, PBS alone, then fixed for 10 minutes with 1% glutaraldehyde in 10mM sodium phosphate buffer. Fixed specimens were washed extensively with distilled H_2O, rapidly frozed and freeze-dried, and rotary coated with platinum or tantalum-tungsten at 45° and carbon at

90° as previously described.

3. RESULTS

3.1 Surface Morphology

Micrographs of the apical surface of BAEC (without flow) reveal a system of pores and finger-like microvilli which extend upwards from the surface (Figure 4.1). The shape and size of the pores are consistent with them being invaginations of membrane used in the trans-endothelial transport of soluble molecules [Simionescu et. al., 1981]. The function of the surface villi is unknown, but most cells in culture have microvilli. Once cells were exposed to laminar shear stress, the villi were removed (Figure 4.1).

There are also many small rods of uniform dimension in the intercellular space, which appear to be holding the cells together. These are present after the cell membrane is extracted (Figure 4.1.c). Their composition is unknown; however, they are in close proximity to peripheral F-actin bands. F-actin does not appear to extend from one cell to the next as has been suggested by others [Gotlieb et. al., 1991].

3.2 Cytoskeletal Composition and Structure

The BAEC cytoskeleton is composed of fibers which interconnect to form a complex network which has the appearance of a porous medium (Figure 4.2). The individual fibers are ~10 nm in diameter and can be seen to bifurcate in many places between intersections with other fibers. Several types of filaments are present: F-actin, intermediate filaments (vimentin), and microtubules. In peripheral regions actin fibers predominate (as proved by S1 labelling, below), with

Figure 4.1: (a) Nonoriented cells prepared without detergent extraction showing pores, microvilli, and rod shaped projections between cells, 25000X., bar is 200 nm. (b) Oriented cells do not exhibit microvilli. (c) After detergent extraction, rod shaped projections between cells are still present, 25000X.


a

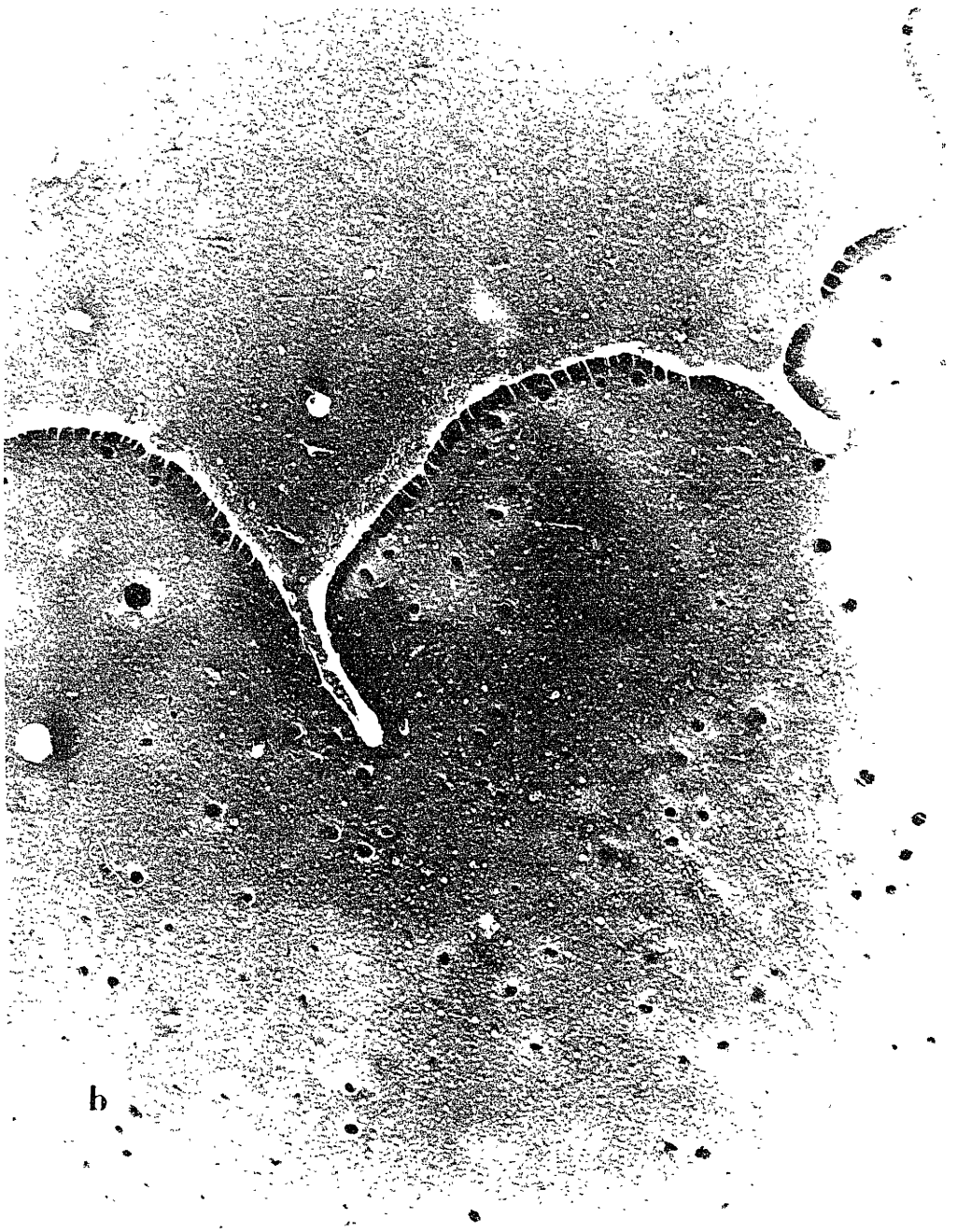
h


c

Figure 4.2: The cytoskeletal network of a nonoriented BAEC at (a) 5000X, bar is 1 μm; and (b) 25000X, bar is 200 nm.

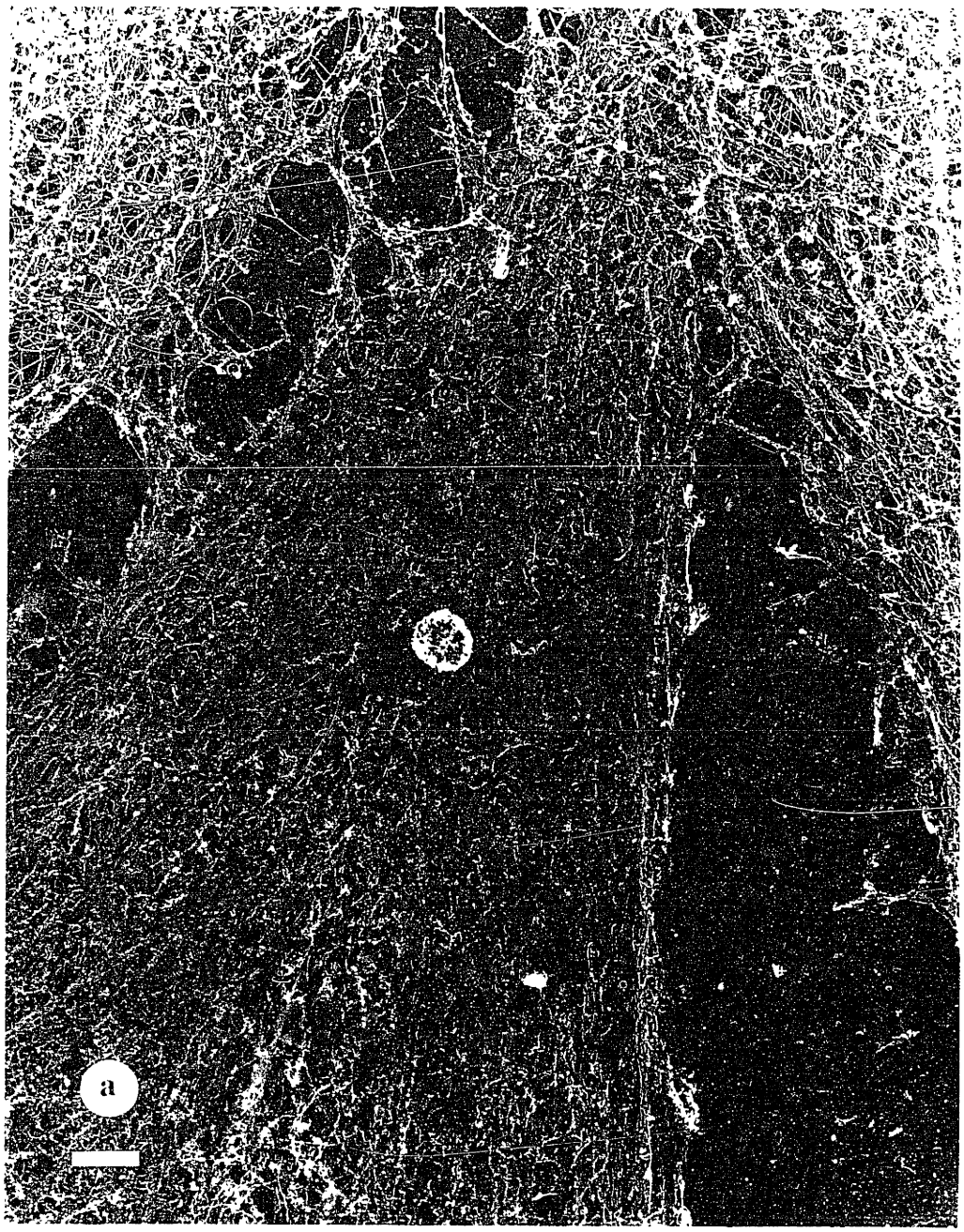
a

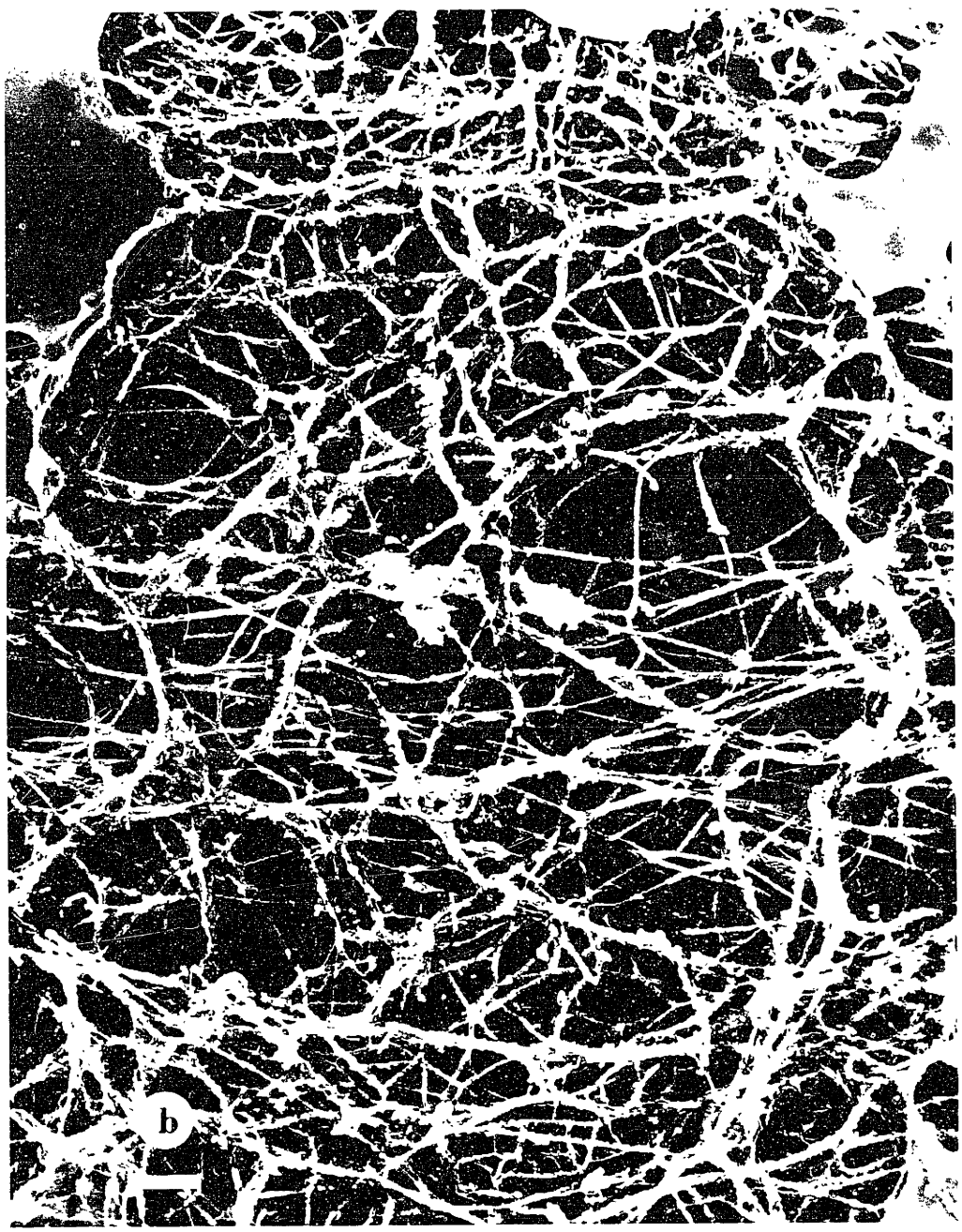
b

Figure 4.3: Oriented BAEC cytoskeleton labelled with antibody coupled to 8 nm colloidal gold to identify vimentin (intermediate filaments). (a) 5000X, bar is 1 μm; (b) paranuclear region at 25000X, bar is 200 nm; and (c) region in cell periphery at 25000X.


a

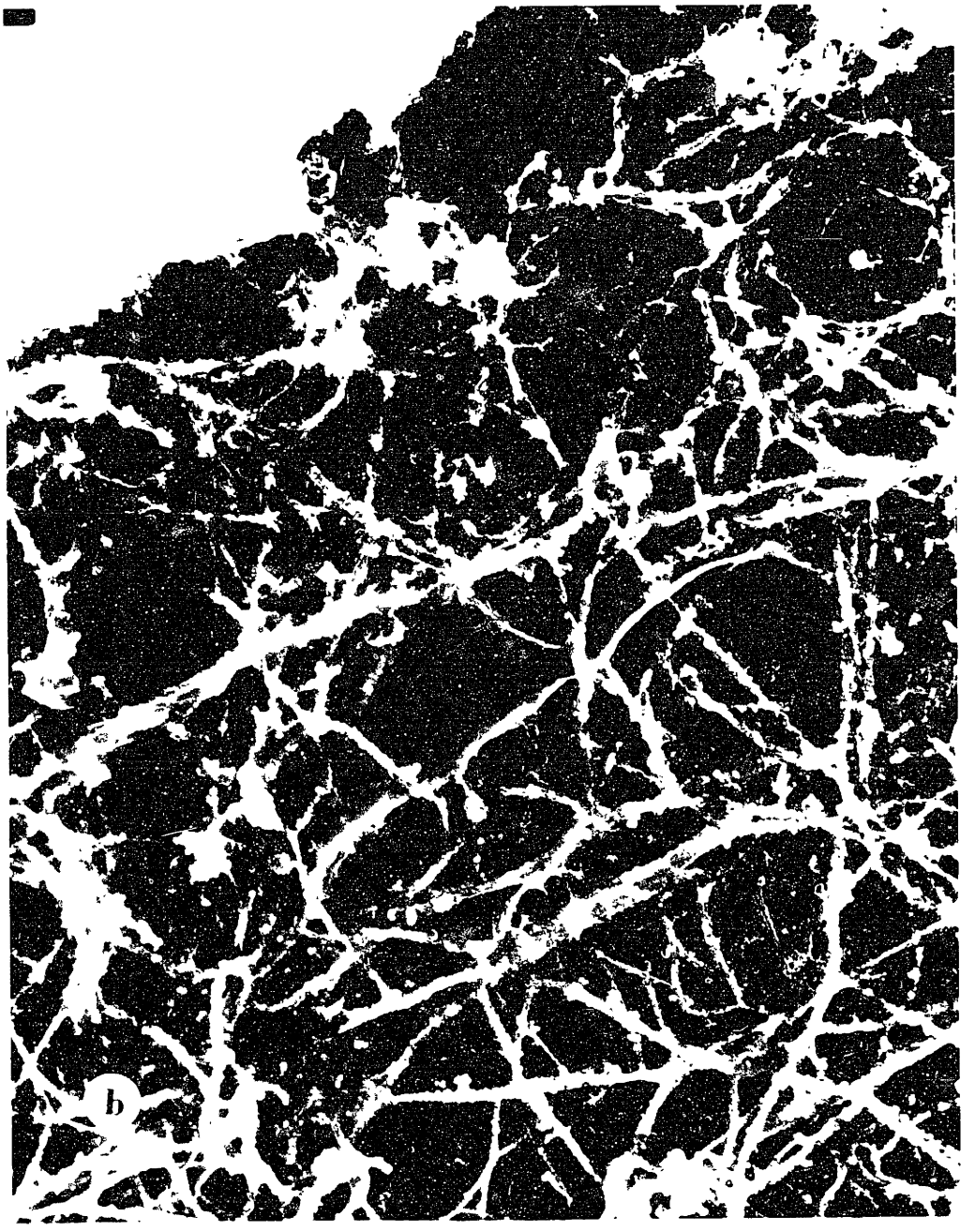
b

low levels of intermediate filaments intermixed (Figures 4.3, 4.4, & 4.5).

Intermediate filaments are found at higher frequency near the nucleus. At the cell periphery, immunogold staining with colloidal gold-coupled antibodies to vimentin is greatly diminished (Figure 4.3.c). The cortical cytoskeleton is almost exclusively F-actin. Towards the nucleus, intermediate filaments concentrate. Individual filaments can be seen in the interstices of the network and have a smooth appearance, in contrast to bundles of actin fibers, whose substructure gives them a more "ropy" appearance. Intermediate filaments do not approach the plasma membrane. In Figure 4.2.b, a section of undissolved plasma membrane remains. Actin filaments are closely apposed to the membrane patch. In some places, filaments coalesce and protrude upward forming clusters which may be the remnants of the surface finger-like villi in nonoriented cells (Figure 4.1). Intermediate filaments and microtubules are present in the actin network below, but do not approach the membrane.

Microtubules have a distribution similar to intermediate filaments, although their frequency of occurrence is lower. In the cortical cytoplasm, microtubules are sparsely distributed. Anti-tubulin gold labelling in Figure 4.4, shows almost no labelling of actin network in the peripheral region of the cell. More labelling occurs near the nucleus; however, the density appears to be less than that for intermediate filaments.

F-actin is arranged as a network of interconnected filaments and bundles consisting of small numbers of filaments; and as thick bundles composed of hundreds of filaments and associated proteins (stress fibers). Stress fibers have been

studied in cells by light microscopy [White et. al., 1983, 1986;

Figure 4.4: Nonoriented cell cytoskeleton immunolabelled with colloidal gold to identify tubulin (microtubules). Paranuclear region is shown at (a) 5000X, bar is 1 μm; and (b) 25000X, bar is 200 nm. In (c) peripheral cell region is shown at 25000X, bar is 200 nm. Gold labelling on cell membrane is artifact.


a

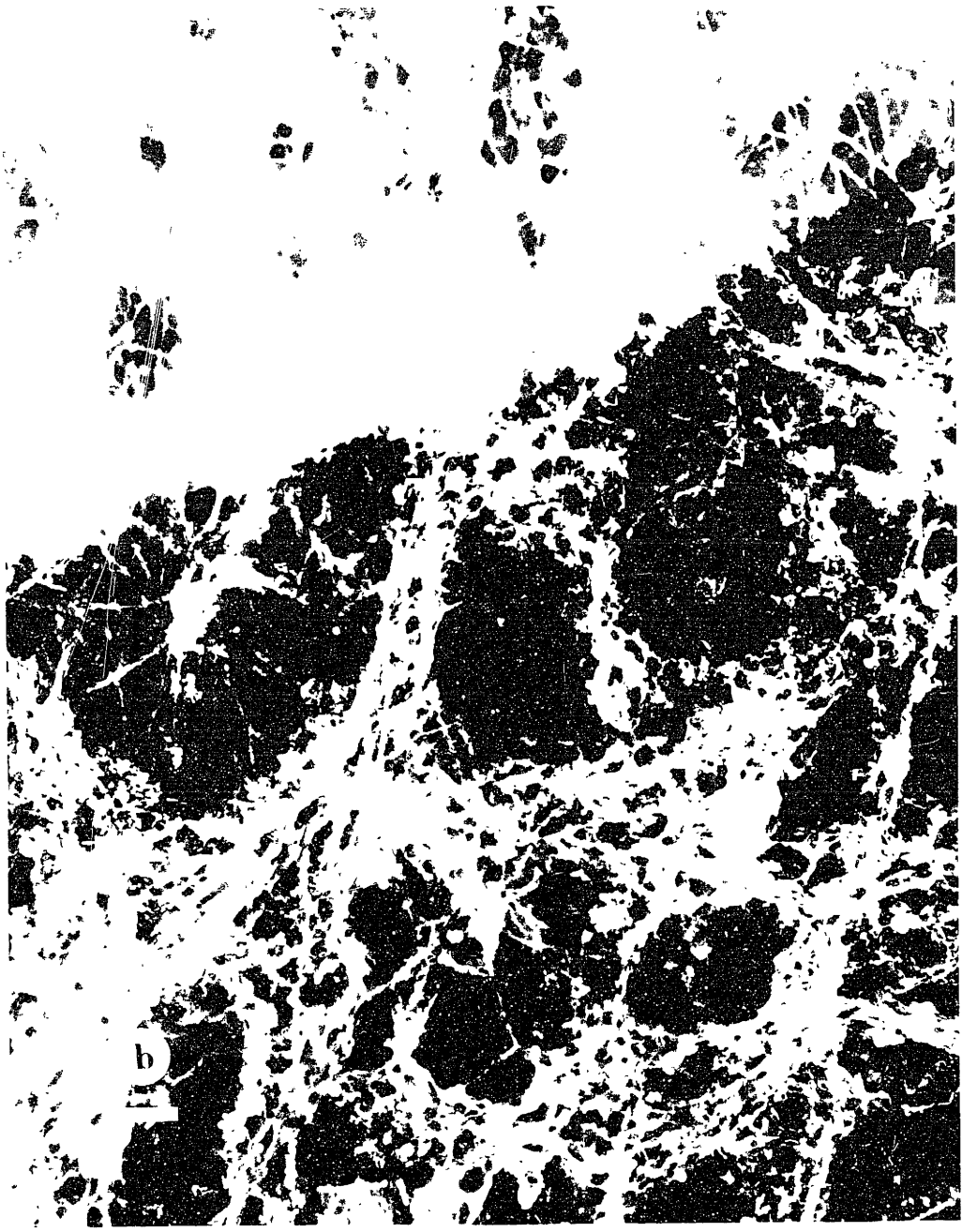
b

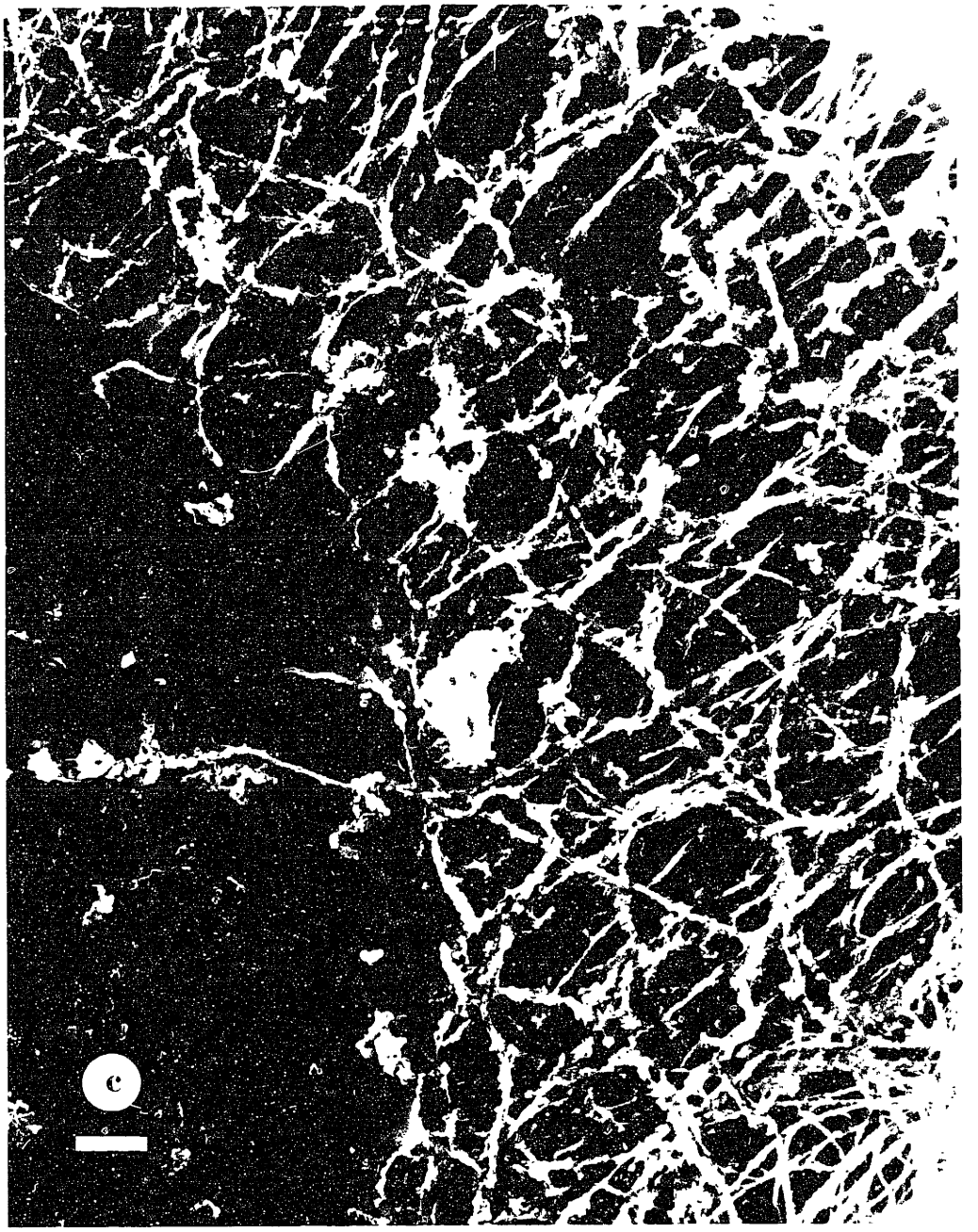
c

-

Figure 4.5: Stress fiber at high magnification showing individual stress fibers; 25000X, bar is 200 nm.

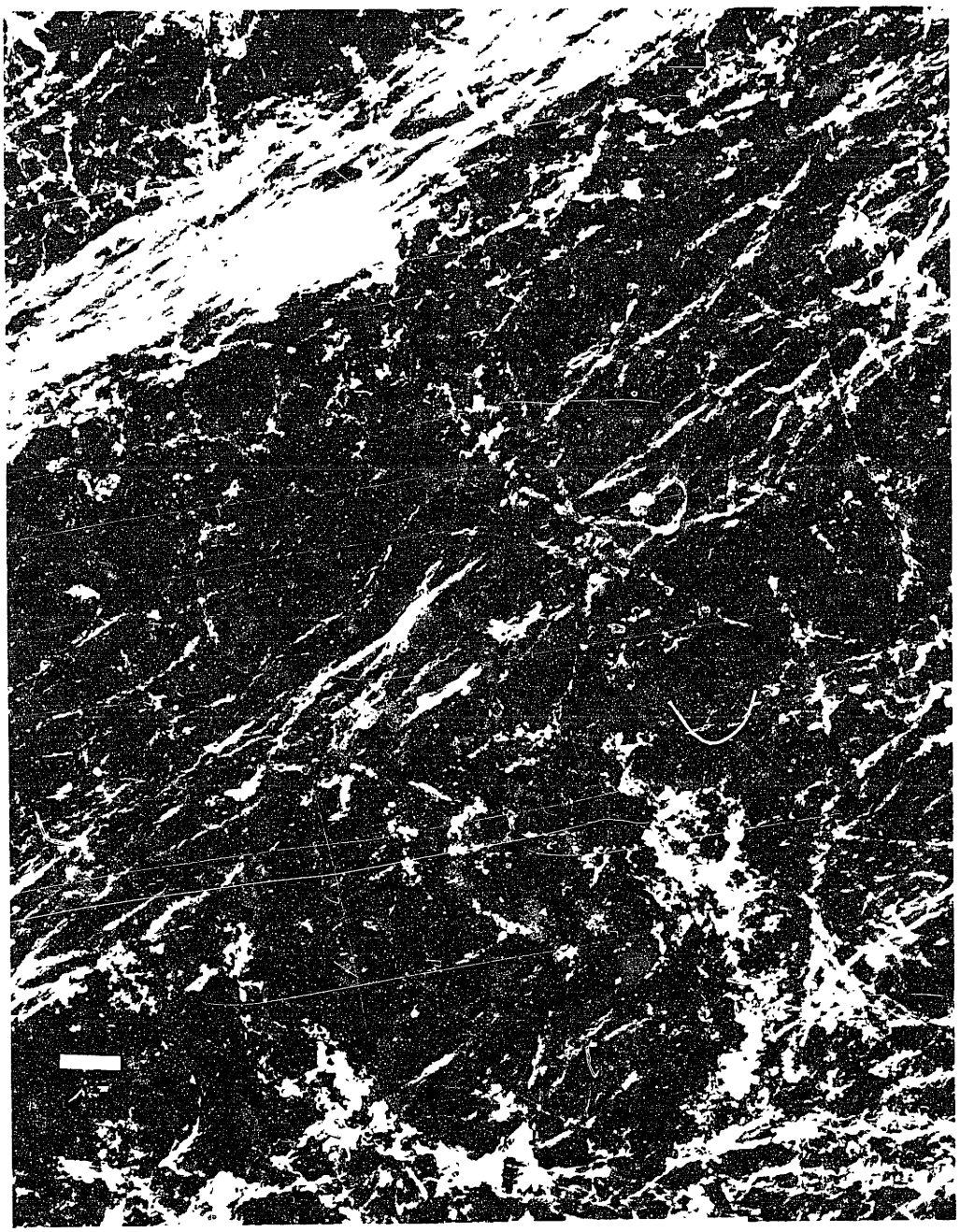

Figure 4.6: High magnification view of cytoskeleton with attached plasma membrane patch. (a) Actin network is seen closely apposed to the membrane patch; (b) Partially extracted cell with most of cell membrane intact; 25000X, bar is 200 nm.

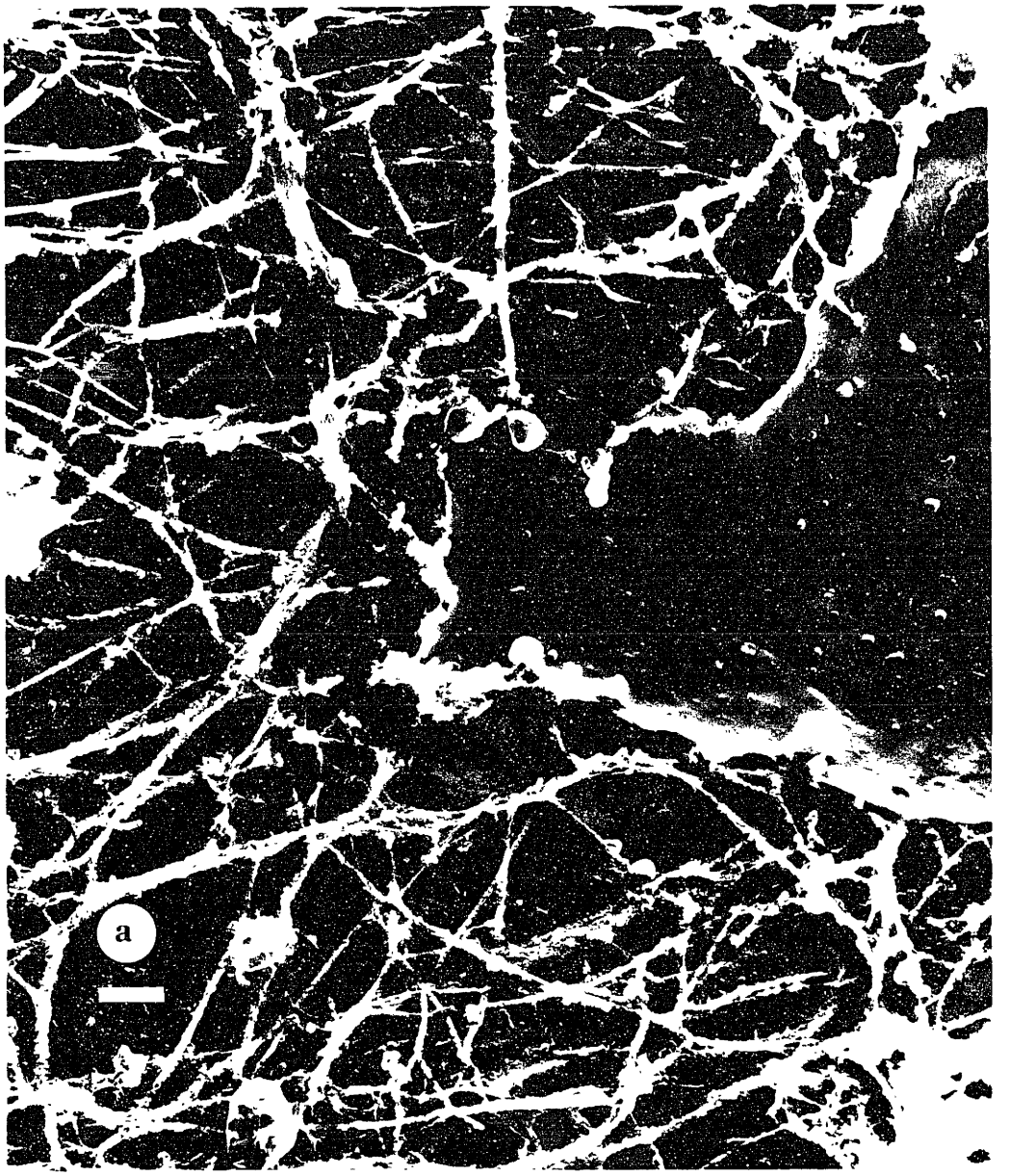
a

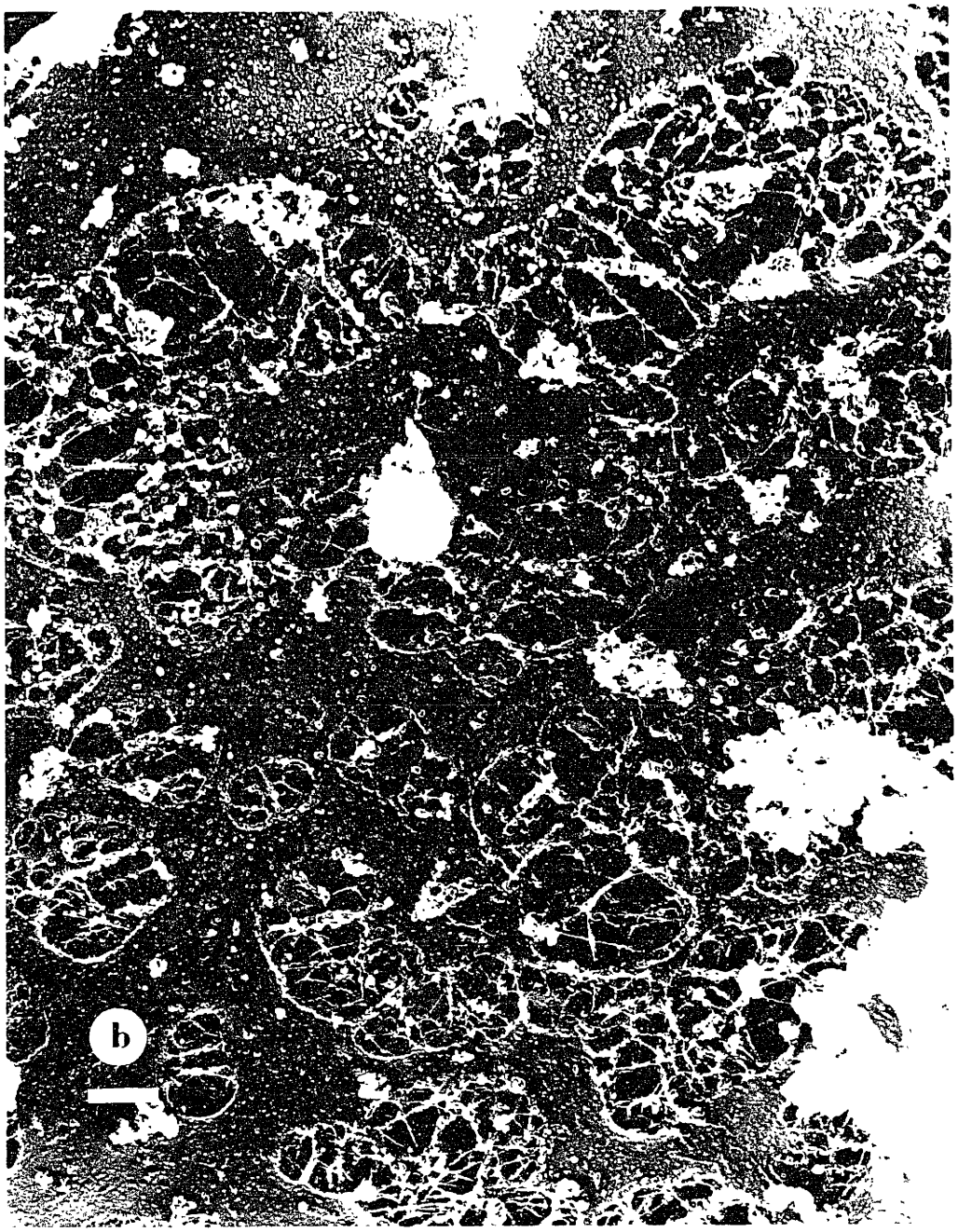
b

Figure 4.7: In nonoriented cells, the direction of orientation of the cortical actin network changes from region-to-region in individual cells. Magnification 5000X, bar is 1 μm.

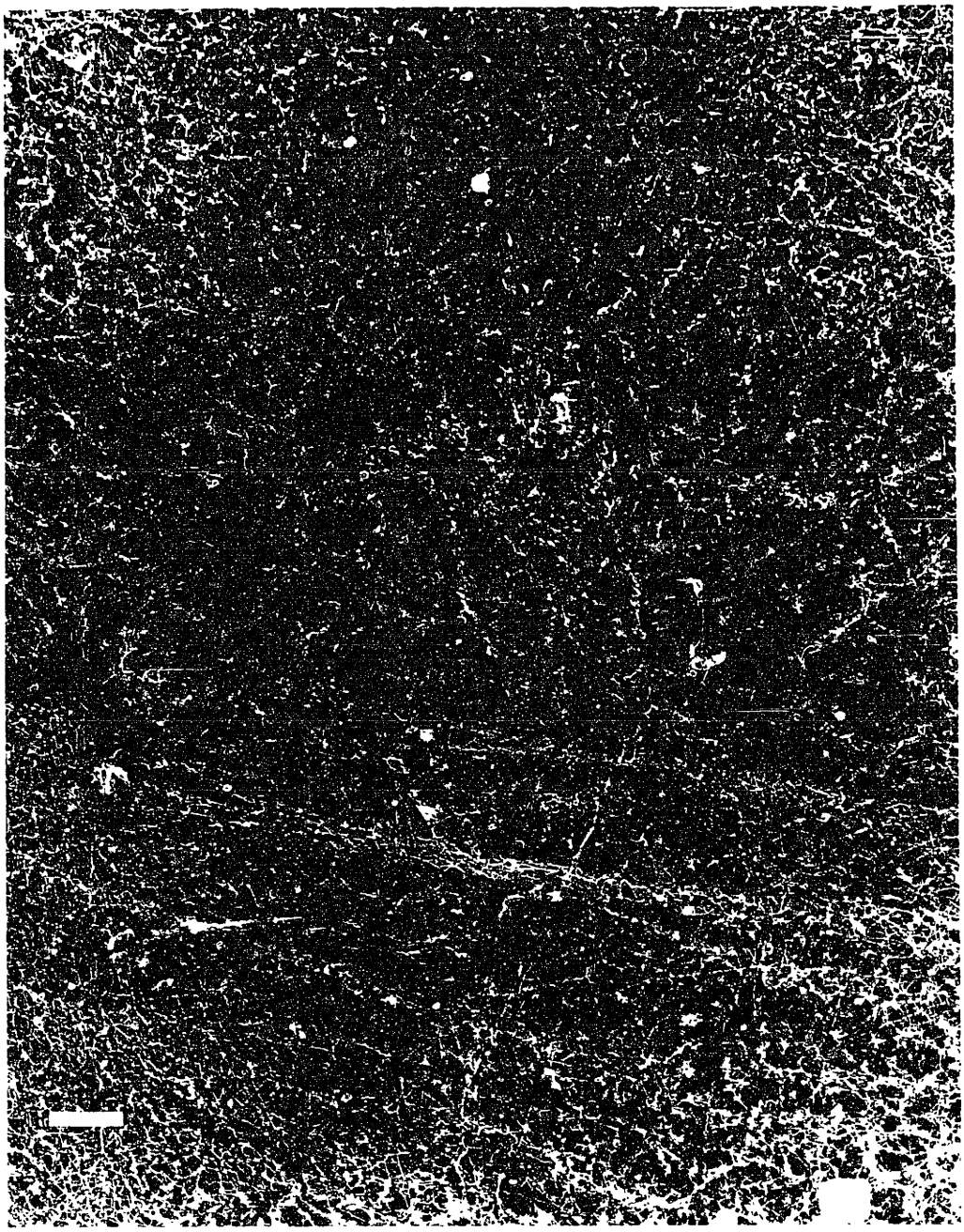

Wong et. al., 1983]. As shown in Figure 4.5, they are composed of many individual F-actin filaments.

In the fibrous network, interconnections between individual filaments criss-crossing in 3D space create pores. These intersections typically occur at acute angles. The submembranous filament network intersects the membrane at many places, as observed in areas where undissolved cell membrane remains (see Figures 4.3 & 4.6).

Network geometry is complex. In nonoriented cells (usually between stress fibers), the meshwork has an apparent direction of orientation. This direction corresponds to stress fiber longitudinal orientation, which varies randomly from region-to-region within an individual cell (see Figures 4.7). Consequently, at low magnification the meshwork appears to have no inherent direction of orientation. In oriented cells, stress fibers are aligned, so that the entire network appears to be oriented (Figure 4.12).

The cytoskeleton is most easily observed at its periphery, where it is thinnest, so that detergent extraction is effective in removing the soluble contents throughout, and metal penetration is sufficient to coat filaments at the bottom. Above the nucleus, the cell is typically 3-4X as thick. Opaque aggregates form and preclude observations of the cytoskeleton with unbleached replicas (data not shown). The situation is improved by (presumably) cleaving DNA with NCS prior to detergent extraction (Figure 4.8). The network above the nucleus has a similar appearance to cortical cytoplasm. Interconnecting fibers create a porous meshwork which connects nuclear membrane to plasma membrane.

Figure 4.8: Cytoskeleton of nonoriented cell treated with NCS. Stress fibers are located in the bottom of the cell, and do not pass over the nucleus. (a) 5000X, bar is 1 μm; (b) 25000X, bar is 200nm.

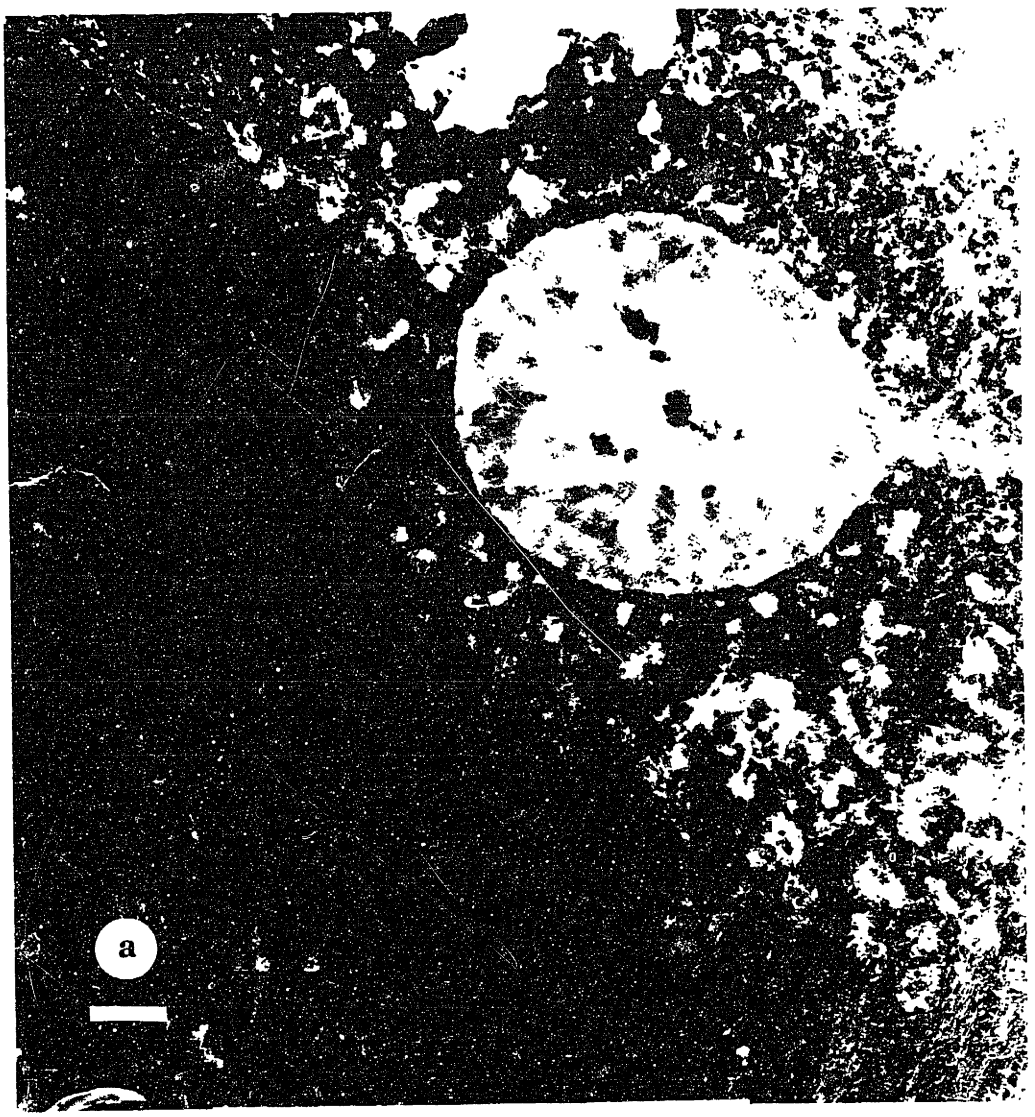
a


b

Figure 4.9: Cytoskeleton of oriented cell treated with NCS, showing stress fibers as they pass over and/or through the nucleus. 25000X, bar is 200 nm.

Figure 4.10: Cytoskeleton of nonoriented cell labelled with myosin head sub-fragment S1 to identifiy F-actin. 25000X, bar is 200 nm.

F-actin filaments can be followed from the surrounding cytoplasm as they pass above or disappear below the nucleus. In oriented cells, stress fibers pass above the nucleus (Figure 4.9). This is in striking contrast to nonoriented cells, where stress fibers are found almost exclusively in basal cell regions (Figure 4.8).

3.3 Actin Organization

That most of the filaments comprising the cytoskeletal network are F-actin can be deomonstrated using myosin S1. This subfragment which contains only the actin binding head of mysosin binds cooperatively to the sides of filaments. Figure 4.10 is a nonoriented cell labelled with the myosin head fragment, S1. Myosin S1 binds to F-actin forming a chain of arrowheads, and appear like twisted cables in frozen and freeze-dried cytoskeletons. The polarity of the filaments can be observed at high magnification. Actin filaments grow preferentially in the direction of the barbed end of the arrowheads [Janmey et. al, 1988; Cortese et. al., 1988]. Stress fibers are also labelled with S1, showing that they consist of bundles of individual filaments (Figure 4.5). Unlabelled 10 nm fibers are shown, therefore, to be intermediate filaments. Microtubules are identified by labelling with colloidal gold, and by their unique 25 nm diameter.

Stress fibers measure 100 nm in breadth, and may extend the full length of cells (~40 μm). Thus, the fibers consist of O(100) individual F-actin filaments bundled together. It is not clear whether individual filaments extend the entire length of the stress fiber, or whether the stress fibers are composed of a series of shorter anastamosed filaments.

-

Figure 4.11: Cytoskeletons of nonoriented cells. The borders between neighboring are seen; stress fibers are located along the cell periphery. 5000X, bar is 1 μm.

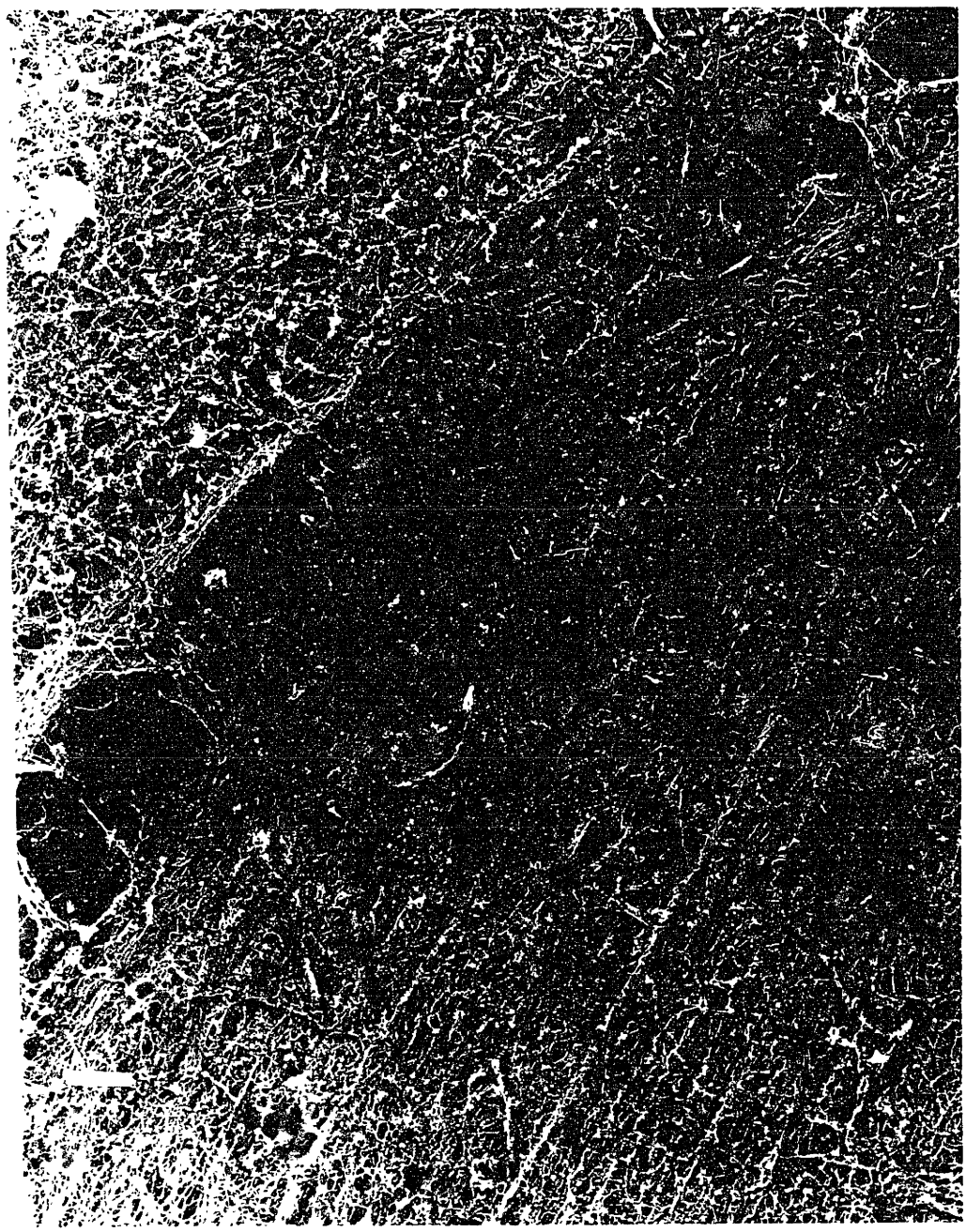

Figure 4.12: Stress fibers in oriented cytoskeletons (a) & (b) at 5000X, bar is 1 μm; and (c) 25000X, bar is 200 nm.

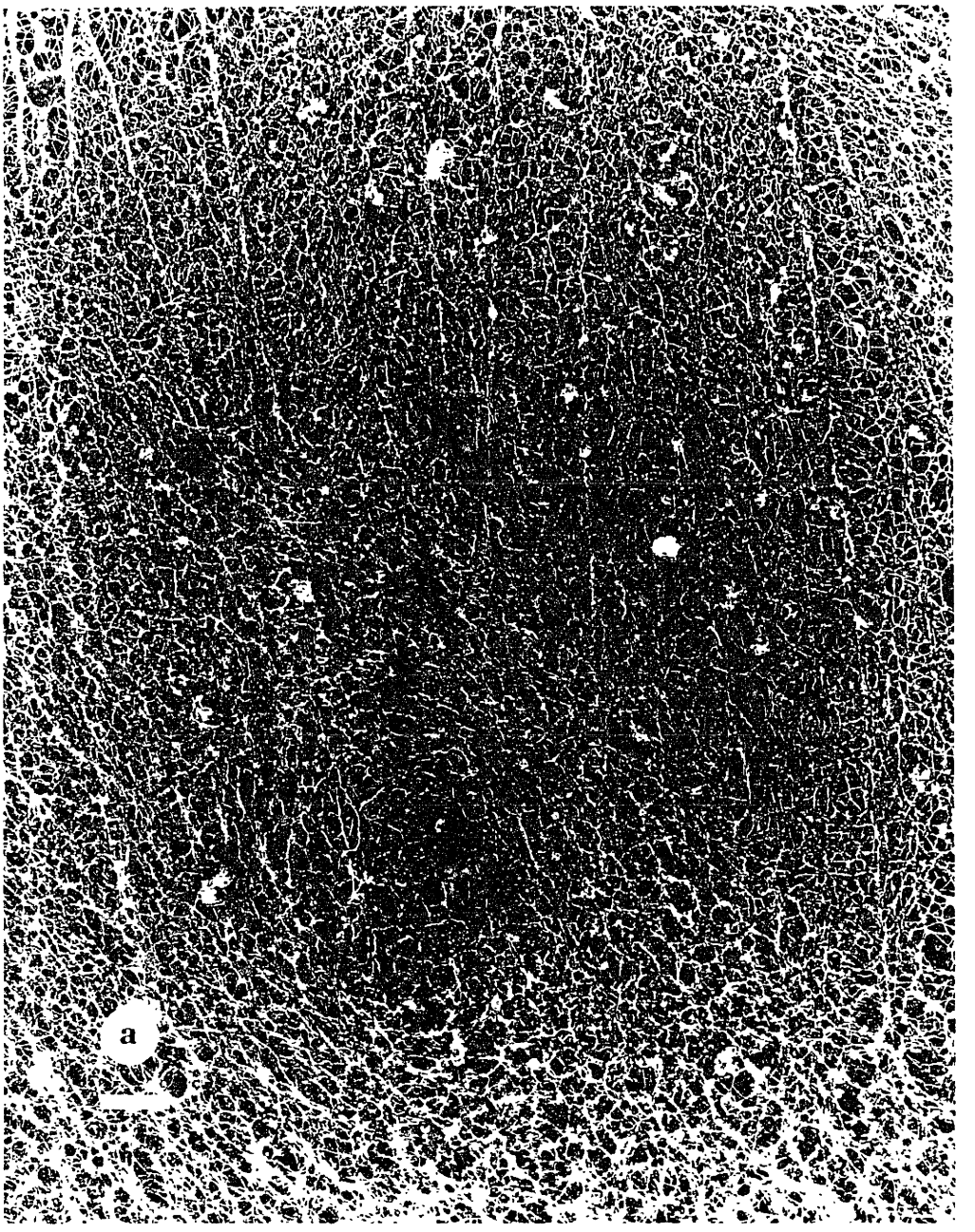
a

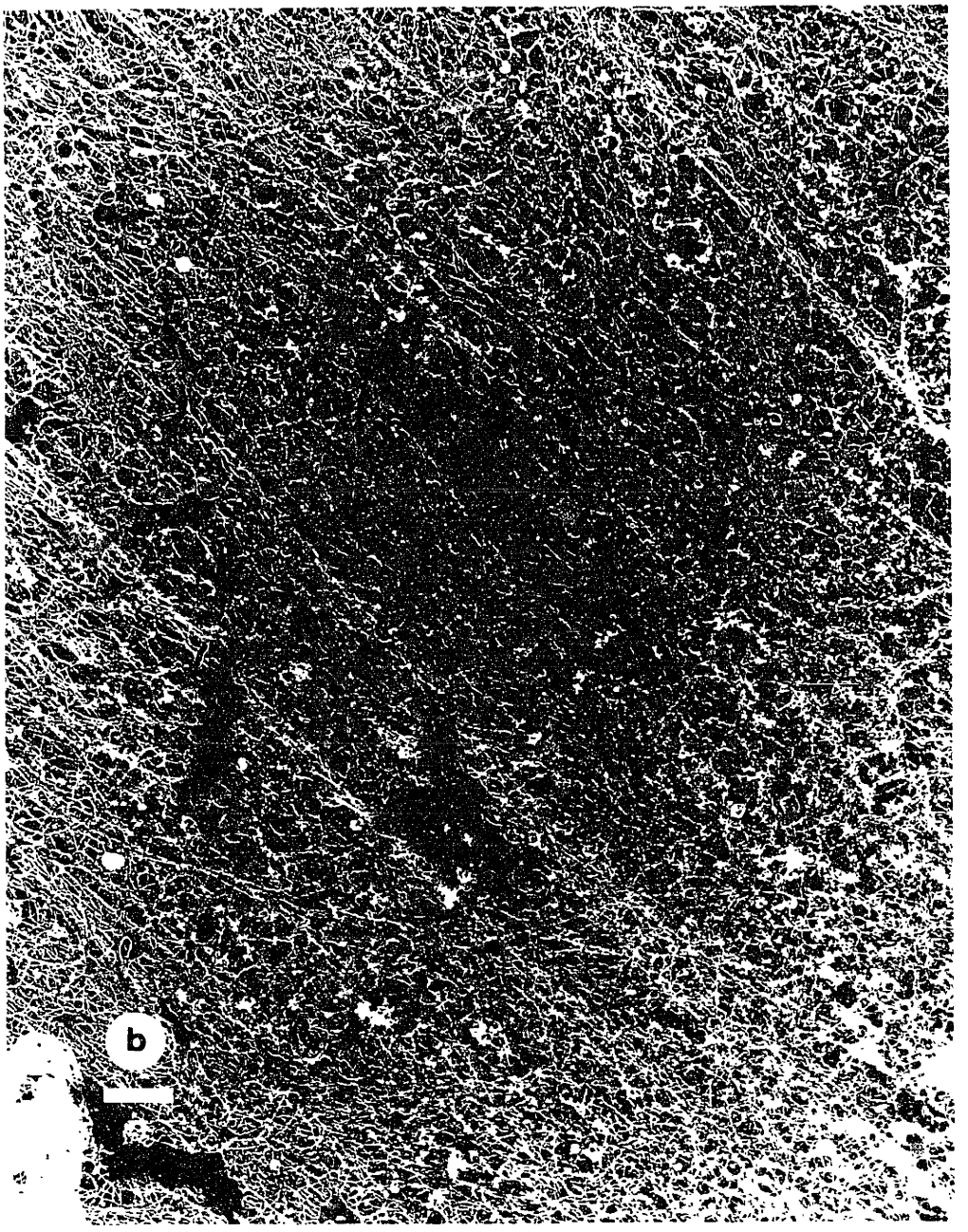
b

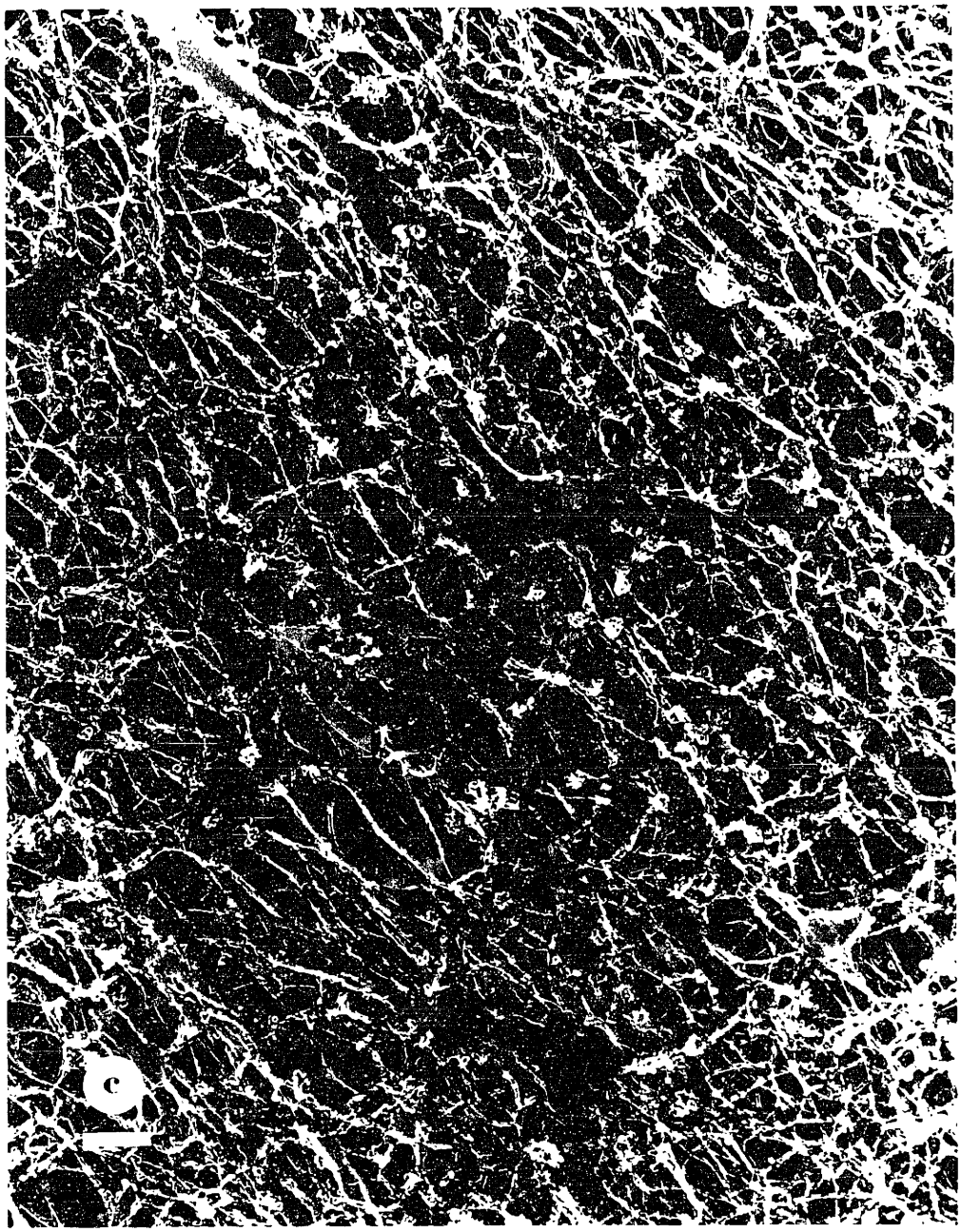
c

In nonoriented cells, stress fibers are prominent along lateral borders contacting neighboring cells and in the cytoplasm periphery (Figure 4.11). Stress fibers are also present beneath nuclei (see Chapter 3). In oriented cells, they course through central regions, passing above the nucleus. They appear to originate (or end) in some cases above the nuclear membrane (Figure 4.9).

3.4 Other Cytoskeletal Changes with Cell Orientation

Exposure to laminar shear stress affects the cytoskeleton, which, with other adjustments, produces the large-scale metamorphosis from a polygonal cell shape to an elongated shape. Stress fibers are modified as described above and has been observed by others [White et. al., 1983; Wong et. al., 1983]. However, it was not previously possible to detect changes in the cortical network, which constitutes the majority of intracellular F-actin.

Nonoriented cytoskeletons have localized patches where the cortical network orientation aligns with stress fibers nearby (Figure 4.11). However, the stress fiber direction varies from region-to-region within the cell, so that the overall appearance of orientation (at lower magnification) is random. In aligned cells, the entire cyto-network is oriented (on average) in the direction of the cell long axis.

Stress fibers in nonoriented cells are located in basal regions and near lateral borders with neighboring cells. In oriented cells, stress fibers become prominent in the central region of the cells, extending towards the top cell membrane. In Figure 4.12, stress fibers can be observed just below the apical

membrane.

Changes in the intermediate filament filaments and microtubules are not dramatic (see Chapter 3). They remain mostly near the nucleus, though small numbers of fibers can be seen intermixed with F-actin in the cortical network.

4. DISCUSSION

High resolution views of cytoskeletons from detergent extracted endothelial cell monolayers reveal a complex system of interconnected fibers. The cytoskeleton is a 3-D structure composed of F-actin, the predominant filament type; and intermediate filaments and microtubles in varying proportions. Figure 4.13 is a schematic of the endothelial cell. Cells are thinnest (~1 μm) in peripheral regions, and bulge to 2-3 X this thickness above the nucleus. The cytoskeleton also connects with the cell membrane, suggesting that it plays a major role stabilizing it, defining the surface topology of the cell, and transmitting forces from the apical membrane to substratum.

4.1 Surface

There are prominent changes in surface topology indicative of the extensive internal adjustments when cells align. Surface villi on nonoriented cells are removed, leaving oriented cells with a smooth surface. There are several possibilities for why this occurs, but an analogy can be drawn to platelets, which store extra membrane internally to be divulged when the platelet is activated and spread. Thus, the disappearance of villi from BAEC could be a redistribution of membrane to satisfy an increase in surface area when cells orient. Another possibility is that removal of the villiw reduces deformations of the cytoskeleton resulting from having these extensions "flapping in the breeze". More work is needed to assess this observation.

Nonoriented

- actin forms cortical network with many connections to cell membrane on top and bottom
- stress fibers in bottom of cell
- intermediate filaments centrally
- surface microvilli

Oriented

- actin increased beneath top membrane (stress fibers)
- smooth apical surface
- stress fibers attach to top membrane, and have many attachments to cortical network

Figure 4.13: Schematic of endothelial cell (nonaligned and aligned)

4.2 Organization of Cytoskeleton

4.2.1 Arrangement

The BAEC cytoskeleton has thin strands (~10 nm) and bundles of filaments interconnected at acute angles. Strands near the apical surface are F-actin extending upwards and intersecting the plasma membrane in many places. Occassionally, fibers coalesce and protrude, forming clusters which may be remnants of surface villi in nonoriented cells. The F-actin network is a component of the cytskeleton which (along with undetermined associated proteins) forms links to the plasma membrane (see section 4.2.3 below).

Stress fibers reinforce the cyto-network. The larger stress fibers are typically 100 nm wide, and may extend the full length of a cell (~ 40 μm). There are many connections between stress fibers and the ctyo-network via actin filaments which branch from stress fibers. The network between stress fibers is usually anisotropic, with the pores elongated in the same direction as stress fibers nearby. In limited regions within a nonaligned cell, there is a predominate direction for stress fibers. However, this direction varies randomly from region to region. In oriented cells stress fibers are aligned in the direction of cell elongation, so that the cortical network has pores which appear elongated in this direction.

For an elongated cell, the tensile strength would be expected to be much greater in the direction of orientation than in perpendicular directions. Nonoriented cells would be expected to have roughly equivalent tensile strength in any direction; however, the overall modulus magnitude would be less than for

elongated cells, which are reinforced with apical stress fibers. Therefore, cells initially experiencing flow might be expected to deform by an amount large enough to affect cell-cell, cell-substrate, and/or cyto-network-membrane attachments. Elongated cells may withstand these forces without similar destabilization due to cytoskeletal adjustments. In the following chapter, we show that the mechanical advantage of stress fiber construction is potentially substantial, increasing the predicted bulk shear modulus by a factor of 10 (chapter 5).

4.2.2 Composition

The endothelial cell filamentous network is primarily composed of actin. It also includes microtubules and intermediate filaments. Actin filaments mediate attachment of the cytoskeleton to the plasma membrane. Intermediate filaments are concentrated around the nucleus. They are interspersed and may be interconnected with the actin network. From fluorescence studies of endothelial cells *in vitro* and *in vivo*, intermediate filaments are believed to compartmentalize the cell, dividing it into various functional regions (i.e. nuclear compartment, organelles, pseudopodia, etc.) [Gotlieb et. al., 1991]. They may contribute to the mechanical properties of the network near the nucleus. However, in peripheral cell regions, intermediate filaments are sparse, and would be expected to contribute little to network mechanics.

Microtubules are also concentrated near the nucleus, but at lower levels than intermediate filaments. They extend into the peripheral cytoplasm at low concentrations relative to the many actin filaments. For microtubules, most evidence suggests that they are used for guidance and orientation. In endothelial

cells, selective transport of upregulated proteins to the apical membrane may be guided by microtubules [Molony et. al., 1991; Kupfer et. al., 1983]. The microtubule organizing center (MTOC) is moved to face the direction of migration or elongation [Gotlieb et. al., 1991]. Others have speculated that microtubules play a structural role [Ingber et. al., 1989], by supporting compressive loads generated intracellularly by tensile elements. Our findings do not repudiate this hypothesis; however, given the low filament numbers in the network relative to actin and intermediate filaments (espically in cortical regions), it seems less likely.

Overall, the mechanical properties probably vary from region to region. Around the nucleus, the network is a composite of properties of intermediate and actin filaments. However, the cell periphery is best characterized as a porous F-actin network, filled with cytoplasm.

4.2.3 Connections to plasma membrane

The connection to the cell membrane is a crucial link through which forces from the apical cell surface are transmitted to the cytoskeleton. On the basal aspect, stress fibers attach to focal adhesions, where the cell is anchored to the underlying matrix (see Chapter 3). The composition of these attachments is partially known, including vinculin, α-actinin, and probably talin, paxillin, tenuin, tensin, and others [Abercrombie et. al., 1971; Burridge et. al., 1988; Luna et. al., 1992]. Studies of focal contact dynamics indicate that the cell adjusts its arrangement of substrate contacts in response to shear stress [Davies et. al., 1992]. This suggests that forces on the cell surface are transmitted to substrate attachments. Our findings support this hypothesis. The composition of membrane-actin

filament attachments is unknown, but the aforementioned molecules are possibilities. Endothelial cells also contain ABP and spectrin, which are used by platelets to attach the actin network to membrane skeleton [Hartwig et. al., 1991].

4.3 Orientation

When cells orient, they change from a polygonal shape to a torpedo-like shape, with less of a relative nuclear bulge. The actin network undergoes extensive modifications. Stress fibers are randomly oriented in nonaligned cells. They are also found at cell margins, giving appearance of what has been labelled the dense peripheral band [Gotlieb et. al., 1991]. Actin filaments appear to be contiguous between cells with light microscopy, so that it is difficult to distinguish the exact boundaries of a cell's network.

With electron microscopy, there is no evidence for direct interaction between actin networks in adjacent cells. The cell periphery contains patches of cyto-network with random orientation. But once a cell orients, patches are rearranged so that the entire network of F-actin is oriented in the direction of flow. Stress fibers are constructed which may extend the length of the cell and which pass above the nucleus and through apical regions of the cell, reinforcing the cyto-network. This should reduce deformations of cell shape, and related sequelae which lead to the observed adjustments when nonoriented cells are exposed to laminar flow.

The normal appearance of endothelium in regions of high shear *in vivo* is the elongated configuration. A different phenotype is associated with this shape:

oriented cells have a lower rate of cell division and activate specific genes [Resnick et. al., 1992]. This adapted state may be necessary for normal cell function. *In vitro* studies are underway by others to determine the biology of endothelial cells in this state. Perhaps their characteriization will improve our ability to study pathologic changes associated with hemodynamics.

Chapter Five

THEORETICAL ESTIMATES OF MECHANICAL PROPERTIES OF ENDOTHELIAL CELLS

1. INTRODUCTION

In chapter 4 we observed the 3-D ultrastructure of vascular endothelial cells in the aligned and non-aligned configurations. The cytoskeleton is a filamentous network composed of 3 types of polymers: F-actin, intermediate filaments, and microtubules. Previous investigators have studied purified solutions of these filaments, and defined the ultrastructure of macrophages, leukocytes, platelets, and erythrocytes [Hartwig et. al., 1989, 1991; Stossel, 1986, 1988; Cassimeris et. al., 1988; Janmey et. al., 1990, 1991; Sato et. al., 1987; Evans et. al., 1975, Chien et. al., 1978]. Consequently, a considerable amount of morphological evidence for cytoskeletal function has accumulated. F-actin is thought to provide structural rigidity, and force generation in cell movement. Intermediate filaments partition the cell and support the F-actin network in some regions. Intermediate filaments can sustain larger strains than F-actin, and thus could resist extreme deformation once the yield stress of the actin network is exceeded [Janmey, 1991]. Microtubules are probably used to guide intracellular movements of organelles and proteins, and to orient the cell for directional movements [Gotlieb, 1991; Daniels, 1975].

Experimental tests of cytoskeletal filaments in endothelial cells have been limited. However, endothelial cells offer a unique opportunity for testing the function of the cytoskeleton. The forces which produce the changes with laminar flow are well characterized [Satcher et. al., 1992]. With other cells (e.g. platelets

and leukocytes), the relevant environmental forces are not as readily estimated. Thus, it is difficult to design and test models for these systems. Shear stress provides the ability to probe the mechanical properties of endothelial cells under physiological conditions. Models can be tested to see if predictions are consistent with observed responses.

Few have attempted to model the mechanical characteristics of endothelial cells. Theoretical treatments have been offered by Fung et. al., 1992; Ingber et. al., 1989; and Theret et. al., 1988. Sato et. al., 1987 & 1990, made measurements of mechanical properties using micropipette aspiration. Theret et. al., 1988, constructed a model to estimate the elastic modulus of the cortical cytoplasm based on the observed length of cell sucked into the micropipette by a specified pressure differential. This model was not based on detailed ultrastructural information. Ingber et. al., proposed that the endothelial cell cytoskeleton can be characterized as a tensegrity structure. According to this hypothesis, stress fibers produce tension which is partially supported by microtubules in compression. The model is primarily based on the observation that endothelial cells exert tension on the underlying substrate [Ingber et. al., 1989]. There is indirect evidence for the tensigrity model with fibroblasts --disruption of microtubules causes an increase in tension exerted on the substrate [Kolodney et. al., 1992]. However, there is no evidence for endothelial cells; and the intracellular architecture predicted by this model has not been demonstrated experimentally. Fung et. al., propose the only model which considers shear stress. A framework is established for analyzing the intracellular stress distribution, and a detailed calculation is performed for the limiting case of the cell membrane acting as the exclusive force bearing structure

in the cell. The alternative is for the load to be borne by a stress distribution arising in a solid (viscoelastic) cytoplasm. This possiblity is not analyzed by Fung et. al., for lack of detailed information about the mechanical properties of cytoplasm in endothelial cells.

In the present investigation, we use prior observations (see Chapter 4) of the endothelial cytoskeleton with high resolution 3-D electron microscopy to estimate mechanical properties. The cytoskeleton is analyzed as a crosslinked F-actin network. Elastic moduli for shear and tension/compression are computed and compared with experimental data. Stress fibers would reinforce the network in tension and shear. However, estimated network moduli (without stress fibers) are of sufficient magnitude to resist forces imparted by physiologic levels of shear stress, with negligible deformation.

2. PROBLEM STATEMENT

Endothelial cells form a monolayer which covers the innermost aspect of arteries, serving as a barrier between flowing blood and artery wall. Figure 5.1 is a highly schematic diagram of this system. Individual cells are surrounded by and in contact with neighboring cells. The flowing blood is in contact with the top surface of the monolayer. Basally, the cells attach to a complex and compliant matrix *in vivo*. In contrast, cells grown for *in vitro* studies, are affixed to a rigid glass coverslip on which glycoproteins (such as vitronectin, fibronectin, and laminin) are layered by the cells themselves. Individual cells have a profile similar to a sunny-side up egg (see Chapter 3). They are flat except for a slight bulge caused by the nucleus. The mechanics of transmission of shear stress on the cell membrane to attachment points is not known. But it is possible to define limiting scenarios. If the cytoplasm is fluid-like, then the cell membrane bears the load. Stress builds up along the membrane until an intercellular junction is reached, where the load can be transmitted to the substrate [Fung et. al., 1992]. Alternatively, if the cytoplasm has solid-like properties, then the load is borne by the cytoplasm. There is a non-zero stress distribution within the cell which transmits stress to substrate attachments.

In Chapter 4, we observed that the "cytoplasm" consists of a porous network of F-actin, intermediate filaments, and microtubules. Cytosol fills the interstices. The network attaches to the cell membrane, and supports the load applied by shear stress. The major difference between

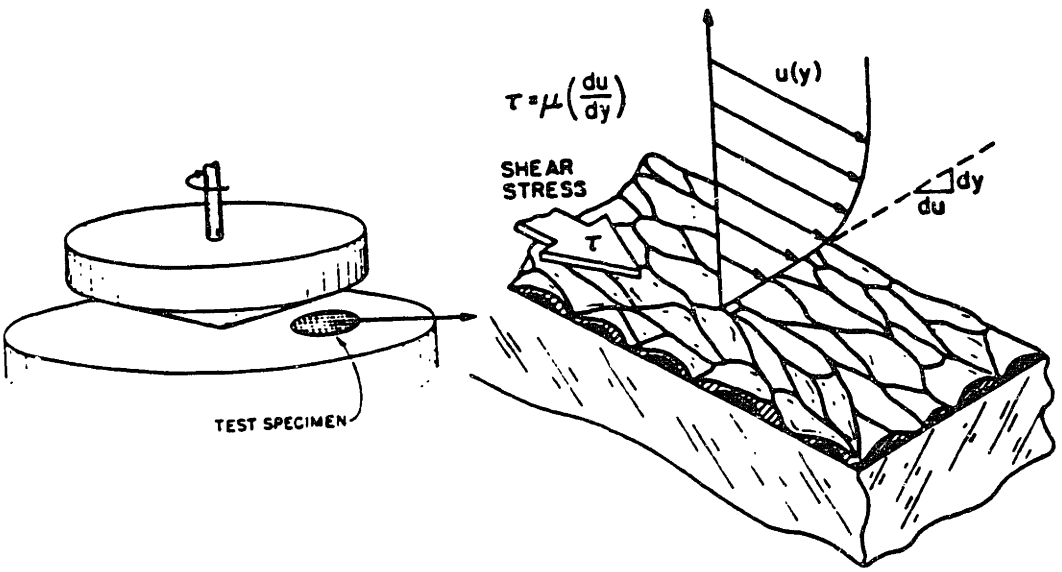

Figure 5.1: Schematic of endothelium [adapted from Dewey et. al., 1981].

aligned and nonaligned cells is the presence of stress fibers in apical regions of the former, which reinforce the network. Stress fibers in aligned cells will be treated as a load-bearing element in series or parallel with the cortical network.

The properties of the internal domain are in reality a composite of constituent filament mechanical properties, cytoplasm, membrane, and organelles. The cortical network is predominantly constructed from F-actin. Intermediate filaments and microtubules are found in increased densities near the nucleus. But they appear at lower frequency than F-actin in the periphery. Moreover, there is little information available about the mechanical properties of these filaments. In one of the only experiments conducted on them, solutions of intermediate filaments and microtubules did not exhibit mechanical properties consistent with a load bearing role under physiological conditions [Janmey et. al., 1991]. Including them in a model requires information for their mechanical behavior which is currently unknown. It also requires a better understanding of the way that intermediate filaments, microtubules, and actin, are interconnected in the cytoskeletal network. We will idealize the internal domain as a porous F-actin network. Thus, the only additional information needed to estimate mechanical properties is the F-actin content per cell.

3. MATERIALS AND METHODS

3.1 Cell Culture

Bovine aortic endothelial cells (BAEC) were grown on 12-mm and 15-mm round glass coverslips as described in previous chapters (see Chapter 3). BAEC were aligned in the cone and plate apparatus for 36 hours at 10 dynes/cm^2 (see Chapter 3 for details).

3.2 Determination of the actin content of cells

The actin content of both aligned and nonaligned BAEC on 15-mm coverslips was determined using the method described by Hartwig and Janmey [1989]. Confluent monolayers of nonaligned BAEC on glass coverslips were lysed by the addition of PHEM buffer (60 mM Pipes, 25 mM Hepes, 10mM EGTA, and 2 mM $MgCl_2$), 0.75% Triton, and 42 mM leupeptin, 10 mM benzamidine, and 0.123 mM aprotinin to inhibit proteases [Schliwa et. al., 1981]. After 2 minutes, the cells were detached from the glass coverslips using a cell scraper. The insoluble material was separated by centrifugation at 15000xg for 30 minutes at room temperature. Supernatents were divided in half for determination of total protein by the modified Folin-phenol method [Lowry et. al., 1951]. This protein assay can be performed in the presence of Triton detergent at concentrations < 1%. The polypetide composition was analyzed by electrophoresis through 5-15% gradient polacrylimide slab gels in the presence of 0.1% sodium dodecyl sulfate [Laemmli, 1970].

Similarly the protein in the insoluble cytoskeleton was measured by resuspending the residue pellet in DPBS (Dulbecco's phosphate buffered saline) and performing the Folin-phenol assay. The polpeptide composition was analyzed by solubilizing with boiling 1% SDS in the gel sample buffer of Laemmli [1970], and electrophoresis on a polacrylimide gel as above. Each measurement was made in duplicate.

The percentages of actin in the insoluble and soluble phases were determined densitometrically from the relative intensities of the Coomassie blue stained polypeptide bands on the polyacrylamide gels. The Coomassie blue staining of actin was directly proportional to the concentration of protein applied in the range of concentrations used [Hartwig et. al., 1986]. The migration of actin on polyacrylamide gels was confirmed by electrophoretic transfer to nitrocellulose paper and identification with anti-actin antibodies [Hartwig et. al., 1986].

The total number of cells on a coverslip was determined by suspending the cells using Trypsin-EGTA, and counting with a haemocytometer. Actin quantitations were repeated with various populations of nonaligned cells (on 12-mm and 15-mm glass coverslips, and 25 cm^2 plastic petri dishes) to check the consistency of the method.

4. EXPERIMENTAL RESULTS

4.1 Protein Quantitation

The protein quantitiation results are summarized in Table 5.1. A photograph of a polyacrylamide gel of endothelial cell lysates used for densitometric analysis is also shown (Figure 5.2). The actin band is indicated. The total actin per cell is ~0.03 ng for both aligned and nonaligned cells. This represents ~10% of total cell protein. Approximately 75% of this actin is in the soluble phase (i.e. the cytoplasm). The remainder is associated with the cytoskeleton and thus is in the form of F-actin and stress fibers.

From the quantity of insoluble actin, we obtain an estimate of the total number of actin monomers, and thus the total length of F-actin (370 monomers polymerize to make 1 μm of F-actin). If we assume an average filament length of 500 monomers (1.4 μm), there are roughly 200000 filaments in nonaligned cells. There is slightly more F-actin in aligned cells; however, this increase is not statistically significant. The actin content of various other cells is included in Table 5.2 for comparison.

-

Cells	Protein per cell (ng)		Actin per cell (ng)		F-actin	no. filaments
	Soluble	Insoluble	G-actin	F-actin	(no. monomers)	(1.4 μm)
Nonaligned	0.370 ±.0772	0.0997 ±.0306	0.02627 ±.00548	0.00798 ±.00245	1.131 ±.347 E8	226000 ±69000
Aligned	0.359 ±.077	0.1151 ±.0225	0.02550 ±.00394	0.00863 ±.00169	1.223 ±.239 E8	245000 ±48000

Table 5.1: Protein quantitation results

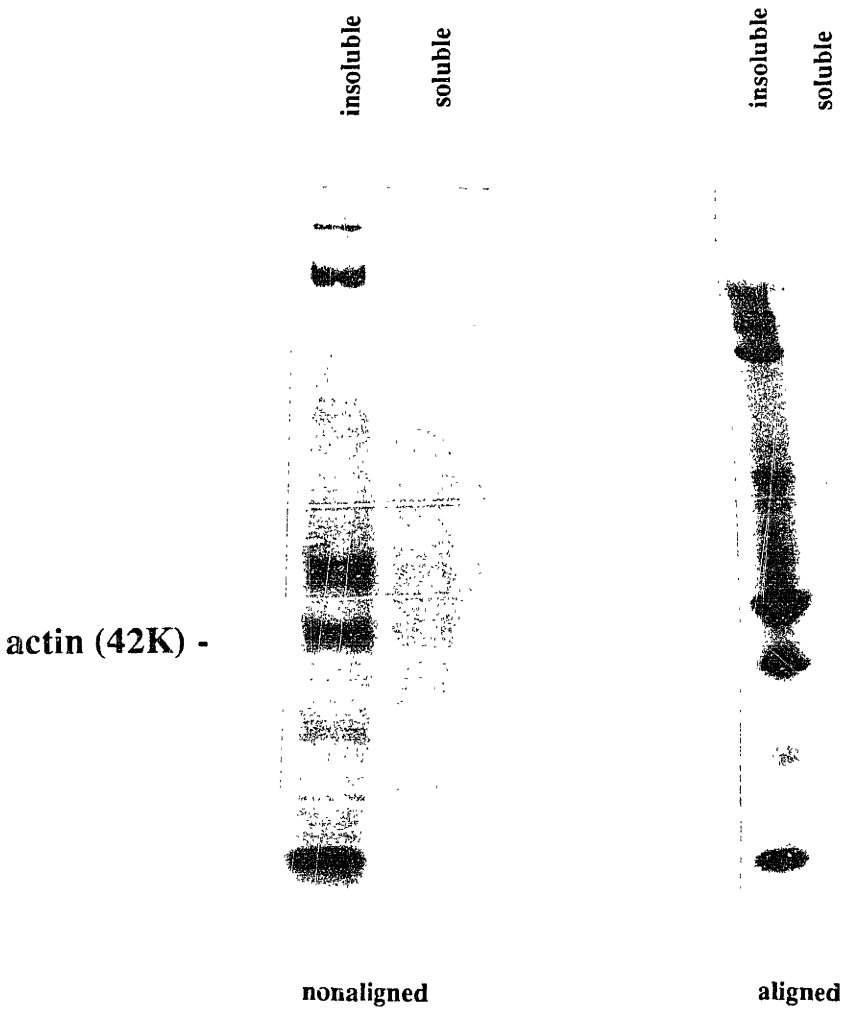

Figure 5.2: SDS-PAGE of BAEC lysates and detergent soluble phase, stained with Coomassie blue to identify protein bands.

Cell type	Reference	F-actin concentration mg/ml
Endothelial		10
Platelets	Hartwig, 1992	5-10
Macrophages	Hartwig & Shevlin, 1986	15

Table 5.2: Actin content of various cells

5. MECHANICS OF ENDOTHELIAL CELLS

In order to estimate the mechanical properties of the cytoskeletal network, we turn to the theory of so-called "cellular solids" [Gibson et. al., 1988]. Cellular solids are made up of an interconnected network of solid struts or plates which form the edges and faces of repeat units called cells. Many natural and synthetic materials are cellular solids: wood, cancellous bone, coral, glass foams, breads, corn flakes, and paper, to name a few. The microscopic structure of these materials resembles the endothelial cytoskeletal network (Figure 5.3.1). In what follows, we outline the theory for estimating mechanical properties of such solids. We will refer to this catagory of substances as "foams" instead of "cellular solids" from henceforth, in order to avoid confusion in terminology.

5.1 Theory of Foams

A comprehensive development of the theory of foams is given by Gibson et. al., 1988. It is based on a very simplified model of an actual foam of the types shown in Figure 5.3.1. Briefly, bulk mechanical properties are derived from considering the mechanism of compression and shearing of the network, as it occurs in the "cells", microscopic repeat units which make up the network. The key network parameters are: geometrical organization; the microscopic mechanism of deformation; and relative density (defined below). The crucial constituent material properties are: density, Young's modulus, yield strength, fracture strength, and creep parameters. Other potential influential factors are strain rate, temperature, anisotropy, and multiaxial loading. The procedure to analyze

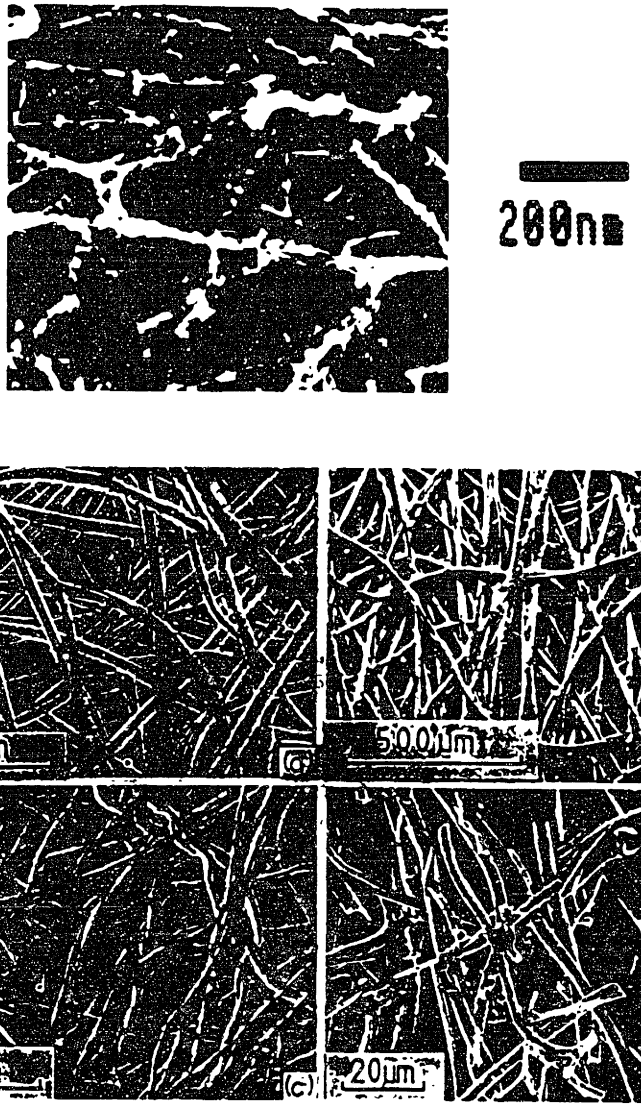

Fibrous materials: (a) felt, (b) paper, (c) cotton wool, (d) space shuttle tile
(courtesy of Nancy Shaw, NASA Lewis Research Center, Cleveland, OH).

Figure 5.3.1: Comparison of endothelial cytoskeleton with microscopic structure of various "cellular solids" [adapted from Gibson et. al., 1988].

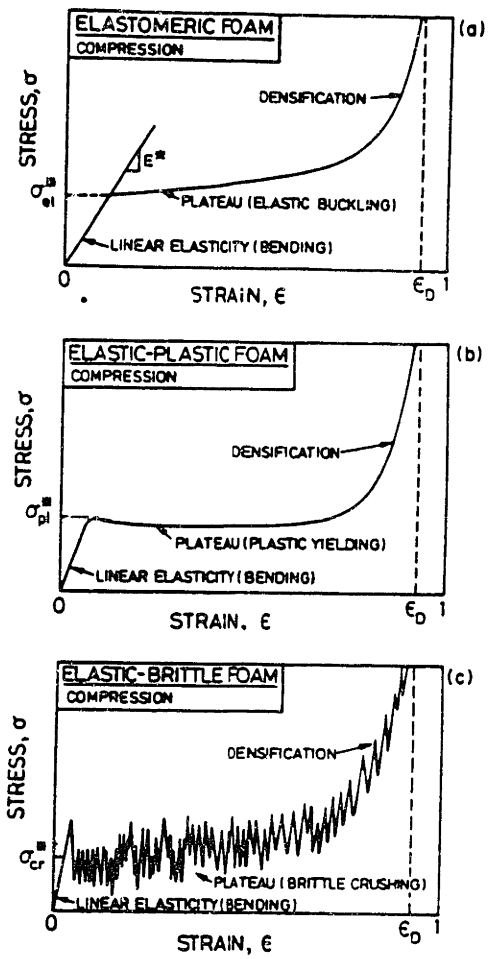

Figure 5.3.2: Schematic compressive stress strain curves for foams, showing 3 regions of linear elasticity, coallapse plateau, and densification for: (a) elastomeric foam; (b) elastic-plastic foam; (c) elatic-brittle foam [adapted from Gibson et. al., 1988].

mechanisms of deformation combines simple mechanics with scaling ideas [Gibson et. al., 1988], and gives results which have been compared to experiments with a variety of materials.

All network geometries are organized as one of, or a combination of, two configurations: open or closed. An open network is one composed of interconnected filaments. Closed networks consist of interconnected walls which enclose volumes within the network. Free fluid flow is possible through an open lattice; whereas, this is not possible with a closed lattice. The geometry in turn determines the class of deformations possible in response to a force. In general, foams in compression or tension exhibit stress-strain curves with 3 regions: 1. linear elasticity at low stress; then, 2. a collapse plateau; truncated by, 3. a regime of densification and sharply increasing stress (Figure 5.3.2). The corresponding mechanisms of deformation for an open lattice in each region are indicated below:

1. In the linear-elastic region, deformation occurs by filament bending or stretching. The Young's and shear moduli determine the slope of the stress-strain curve.

2. In the plateau region, collapse of the cells which constitute the network occurs by elastic buckling, plastic hinges, and brittle crushing/fracture. If the network is fluid filled, viscous work must be performed to move the fluid in addition to deforming the cells. This tends to increase the stiffness of the network.

3. In the regime of densification, opposing cell walls touch so that additional deformation is by direct compression/stretching of the solid itself.

With closed lattices, bending also occurs; but the enclosed volumes within the network affect mechanical properties, since any volume change requires that the encapsulated fluid be compressed or expanded.

For the endothelial cytoskeleton, we are restricted to analyzing linear-elastic deformations since we lack information relevant to regions of larger distortion. For the period before active adjustments are made by the cells, small deformations are determined by the constitutent filament (or wall) properties scaled by their concentration in space; therefore, the most important (by far) characteristic of the network for estimating mechanical properties is its density. The precise arrangment of filaments is not as important (for this method). The integrated response of the network is primarily a function of the amount of material per unit volume (and of course, the type of material). Consequently, analysis of an open-lattice such as the endothelial cytoskeleton can be simplified by modelling the network as an array of filaments of length l and square cross-section of side t [Gibson et. al., 1988] (see Figure 5.4). Adjoining network "cells" are staggered so that members meet at their midpoints. The actual network geometry is much more complex--but as long as the density of the model is similar, mechanical properties will be similar. The model geometry qualitatively reproduces the response of the real network: deformations are produced by bending or stretching of constituent filaments. We now define the relative density:

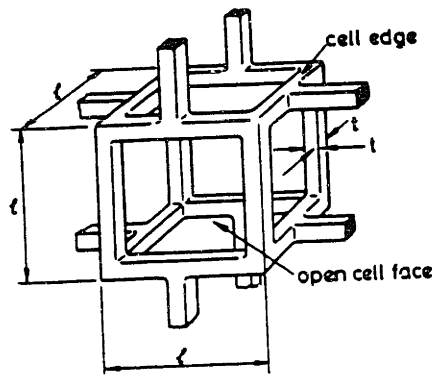

Figure 5.4: Unit cell of open-lattice model for cytoskeleton [adapted from Gibson et. al., 1988].

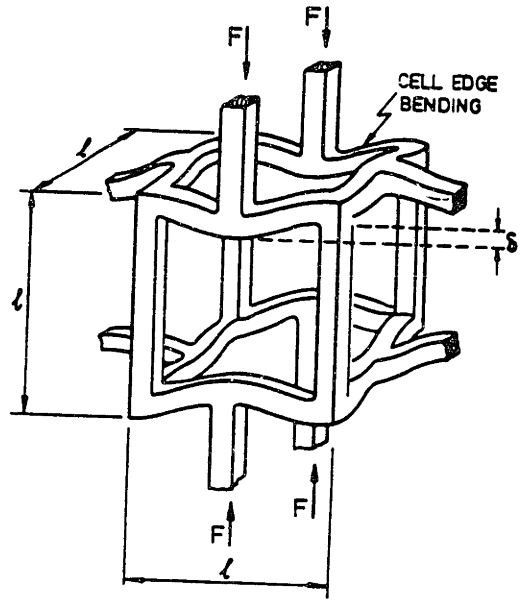

Figure 5.5: Loading of unit cell due to shear stress, indicating mechanism of deformation [adapted from Gibson et. al., 1988].

$$\frac{\rho^*}{\rho_s} \equiv relative \;\; density$$

where ρ^* is the average density of the network; and ρ_s is the density of the struts (in our case F-actin). The relative density is related to the unit cell dimensions by:

$$\frac{\rho^*}{\rho_s} \alpha \left\{\frac{t}{l}\right\}^2 \tag{5.1}$$

If we consider the filaments to be beams, the second moment of area, I, of a member scales with the elemental thickness according to,

$$I \alpha t^4 \tag{5.2}$$

Young's modulus is calculated by considering a mechanical deformation of the foam. A uniaxial loading on the foam causes each unit cell edge to transmit a force F, as illustrated in Figure 5.5. Beam bending is the mechanism of compression. The beams of length l are loaded at their midpoints with force F. The consequent linear-elastic deflection of the unit cell structure is estimated as:

$$\delta \alpha \frac{Fl^3}{E_s I} \tag{5.3}$$

where E_s is Young's modulus; and δ is the linear-elastic deflection. F is related to the remote compressive stress on the foam, σ by:

$$F \alpha \sigma l^2 \tag{5.4}$$

and the strain ε is related to unit cell displacement δ by:

$$\varepsilon \alpha \frac{\delta}{l} \tag{5.5}$$

For the foam, Young's modulus is defined as:

$$E^* \equiv \frac{\sigma}{\varepsilon} = \frac{C_1 E_s I}{l^4} \tag{5.6}$$

where C_1 is a constant. Substituting equations 5.1 and 5.2 in 5.6, we get:

$$\frac{E^*}{E_s} = C_1\left\{\frac{\rho^*}{\rho_s}\right\}^2 \tag{5.7}$$

For the shear modulus, G^*, we consider a shear stress τ applied to the foam, causing strain γ. Unit cell members respond as before by bending, so that:

$$\tau \alpha \frac{F}{l^2} \tag{5.8}$$

$$\gamma \alpha \frac{\delta}{l} \tag{5.9}$$

and δ is given by equation 5.3. Now:

$$G^* \equiv \frac{\tau}{\gamma} = \frac{C_2 E_s I}{l^4} \tag{5.10}$$

Substituting equations 5.1 and 5.2 in 5.10, we get:

$$\frac{G^*}{E_s} = C_2\left\{\frac{\rho^*}{\rho_s}\right\}^2 \tag{5.11}$$

Data are available for the Young's modulus and shear modulus of foams with a wide range of relative densities [Figure 5.6]. The best fit is for $C_1 \sim 1$; $C_2 \sim 3/8$ [Gibson et. al., 1988]. Therefore:

$$\frac{G^*}{E_s} \approx \frac{3}{8}\left\{\frac{\rho^*}{\rho_s}\right\}^2 \tag{5.12}$$

$$\frac{E^*}{E_s} \approx \left\{\frac{\rho^*}{\rho_s}\right\}^2 \tag{5.13}$$

Data for synthetic materials and natural materials are included in the graph. Thus, the correlation between modulus and relative density strongly depends on similarities in structure rather than material properties, and should be representative of actin network structure.

5.2 F-actin Network Properties

In order to estimate G^* and E^* for a network of F-actin, we must first know ρ^*, ρ_s, and E_s. Density data for F-actin indicate [CRC Handbook of Biochemistry]:

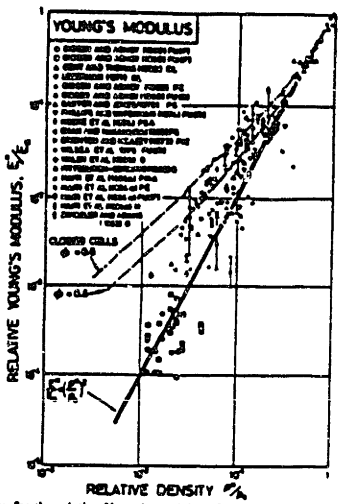

Data for the relative Young's modulus of foams, E^*/E_s, plotted against relative density, ρ^*/ρ_s. The solid line represents the theory for open-cell foams. The two dashed lines represent the theory for closed-cell foams (eqn 5.13) with $\phi = 0.8$ and $\phi = 0.6$.

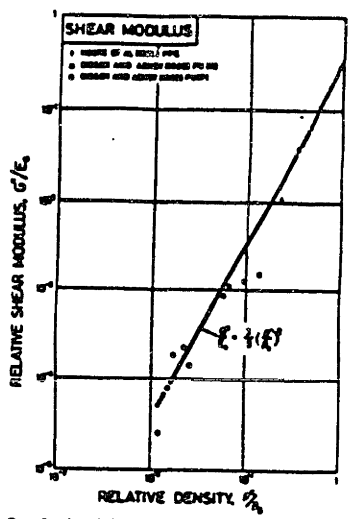

Data for the relative shear modulus of foams, G^*/E_s, plotted against relative density, ρ^*/ρ_s. The solid line represents the theory for open-cell foams.

$$\frac{E^*}{E_s} \approx \left\{\frac{\rho^*}{\rho_s}\right\}^2$$

$$\frac{G^*}{E_s} \approx \frac{3}{8}\left\{\frac{\rho^*}{\rho_s}\right\}^2$$

Figure 5.6: Moduli vs relative density [adapted from Gibson et. al., 1988]

$$\rho_s = 732 \ \frac{mg}{ml}$$

For a second estimate, x-ray crystallography studies show [Taniguchi et. al., 1983] that the unit cell of crystalline G-actin contains one molecule (MW 42500) and has dimensions: a = 61 Angstrom; b = 41 Angstrom; c = 33 Angstrom; and $\alpha = \beta = \gamma = 90°$. The calculated density is (for a fully packed crystal):

$$\rho_s = 845 \ \frac{mg}{ml}$$

There is intermolecular space in F-actin, thus the experimentally measured value of 732 *mg/ml* is taken as being more representative, and used in subsequent calculations. We measure F-actin content (equivalent to average network density) of nonoriented BAEC to be

$$\rho^* = 10 \frac{mg}{ml}$$

This is consistent with other investigators, who estimate that the concentration of F-actin in the cytoplasm of eukaryotic cells is 10-20 *mg/ml* [Hartwig et. al., 1989; Stossel et. al., 1988]. The relative density is thus of the order of $1.3 \ x \ 10^{-2}$.

Young's modulus of F-actin is estimated from the bending modulus, Γ [Oosawa, 1977; Kishino et. al., 1988]:

$$E_s = \frac{\Gamma}{I}$$

For F-actin:

$$\Gamma = 1.7\,x\ 10^{-17}\ dyne\text{-}cm^2; \text{ and } I = \frac{\pi a^4}{4}$$

for a cylinder of radius a. Using a = 3.5 nm, we get

$$E_s = 1.44\,x\ 10^9\ \frac{dyne}{cm^2}$$

Substituting these values in equations 5.12 and 5.13 gives

$$E^* = 2.4\,x\ 10^5 \frac{dyne}{cm^2} = 2.4\,x\ 10^4 \frac{N}{m^2} \qquad (5.14)$$

$$G^* = 0.9\ x\ 10^5 \frac{dyne}{cm^2} = 0.9\ x\ 10^4 \frac{N}{m^2} \tag{5.15}$$

These estimates are for cortical actin alone, without stress fibers.

Table 5.3 lists experimental measurements of the elastic shear modulus. Our estimates compare favorably with F-actin solutions of concentration approaching 10 mg/ml; and with cytoplasm from *Physarum polycephalum*, a slime mold. The measurements on BAEC by Theret et. al., 1988, do not agree. However, in these experiments, cells were detached from the substrate before measurements were made, and the elastic moduli are estimated from modelling the cells as half infinite spaces (since there was no knowledge of detailed cytoskeletal structure).

Reference	Material	Concentration (mg/ml)	Elastic Modulus (dynes/cm^2)
Janmey et. al., 1991	F-actin	10	10^4 - 10^5 (shearing)
Adams et. al., 1992	cytoplasm	-	~ 10^5 (stretching)
Theret et. al., 1988	nonoriented baec	-	~ 10^3
	oriented baec	-	~ 10^4

Table 5.3: Computed and experimental estimates of elastic shear modulus.

5.3 Network Properties with Stress Fibers

Stress fibers could conceivably act in parallel or in series to the cortical cytoskeleton, transmitting surface loads to substrate and intercellular attachments. The predominant modes of loading on cells from shear stress are tension and shearing. Treating the two cases separately, we estimate the effects of stress fibers via simple models. In Figure 5.7, uniaxial tension is resisted by (A) stress fibers (element 2) in parallel with the actin network (element 1). In (B) they are arranged in series.

5.3.1 Parallel elements in tension Consider element 1 in parallel with element 2, with tensile force T applied to the composite structure (see Figure 5.8). System constraints are expressed as:

$$T_1 + T_2 = T \tag{5.16}$$

$$\varepsilon_1 = \varepsilon_2 = \varepsilon \tag{5.17}$$

where T_n is the tension in element n; and ε_n is the strain in element n. For the composite,

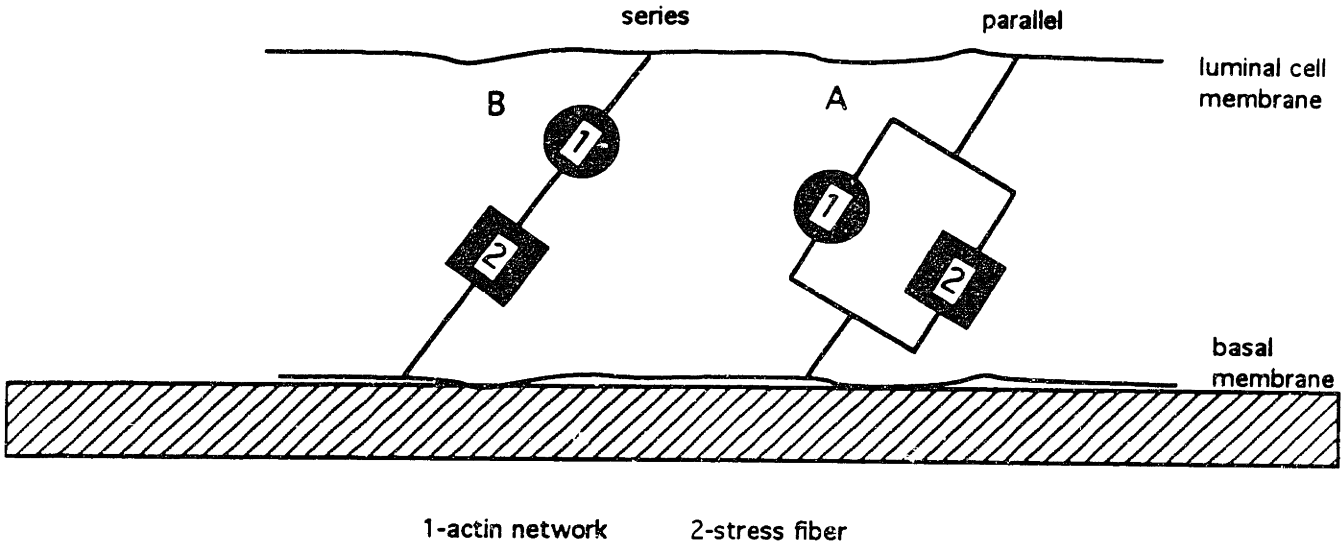

Figure 5.7: Stress fibers as parallel and series elements with actin network for case of tensile loading

$$\sigma = \frac{T}{A} = \frac{T_1 + T_2}{A} \tag{5.18}$$

where A is the relevant membrane area, and σ is the stress on the membrane. Thus,

$$E = \frac{\sigma}{\varepsilon} = \frac{T_1 + T_2}{\varepsilon A} = \frac{A_1\sigma_1 + A_2\sigma_2}{\varepsilon A} = \frac{A_1E_1 + A_2E_2}{A} \tag{5.19a}$$

or in condensed notation,

$$E = \sum_{n=1}^{2} \frac{A_n E_n}{A} \tag{5.19b}$$

The contributions of constituent moduli to the composite modulus are additive for parallel elements.

5.3.2 Series elements in tension Now consider element 1 in series with element 2, with tensile force T applied (see Figure 5.9). The constraining equations are now:

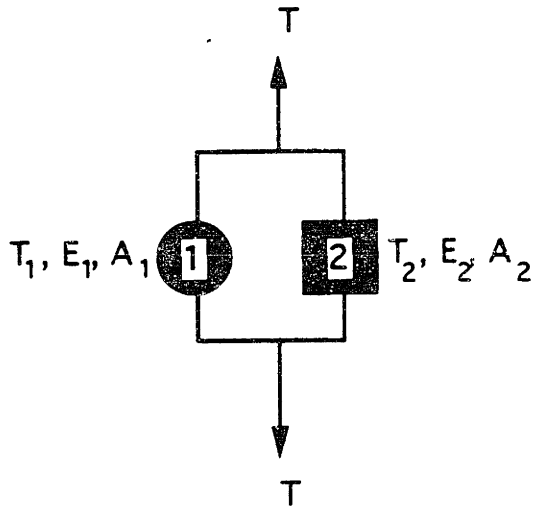

Figure 5.8: Parallel elements

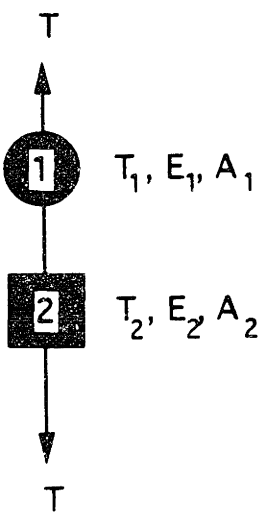

Figure 5.9: Series elements.

$$T = T_1 = T_2 \tag{5.20}$$

$$\Delta l = \Delta l_1 + \Delta l_2 \tag{5.21}$$

Thus,

$$\varepsilon = \frac{\Delta l}{l} = \frac{\Delta l_1 + \Delta l_2}{l} = \varepsilon_1 \frac{l_1}{l} + \varepsilon_2 \frac{l_2}{l} \tag{5.22}$$

substituting for ε_n,

$$\varepsilon = \frac{\sigma_1 l_1}{E_1 l} + \frac{\sigma_2 l_2}{E_2 l} = \frac{T l_1}{A_1 E_1 l} + \frac{T l_2}{A_2 E_2 l} \tag{5.23}$$

and substituting $T = A\,\sigma$, we obtain

$$\varepsilon = \left\{ \frac{A l_1}{A_1 l E_1} + \frac{A l_2}{A_2 l E_2} \right\} \sigma \tag{5.24}$$

For the composite structure:

$$E = \frac{\sigma}{\varepsilon} \tag{5.25}$$

substituting Equation 5.24 in Eq. 5.25, gives

$$\frac{1}{E} = \frac{Al_1}{A_1 l E_1} + \frac{Al_2}{A_2 l E_2} \tag{5.26}$$

or in condensed notation:

$$\frac{1}{E} = \frac{A}{l} \sum_{n=1}^{2} \frac{l_n}{A_n E_n} \tag{5.27}$$

To obtain the composite modulus we add the inverse of constituent moduli.

In the case of series elements (Eq. 5.27), and with parallel elements (Eq. 5.19), the constituent modulus is scaled by the area ratio A_n/A. These ratios can be estimated directly, or by using a scaling argument. Endothelial cells typically have ~10 stress fibers per cell [Gotlieb et. al., 1991]. If we assume that each connects to the top membrane, the force on 1/10 of the membrane (on average) is the relevant tension for the series and parallel elements of Figures 5.8 and 5.9. Thus, the area of the membrane, A, is 1/10 the total apical membrane

$$\frac{E_2}{E_1} \approx \frac{10^9}{10^5} = 10^4$$

where the subscript designations are: 1-network; 2-stress fibers; 3-composite element

From direct area estimate:

$$\frac{A_2}{A_3} = \frac{A_2}{A_1} \approx 10^{-3}$$

From number density:

$$\frac{A_2}{A_1} \approx 10^{-4}$$

Type	Area ratio	Modulus ratio (E_3/E_1)
Parallel	direct	11
	number density	2
Series	direct	1.8
	number density	1

Table 5.4: Stress fiber enhancement of network strength

area. Next, we equate the network area (A_1) to A, since the tensile force will be resisted by network beneath the membrane with equivalent cross sectional area. Finally, we estimate the cross sectional area of a stress fiber from morphological data. A typical stress fiber is 0.2 μm in diameter. The cross section is idealized as a circle. The Young's modulus of the network is known (Table 5.3); and the modulus of stress fibers is assumed to be the same as F-actin. These values are substituted in equations 5.19a and 5.26 to yield an estimate for the composite element modulus, shown in Table 5.4.

We can also estimate the area ratio based on the numbers of F-actin filaments and stress fibers. It can be argued that the area ratio A_2/A_1 scales as the ratio of filament numbers (since network properties are determined by the density of filaments). Thus: A_2/A_1 = N(stress fibers)/N(F-actin filaments) = $10/10^5$ = 10^{-4}. The predicted modulus enhancement using this ratio is included in Table 5.4.

In all cases except for the last, stress fibers significantly enhance the Young's modulus. There is more augmentation with the parallel arrangement than with the series arrangement.

Finally, if we estimate the network strain (without stress fibers) using physiological levels of shear stress (20 dynes/cm^2):

$$\varepsilon = \frac{\tau}{E^*} = 10^{-4}\ (0.01\%)$$

A deformation of 0.01% is probably too small to affect network crosslinks.

5.3.3 Elements in shear Analysis for series and parallel elements with shear loading yields the same equations as for tensile loading (see equations 5.19 and 5.26). Stress fibers in aligned cells are located just below the top membrane. They may attach apically as they do along the bottom membrane to focal adhesions. However, the length of aligned BAEC (typical length ~40 μm) is much larger than the top to bottom thickness (<1.0 μm). Stress fibers can extend for the length of a cell; thus, they are essentially parallel to the top membrane. There are many actin filaments which branch from stress fibers and attach to the surrounding network (see chapter 4), which fills the space between the top membrane and a stress fiber. This is represented schematically in Figure 5.10. The shear modulus of stress fibers is assumed to be identical to F-actin ($\approx 10^9$ *dynes*$/cm^2$); which is much more than the shear modulus of the network (0.9×10^5*dynes*$/cm^2$). We can estimate if the presence of stress fibers in apical regions significantly reduces the deformation caused by shear stress. With network alone, the deformation angle, γ, is (see Figure 5.11):

$$\gamma = \frac{\tau}{G} = 2 \times 10^{-4} radians \ (0.01^o)$$

for $\tau = 20$ *dynes*$/cm^2$. Thus, the cell is not significantly distorted by physiological levels of shear stress in the absence of stress fibers.

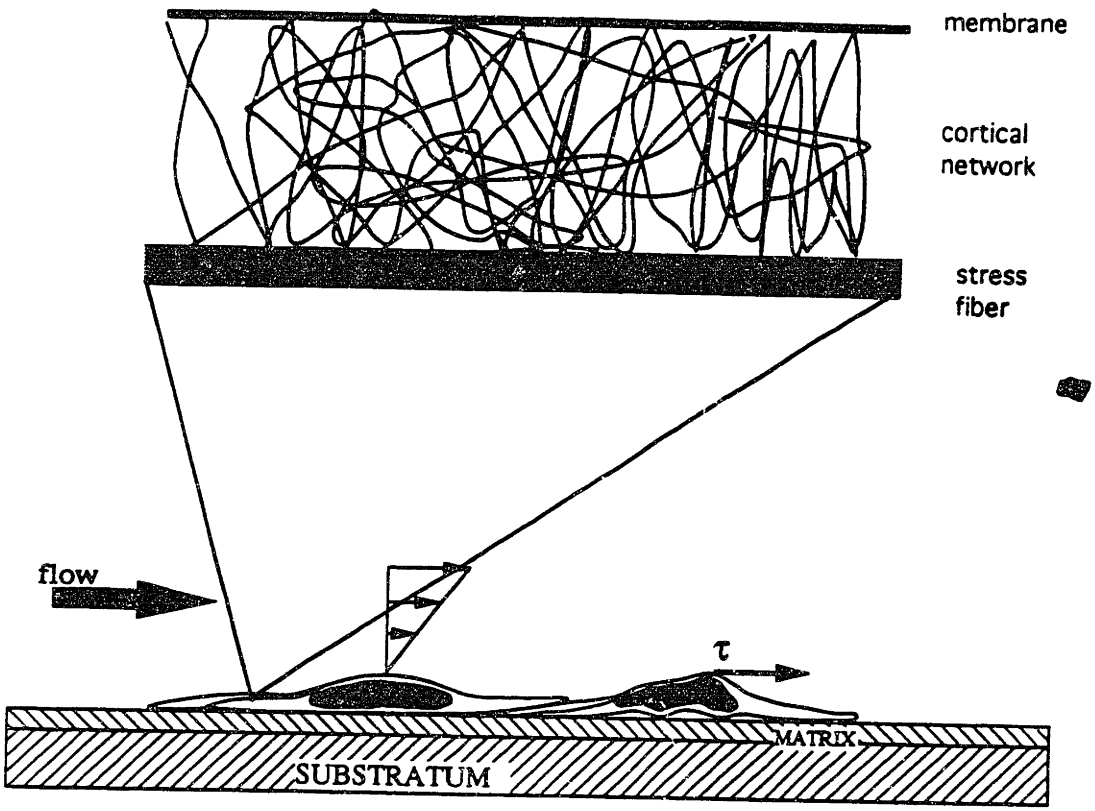

Figure 5.10: Schematic of stress fiber beneath top membrane, with many attachments to intervening network

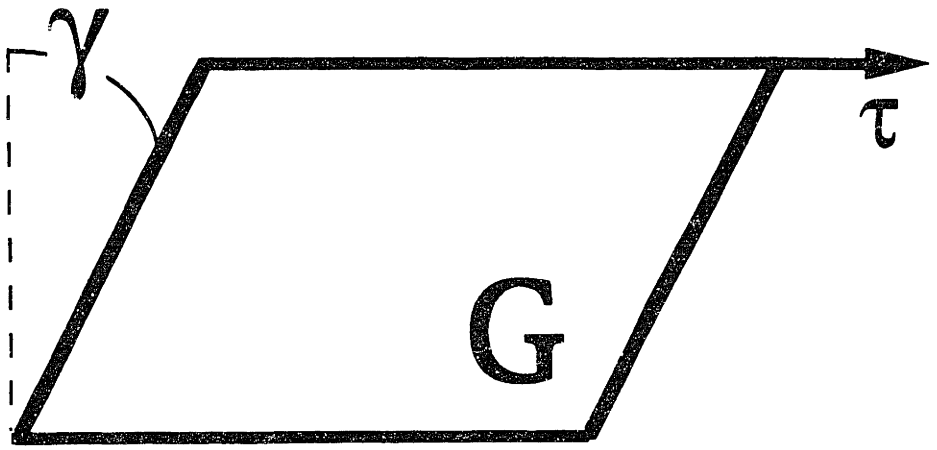

τ - shear stress

G - shear modulus

γ - deformation angle

Figure 5.11: Deformation angle caused by uniaxial shear stress

6. DISCUSSION

Vascular endothelium grows as a monolayer of cells on the innermost aspect of the artery wall. As the interface between flowing blood and artery, the endothelial cells are able to withstand shear stress without mechanical damage. Cells are attached to the substrate below and neighboring cells on the sides. Forces on the top cell membrane are transmitted to attachment sites. It had been postulated that this could occur via tension in the cell membrane [Fung et. al., 1992]. However, from 3-D ultrastructural studies, the cytoskeleton was identified as the probable load bearing element in endothelium (Chapter 4). It attaches to the apical membrane and is primarily composed of F-actin crosslinked to form a porous network.

The bulk elastic shear and compressive/tension moduli were estimated using the theory of foams [Gibson et. al., 1988]. Calculated values are in good agreement with experimental measurements on cytoplasm from *Physarum polycephalum* and F-actin gels (Table 5.3). Experimental measurements by Theret et. al., 1988, on BAEC give values for the modulus which do not agree. However, the technique used to measure mechanical properties (micropipette aspiration) required a probe which is 1/4 the size of the cell; the cells were detached from the substrate before measurements were made, disrupting intercellular and cell-substrate attachments; and the model used for estimating the elastic modulus treats cells as half infinite spaces.

Stress fibers reinforce the network in our simple conceptualization, where they are in series or parallel with the network for a tensile loading. The stress

fibers are oriented to take axial tension/compression; whereas the cortical network would be deformed by beam bending. Thus, a given density of stress fibers will be more able to carry a load than an equivalent weight of cortical network. In aligned cells, there are many attachments between network actin filaments and stress fibers, which start at focal adhesions in the basal region, and may end with an attachment to the top membrane. Aligned cells are much longer than they are thick (from top to bottom); thus, stress fibers extending for the length of the cell are essentially parallel to the top membrane. For shear deformations, stress fibers are in series with the network. Actin network is able to withstand physiologic forces without stress fibers, using estimates of the shear modulus from the theory of foams. However, the possibility remains that cross-linking between actin filaments is not of sufficient strength in nonaligned cells to support shear stress on the network. Nonaligned BAEC had lower modulus than aligned cells as measured by Theret et. al., 1988, despite considerable manipulations and less than optimal measurements. A critical change which occurs with alignment (which is not explored in our model) could be stronger cross-linking in the network.

Despite much speculation, a definitive structure-function relationship for the endothelial cytoskeleton has not been proven [Gotlieb et. al., 1991]. Our findings and observations of others are consistent with the cytoskeleton serving as the stress bearing element [Dewey et. al., 1981; Hartwig et. al., 1991; Wong et. al., 1983; White et. al., 1983]. Cells exposed to shear stress adjust their substrate attachment plaques (focal contacts) [Davies et. al., 1992]; implying that forces are transmitted via the cytoskeleton to substrate attachments. If physiologic forces are not of sufficient magnitude to significantly distort the network, or the cell (by

inference), it is less likely that cell-cell attachments are disrupted by mechanical forces. It is possible that the active response triggered by shear stress produces the changes observed at intercellular attachments.

An additional point of controversy is how shear stresses elicit an intracellular signal. Shen et. al., 1992, have measured increases in intracellular Ca^{++} in BAEC in response to shear stress. Others have postulated the existence of stretch receptors and stretch sensitive channels in the apical cell membrane [Harrigan, 1990; Sachs, 1988]. Our findings are consistent with these observations. A protein which links the cytoskeleton to the top membrane could activate intracellular signals. Actin filaments attach to the overlying membrane in many places. In other cell types (platelets and erythrocytes) linkages between actin network and plasma membrane have been identified [Hartwig et. al., 1991; Fox 1985; Lux, 1979; Branton et. al., 1981]. Proteins that compose these complexes include actin binding protein (ABP), spectrin, and integral membrane proteins such as GP IX-1b. Endothelial cells may use these and/or other molecules for the linkage [Gorlin et. al., 1990]. Shearing forces would displace the membrane relative to the cytoskeleton, so that the linkage molecules would be deformed, perhaps causing cytosoloic Ca^{++} or K^{+} transients [Shen et. al., 1992].

In the case of laminar flow, transcellular stress fibers are constructed as cells orient in the direction of flow. Buxbaum et. al., 1987, have performed experiments comparing the viscoelastic characteristics of cytoplasm and F-actin gels which provides an additional explanation for stress fiber production. Cytoplasm behaves as a thixotropic viscoelastic material *in vitro*--it deforms

elastically until a critical yield stress is reached, then flows as an indeterminate fluid. The shear stress in flowing cytoplasm is independent of shear rate since there is an inverse proportionality between viscosity and shear rate [Buxbaum et. al., 1987]. The yield stress of pure F-actin solutions (of ~10 mg/ml, the concentration of cytoplasm) is ~10 dynes/cm^2 [Kerst et. al., 1990]. However, F-actin in these solutions is not crosslinked as in a cell. The threshold shear stress for endothelial cell alignment is ~8 dynes/cm^2 [Dewey et. al., 1981]. If the cytoplasm flows at the points of highest shear stress, this could align actin filaments which are subsequently bundled together to form stress fibers. Since stress fibers increase the modulus of the network locally, the cytoplasmic streaming would be self-limited, stopping soon after stress fibers achieve a certain length (in this scenario). When purified actin gels are subjected to shear stress, regions of aligned fibers aggregrate to form a crystalline phase which is very similar in morphology to stress fibers [Cortese et. al., 1988; Suzuki et. al., 1989; Buxbaum et. al., 1987, Ito et. al., 1987]. Moreover, ultrastructural studies show that many stress fibers in oriented cells tend to have one attachment at or around the nucleus, where stresses would be maximum (Chapter 4).

Several observations make this hypothesis less likely. There are important differences between purified F-actin solutions and the cortical network. In the cell there are many architectural proteins which produce cross-links between filaments, bundle filaments, and regulate construction/degradation of filaments. These could have profound effects on mechanical properties of the network. This potentially crucial characteristic is not accounted for; moreover, intracellular streaming of cytoplasm has never been observed in BAEC. Further studies are

needed to assess the possibilities.

F-actin filaments interact with microtubules and intermediate filaments. Our model does not account for other filaments, in part because the precise nature of interfilament interactions is unknown. The role of stress fibers in alignment has been studied, but little is known about the role of cortical network actin, intermediate filaments, or microtubules for normal adjustments. This could be tested by observing alignment in the presence of agents which disrupt these filament systems.

Our conceptualization also does not explain endothelial response to turbulent flow [Davies et. al., 1986]. In this case, cells respond by dividing at average shear stresses below those needed to align cells (~ 2-3 dynes/cm^2). The cell is unable to adjust to the inherent chaotic variations in shear stress with turbulent flow. Further studies of cells in these conditions are needed to identify the mechanism involved.

Finally, the temporal relationships between observable events, namely:

- force on top membrane
- intracellular signal
- peripheral manifestations, such as stress fiber construction and disruption of intercellular attachments

must be clarified.

Chapter Six

CONCLUSIONS

Atheresclerosis develops at focal sites in arteries. Thus, hemodynamics has been implicated as an important factor in the pathogenesis of the disease. Studies have shown that endothelial cells respond to shear stress with: changes in gene transcription, increases in cytosolic Ca^{++}, K^{+} currents, and adaptions in morphology. Cells also respond to turbulent and distrubed flows by migration and increased rate of division. These observations correlate response with stimulus but do not explain the mechanism of action.

Structure-function relationships must be defined in order to construct the mechanism. Specifically, one must know how endothelial cells withstand luminal shearing forces. The cytoskeleton was presumed to fulfill this function, although there was only indirect evidence for this hypothesis. Earlier studies did not determine whether the cytoskeleton was connected to the membrane, which would be necessary for forces to be absorbed.

This thesis is a first attempt to construct a model for the mechanism of adjustment in response to shear stress. We have been able to assign the function of load-bearing to the cytoskeleton based on ultrastructural studies, and modelling which predicts experimentally measured mechanical properties.

We began by defining the detailed forces acting on a monolayer resulting from laminar flow. The "bumpiness" of the monolayer creates an additional gradient of significant maginitude. The shear stress can vary by 30-40% of

average wall shear across individual cells. An imbalance in forces created by the gradient is enough to disturb intercellular adhesions, although it is of insufficient magnitude to remove a cell from the monolayer. Thus, the calculations predicted that cell-cell attachments would be preferentially disturbed in a laminar flow; and by inference, in turbulent flow (since responses are elicited at lower average wall shear). Moreover, we envisioned a specific role for stress fibers. They (as their name implies) might help transmit forces to the substrate, thereby sparing cell-cell attachments. This would have a stabilizing effect so that the monolayer could adjust and function normally with a constant load due to shear stress on the apical membrane. Observations of other investigators support this view; but we needed detailed ultrastructural information in order to asses our predictions. A method was desired which would provide information about 3-dimensional cytoarchitecture, cell-cell attachment structure, and the arrangement of stress fibers in the cell. In particular, Do stress fibers attach apically in aligned cells?; and, Were there additional changes in the cytoskeleton suggesting that stress fibers support loads on the top membrane?

Our first approach was to use confocal microscopy. Confocal imaging allows examination of 3-dimensional structure by focussing on specific planes within the cell, i.e. optically sectioning the cell. It was combined with immunofluorescence to examine microfilaments, stress fibers, and other architectural proteins associated with intercellular and cell-substrate adhesions.

Our studies confirmed that endothelial cells have a "fried-egg" shape *in vitro*. The cell periphery is flat. The nucleus creates a bulge in the center of the

cell, increasing the top to bottom thickness by 3-4X compared to the periphery. As cells orient, they adapt a "torpedo-like" shape where the central bulge is less pronounced. Moreover, stress fibers are redistributed from basal and peripheral locations. In aligned cells, elongated and aligned stress fibers are present in apical cell regions (such as above the nucleus). There are also changes in the cortical actin network, indicated by increased staining for F-actin with a diffuse pattern in apical regions.

Cell-cell attachment regions were altered by fluid flow as well. Both laminar and turbulent shear stress caused the removal of border staining for endoCAM, a probable cell-cell adhesion molecule which stains confluent BAEC along cell-cell attachments. Our hypothesis is that staining will reappear in the case of laminar flow, once cell adjustments are complete. BAEC in static culture do not silver stain at borders as well as BAEC *in vivo* [unpublished data]; and, vinculin and α-actinin staining is reduced from the borders of cells aligned for 36 hours compared to static controls. Thus, BAEC *in vitro* probably do not construct intercellular adhesions which are identical to BAEC *in vivo*. The situation worsens for cells exposed to flow--for comparable intercellular junctions to be reestablished may take additional time. Longer term experiments are needed to assess this possibility.

Apical attachments of stress fibers may include proteins used in focal adhesions. Thus, the arrangements of the architectural proteins vinculin and α-actinin were examined with confocal microscopy. Changes in α-actinin staining patterns suggested the existence of apical attachment complexes. A distinct punctate

pattern of staining was present in the apical regions of oriented cells which could not be detected in nonoriented cells. Moreover, increased diffuse cortical network staining suggested augumented F-actin crosslinking in the apical cytoplasm. In total, these findings reinforce the notion that F-actin and the cytoskeleton are important for force transmission. Stress fibers help to redistribute stresses from cell-cell junctions to focal contacts. The changes in junctional integrity, demonstrated by interruption of cell-cell border staining, may be a stimulus which drives intracellular events leading to shape change and/or migration and cell division (with turbulent shear stress).

The amount of useful information which could be obtained using confocal microscopy was limited. This technique has the transverse resolution of light microscopy, while structural details in cells can be on the scale of nanometers. Thus we turned to electron microscopy.

Examination of the cytoskeleton required a specialized technique whereby the membrane and cytoplasm are detergent extracted, leaving behind the cytoskeleton (and other insoluble proteins) which can be rotary shadowed with metal, creating a replica which is viewed on a tilting stage in order to obtain stereoscopic photographs. This technique can be used with thin cells, and preserves the 3-dimensional arrangement of the cytoskeleton. It has been previously used to study platelets, macrophages, and leukocytes. Endothelial cells are larger and more complex in structure; moreover, they grow in a monolayer so that the cells must be observed as a group instead of individually as is possible with the other cell types mentioned. Thus, the technique was modified in some ways

to achieve comparable results, and eventually yielded the first detailed images of the endothelial cytoskeleton.

The cytoskeleton is a porous network created by intersecting filaments which are predominantly F-actin. The network fills the cytoplasm between top and bottom cell membranes, and connects to both in many places. Along the top membrane of nonaligned cells, fibers occassionally coalesce and protrude as globular structures which are remnants of microvilli. Actin filaments were the only type attaching to the cell membrane. Intermediate filaments are in lower concentrations throughout the cell except near the nucleus. Microtubules were seldom observed. Our findings support the hypothesis that intermediate filaments partition the cell into various compartments; and that microtubules serve as a guidance system.

Stress fibers pass above the nuclei of aligned cells, reinforcing the network in the apical regions. Actin in cells is distributed between several major pools [Hartwig, 1991; Stossel, 1986]:

- the monomeric form is present in the cytoplasm.
- filaments are used to create space filling networks such as the cortical network.
- filaments are used to created lamellar submembranous networks, as has been demonstrated in platelets and erythrocytes.

• filaments are grouped together into bundles, such as stress fibers in BAEC.

The cell has an extensive complement of proteins which regulate actin. Based on function, there are three major groups of regulatory proteins [Hartwig, 1991]: architectural proteins (which create higher-order actin filament structures); assembly proteins (which regulate the assembly state of actin between monomers and filaments); and proteins regulating interactions with myosin. Changes in one component of a cell's actin are produced by shifts from other pools. In the endothelial cell, we have detected actin in the cortical network, as stress fibers, and cytoplasmic pools of monomeric actin (G-actin). There is no evidence for a lamellar network. When stress fibers appear in aligned cells, they must either be synthesized from monomeric actin; or they are produced by coalescing pre-existing F-actin. Thixotropy studies of cytoplasm and F-actin solutions by others imply that stress fibers may be formed as a result of cytoplasmic streaming [Buxbaum et. al., 1987]. According to this hypothesis, when one region of cytoplasm is displaced relative to another, intervening F-actin is aligned and possibly bundled to form stress fibers. This could be a self perpetuating process, since the bundles tend to concentrate stress locally--thus the fiber could propogate until a substrate or membrane attachment point is reached which can support the locally elevated stress. Further experiments are required to asses these possibilities.

Our findings strongly implicate the cytoskeleton as the load bearing element inside of the cell. Therefore, we analyzed the mechanical properties of the network in order to quantitatively assess this possibility. Modelling the actin network as an open cell foam, we obtained estimates of the elastic moduli. These predictions were in excellent agreement with experimental measurements in the

literature using cytoplasm and F-actin solutions. Stress fibers would serve to increase the overall network modulus, and thus decrease the deformability of the cells. Moreover, they serve as stress concentration markers within the network--their redistribution when the cells experience shear stress may indicate where resultant stress becomes concentrated within the cell. In support of this concept is the observation that stress fibers usually have one attachment point near the nucleus, which would be expected to be a high stress region due to the nuclear bulge; and because the nuclear space represents a discontinuity in the actin network. These tend to concentrate stress just as a hole in a metal sheet is a site of increased stress with an applied load.

The network shear modulus is of sufficient magnitude to withstand physiologic shear stress without significant deformation of the cell. Thus, there is seemingly no functional advantage achieved by reinforcing the network with stress fibers. However, our modelling does not account for changes in network cross-linking when cells align. The cortical actin filaments are assumed to be rigidly cross-linked. This is not the case in cells, where there are specific proteins which create these junctions with finite bond strengths (noncovalent protein-protein bonds). The cortical network in nonaligned cells may be cross-linked with less intrinsic mechanical strength, since these cells have not been exposed to fluid flow. One major change which may occur with alignment is reinforcement of the network by increasing cross-linking (or creating stronger cross-links). Stress fibers would be of benefit in this case, reinforcing the network before and/or while cross-links are constructed.

The possiblity that forces are easily resisted by cortical network focuses attention on the network-membrane interactions. The structures connecting the cytoskeletal network to the plasma membrane should be explored in further detail. They may be the "switch" which "turns-on" the cells when they are exposed to flow.

Overall, work in this thesis brings us closer to understanding the mechanism of flow induced response in endothelium. A structure-function relationship is established: the cytoskeleton supports loads on the cell from shear stress. Understanding the cell response to shear stress will aid efforts to define the role of hemodynamics in the pathogenesis of athersclerosis.

REFERENCES

1. Abercrombie, M, Heagsren, J, Pegrum, SM, Exp. Cell. Res. (1971) 67: 359.
2. Adams, DS "Mechanisms of cell shape change: the cytomechanics of cellular response to chemical environment and mechanicsl loading", Journal of Cell Biology (1992) 1127: 83-93.
3. Albelda, SM, Muller, WA, Buck, CA, Newman, PJ "Molecular and cellular properties of PECAM-1 (endoCAM/CD31): A novel vascular cell-cell adhesion molecule", Journal of Cell Biol. (1991)114(5): 1059-1068.
4. Albelda, SM, Oliver, PM, Rower, LH, Buck, CA "EndoCAM: A novel endotheiial cell-cell adhesion molecule", Journal of Cell Biol. (1990)110: 1227-1237.
5. Baron, MD, Davison, MD, Jones, P, Critchley, DR "The structure and function of α-actinin", Biochemical Society Transactions (1987)15: 796-798.
6. Bell, GI "Models for the specific adhesion of cells to ceils", Science (1978) 200: 618.
7. Benjamin, TB "Shearing flow over a wavy boundary", J. of Fluid Mechanics (1959) 6: 161-205.
8. Blanchard, A, Ohanian, V, Critchley, DR "The structure and function of α-actinin", Journal of Muscle Research and Cell Motility (1989)10: 280-289.
9. Branton, DC, Cohen, CM, Tyler, J "Interaction of cytyskeletal proteins on the human erythrocyte membrane", Cell (1981) 24: 24-32.
10. Burridge, K, Fath, K, Kelly, T, Nuckolls, G, Turner, C, Ann. Rev. Cell Biol. (1988) 4: 487.
11. Bussolari, SR "The dynamic response of vascular endothelium to fluid shear stress *in vitro*", Ph.D. Thesis, MIT, 1983.
12. Bussolari, SR, Dewey, CF Jr, Gimbrone, MA Jr "Apparatus for subjecting living cells to fluid shear stress", Rev. Sci. Instruments (1982) 53(12): 1851-1854.
13. Buxbaum, RE, Dennerll, T, Weiss, S, Heidemann, SR "F-actin and microtubule suspensions as indeterminate fluids", Science (1987) 235:

1511-14.

14. Caponi, EA, Fornberg, B, Knight, DD, McLean, JW, Saffman, PG, Yuen, HC "Calculations of laminar viscous flow over a moving wavy surface", J. of Fluid Mechanics (1982) 124: 347-362.

15. Caro, CG, Fitz-Gerald, JM, Schroter, RC "Atheroma and arterial wall shear. Observation, correlation and proposal of a shear-dependent mass transfer mechanism for atherogenesis", Proc. R. Soc. Lond. B Biol. Sci. (1971) 365: 92.

16. Cassimeris, L, Pryer, NK, Salmon, ED "Real time observations of microtubule dynamic instability in living cells", Journal of Cell Biology (1988) 107: 2223-31.

17. Chien, S, Sang, KP, Skalak, R, Usumi, S, Tozoren, A "Theoretical and experimental studies on viscoelastic properties of erythrocyte membrane", Biophysical Journal (1978) 24: 463-87.

18. Cortese, JD, Frieden, C "Microheterogeneity of actin gels formed under controlled linear shear", Journal of Cell Biology (1988) 107: 1477-87.

19. Daniels, M "The role of microtubules in the growth and stabilization of nerve fibers", Annu. N.Y. Acad. Sci. (1975) 253: 535-44.

20. Davies, PF "Flow modulation of endothelial stimulus-response coupling and transduction", 31st annual meeting of The American Society for Cell Biology, Boston, MA (1991).

21. Davies, PF, Dewey, CF Jr, Bussolari, SR, Gordon, EJ, Gimbrone, MA Jr "Influence of hemodynamic forces on vascular endothelial function: *In vitro* studies of shear stress and pinocytosis in bovine aortic cells" J. Clin. Invest. (1984)73: 1121-1129.

22. Davies, PF, Remuzzi, A, Gordon, EJ, Dewey, CF Jr, Gimbrone, MA Jr "Turbulent fluid shear stress induces vascular endothelial cell turnover *in vitro*", Proc. Natl. Acad. Sci. USA (1986) 83: 2114-2117.

23. Davies, PF, Robotenskyj, A, McKibben, S, Dull, RO, Griem, MC "Measurements of endothelial cell adhesion and the dynamics of focal contacts in real time using confocal image analysis" (1992) submitted.

24. Davis, PH "Effects of non-Newtonian fluid behavior on wall shear in a separated flow region", Abstract of First World Congress of Biomechanics, Vol. 2 (1990) 301.

25. Deforrest, JM, Hollis, TM "Shear stress and aortic histamine synthesis", Am. J. Physiol. (1978)236: H701-H705.

26. Dejana, E, Colella, S, Conforti, G, Abbadini, M, Gaboli, M, Marchisto, PC "Fibronectin and vitronectin regulate the organization of their respective Arg-Gly-Asp adhesion receptors in cultured human endothelial cells", Journal of Cell Biology (1988) 107: 1215-23.

27. DePaola, N "Focal and regional responses of endothelium to disturbed flow *in vitro*", MIT Ph.D. Thesis (1991).

28. DePaola, N, Gimbrone, MA Jr, Dewey, CF Jr "Vascular endothelium responds to fluid shear stress gradients", Arteriosclerosis and Thrombosis (1992) 12: 1254-57.

29. DePaola, N, Ronquist, EM, Dewey, CF Jr "Wall shear stresses produced by surface protuberances in a linear shear flow", International Conference on Spectral and High Order Methods for Partial differential equations, ICOSA-HAM (1989) Como, Italy.

30. Dewey, CF "Dynamics of arterial flow", Adv. Exp. Med. Biol. (1979) 115: 55.

31. Dewey, CF Jr, Bussolari, SR, Gimbrone, MA Jr, Davies, PF "The dynamic response of vascular endothelial cells to fluid shear stress", Journal of Biomechanical Engineering (1981)103: 177.

32. Dewey, CF Jr, DePaola, N "Exploring flow-cell interactions using computational fluid dynamics", ASME/JSME Tissue Engineering Symposium, ASME Winter Annual Meeting (1989) San Franscisco.

33. Dewey, CF Jr., Gimbrone, MA Jr., Bussolari, SR, White, GE, Davies, PF "Response of vascular endothelium to unsteady fluid shear stress *in vitro*", Fluid Dynamics as a Localizing Factor for Atherosclerosis, G. Schettler et al., eds., Springer-Verlag (1983) 182-187.

34. DHEW publication no. (NIH) 82-2035, Report of the working group of arteriosclerosis of the Natl. Heart, Lung, and Blood Inst., vol. 2, Washington DC: Government printing office (1981).

35. Diamond, SL, Eskin, SG, McIntire, LV "Fluid flow stimulates tissue plasminogen activator secretion by cultured human endothelial cells", Science (1989)253: 1483-1485.

36. Duguid, JB "Thrombosis as a factor in the pathogenesis of coronary atherosclerosis", J. Pathol. Bacteriol. (1948) 58: 207-12.

37. Ettenson, DS, Gotlieb, AI "Centrosomes, microtubules, and microfilaments in the reendotheliazation and remodeling of double-sided *in vitro* wounds", Lab. Invest. (1992) 66: 722-33.

38. Evans, EA, LaCelle, PL "Intrinsic material properties of the erythrocyte membrane indicated by mechanicsl analysis of deformation", Blood (1975) 45: 29-43.

39. Fischer, PF, Patera, AT "Parallel spectral element solution of the Stokes problem", J. Comput. Phys., submitted.

40. Flaherty, JR, Pierce, JR, Ferrars, VJ, Patel, DJ, Tucker, WK, Fry, DL "Endothelial nuclear patterns in the canine arterial tree with particular reference to hemodynamic events", Circ. Res. (1972) 30: 23.

41. Folie, BJ, McIntire, LV "Mathematical analysis of mural thrombogenesis", Biophysical Journal (1989) 56: 1121-1141.

42. Fox, JA, Hugh, AE "Localization of atheroma: A theory based on boundary layer separation", British Heart Journal (1966) 28: 388-399.

43. Fox, JEB "Linkage of a membrane skeleton to integral membrane glycoproteins in human platelets", J. Clin. Invest. (1985) 767: 1673-83.

44. Franke, R-P, Grafe, M, Schnittler, H, Seiffge, D, Mittermayer, C, Drenckhahn, D "Induction of human vascular endothelial stress fibers by fluid shear stress", Nature (1984)307: 648-649.

45. Friedman, MH, Bargeron, CB, Hutchins, GM, Mark FF, Deters, OJ "Hemodynamic measufements in human arterial casts and their correlation with histology and luminal area", J. Biomech. Eng. (1980) 102: 247.

46. Friedman, MH, Peters, OJ, Bargeron, CB, Hutchins, GM, Mark, FF "Shear dependent thickening of the human arterial intima", Atherosclerosis (1986) 60: 161-171.

47. Frokjaer-Jensen, J "The plasmalemmal vesicular system in capillary endothelium" , in Prog. Appl. Microcirc., vol. 1 (1983) 17-34.

48. Fry, DL "Acute vascular endothelial changes associated with increased blood velocity gradients", Circulation Research (1968)22: 165-197.

49. Fry, DL "Response of arteral wa. to certain physical factors", Ciba Found. Symp. (1972)12: 93-110.

50. Fry, DL "Hemodynamic forces in atherogenesis", Cerebrovascular Diseases, P. Scheinberg, ed., Raven Press. (1976) 77-95.

51. Fung, YC, Liu, SQ "Elementary mechanics of the endothelium of blood vessels" (1992) submitted.

52. Furchgott, RF, Zawadzki, JV "The obligatory role of endothelial cells in the relaxation of arterial smooth muscle by acetylcholine", Nature (1986) 288:

373-376.

53. Fuster, V, Badimon, JJ, Chesebro, JH "The pathogenesis of coronary artery disease and the acute coronary syndromes", New England Journal of Medicine (1992) 326: 242-50, 310-18.

54. Geiger, B, J. Cell Science Suppl. (1987) 8: 251.

55. Geiger, B "Cytoskeleton-associated cell contacts", Current Opinion in Cell Biology", (1989)1: 103-109.

56. Gibson, LJ, Ashby, MF, Cellular Solids: Structure and Properties (1988) Pergamon Press, Oxford.

57. Giddens, DP, Zarins, CK, Glagov, S, Bharadraj, BK, Ku, DN "Flow and atherogenesis in the human carotid bifurcation", in Fluid dynamics as a localizing factor in atherosclerosis, Schnettler, G ed., Springer-Verlag (1983) 38-45.

58. Gimbrone, MA Jr., personal communication.

59. Gimbrone, MA Jr. "Culture of vascular endothelium", Chapter 1 in Progress in Hemostasis and Thrombosis, Vol. 3, Spaet, T ed.; New York: Grune and Stratton (1976) 1-28.

60. Gimbrone, MA "Vascular endothelium: nature's blood container", in Vascular Endothelium in Hemostasis and Thrombosis (Chapter 3), Gimbrone, MA ed., Churchill Livingstone, Edinburgh (1986) 1-13.

61. Gimbrone, MA "Vascular endothelium: nature's blood compatible container", Ann. N.Y. Acad. Sci. (1987) 100: 5-10.

62. Gimbrone, MA Jr "Endothelial dysfunction and atherosclerosis", J. Cardiac. Surgery (1989) 4(2): 180-183.

63. Gimbrone, MA Jr "Endothelial dysfunction and the pathogenesis of atherosclerosis", In: Fidge, NH, Nestel, PJ, eds, Atherosclerosis VII, Proc. 7th Intl. Symp. on Atherosclerosis, Amsterdam: Excerpta Medica, (1986) 367-369.

64. Gimbrone, MA Jr., unpublished data.

65. Gimbrone, MA Jr, Bevilacqua, MP, Cybulsky, MI "Endothelial-dependent mechanisms of leukocyte adhesion in inflammation and atherosclerosis", Annals NY Acad. Sci. (1990) 598: 77-85.

66. Goldberg, IH "Mechanism of neocarzinostatin action: role of DNA microstructure in determination of chemistry of bistranded oxidative damage", Accounds of Chemical Research (1991) 24: 191-96.

67. Gorlin, JB, Yamin, R, Egan, S, Stewart, M, Stossel, TP, Kwiatkowski, DJ, Hartwig, JH "Human endothelial actin-binding protein: A molecular leaf spring", Journal of Cell Biology *1990) 111: 1089-1105.

68. Gotlieb, AI, Langille, BL, Wong, MKK, Kim, DW "Biology of disease: Structure and function of the endothelial cytoskeleton", Lab. Invest. (1991)65(2): 123.

69. Gotlieb, AI, McBurnie-May, I, Subrahmanyan, L, Kalmins, VI, Journal of Cell Biology (1981) 91: 589-94.

70. Gotlieb. AI, Subrahmanyan, L, Kalmins, VI, Journal of Cell Biology (1983) 96: 1266-72.

71. Hara, T, Mei, CC "Oscillating flows over periodic ripples", J. of Fluid Mechanics (1990) 211: 183-209.

72. Harrigan, TP "Transduction of stress to cellular signals", Abstract: First World Congress of Biomechanics (1990) vol. II: 51.

73. Hartwig, JH "Mechanisms of cell movement", in The Lung: Scientific Foundations; Crystal, RG, West, JB, eds. Raven Press (1991) 141-53.

74. Hartwig, JH "Mechanisms of actin rearrangements mediating platelet activation", Journal of Cell Biology (1992) 118: 1421-1442.

75. Hartwig, JH, Chambers, KA, Stossel, TP "Asociation of gelsolin with actin filaments and cell membranes of macrophages and platelets", Journal of Cell Biology (1989) 108: 467-79.

76. Hartwig, JH, Desisto, M "The cytoskeleton of the resting human blood platelet: Structure of the membrane skeleton and its attachments to actin filaments", Journal of Cell Biology (1991) 112: 407-25.

77. Hartwig, JH, Janmey, P "Stimulation of a calcium dependent actin nucleation activity by phorbol 12-myristate 13-acetate in rabbit macrophage cytoskeletons", Biochim. Biophys. Acta (1989) 1010: 64-71.

78. Hartwig, JH, Kwiatkowski, DJ "Actin binding protein", Curr. Opinion in Cell Biology (1991) 3: 87-97.

79. Hartwig, JH, Shevlin, P, Journal of Cell Biology (1986) 103: 1007-1020.

80. Haugland, RP Molecular Probes: Handbook of fluorescent probes and research chemicals (1989).

81. Heuser, JE, Kirschner, MW "Filament organization revealed in platinum replicas of freeze-dried cytoskeletons", Journal of Cell Biology (1980) 86: 212-34.

82. Hubbe, MA "Adhesion and detachment of biological cells *in vitro*", Progress in Surface Science (1981) 11: 65.

83. Hyman, WA "Shear flow over a protrusion from a plane wall", J. Biomechanics (1972) 5: 45-48.

84. Ingber, DE "Fibronectin controls capillary endothelial cell growth by modulating cell shape", Proc. Natl. Acad. Sci. USA (1990) 87: 3579-3583.

85. Ingber, DE, Folkman, J "Tension and compression as basic determinants of cell form and frunction: utilization of a cellular tensegrity mechanism", in Cell Shape: Determinants, Regulation, and Regulatory Role, Academic Press (1989) 4-31.

86. Ito, J, Zaner, KS, Stossel, TP "Nonideality of volume flows and phase transitions of F-actin solutions in response to osmotic stress", Biophysical Journal (1987) 51: 745-53.

87. Janmey, PA, Hvidt, S, Lamb, J, Stossel, TP "Resemblance of actin-binding protein/actin gels to covalently crosslinked networks", Nature (1990) 345: 89-92.

88. Janmey, PA, Hvidt, S, Peetermans, J, Lamb, J, Ferry, JD, Stossel, TP, Biochemistry (1988) 27: 8218-28.

89. Janmey, PA, Euteneuer, U, Traub, P, Schliwa, M "Viscoelastic properties of vimentin compared with other filamentous biopolymer networks", Journal of Cell Biology (1991) 113(1): 155-160.

90. Jo, H, Dull, RO, Hollis, TM, Tarbell, JM "Endothelial albumin permeability is shear dependent, time dependent, and reversible", Am. J. Physiology, Heart & Circulation Physiology (1991) 260: H1992-H1996.

91. Kappen, LS, Goldberg, IH "Stabilization of neocarzinostatin nonprotien chromophore activity by interaction with apoprotein and with HeLa cells", Biochemistry (1980) 19: 4786-90.

92. Kappen, LS, Napier, MA, Goldberg, IH "Roles of chromophore and apoprotien in neocarzinostatin action", Proc. Natl. Acad. Sci. USA (1980) 77: 1970-74.

93. Karino, T, Goldsmith, HL "Distorted flow in models of branching vessels", Trans. Am. Soc. Artif. Internal Organs (1980) 26: 500.

94. Karino, T, Montomiya, M, Goldsmity, HL "Flow patterns in model and natural branching vessels", in Fluid dynamics as a localizing factor in atherosclerosis, Schnettler, G ed., Springer-Verlag (1983) 60-83.

95. Kerst, A, Chmielewski, C, Livesay, C, Buxbaum, RE, Heidemann, SR "Liquid crystal domains and thixotropy of filamentous actin suspensions", Proc. Natl. Acad. Sci. USA (1990) 87: 4241-45.

96. Killer A, Kaley, G "Prostaglandins mediate arteriolar dilation to increased blood flow velocity in skeletal muscle microcirculation", Circ. Res. (1990) 67: 529-34.

97. Kim, DW, Langille, BL, Wong, MKK, Gotlieb, AI "Patterns of endothelial microfilament distribution in the rabbit aorta *in situ*", Cir. Res. (1989)64: 21.

98. Kim, DW, Gotlieb, AI, Langille, BL "*In vivo* modulation of endothelial F-actin microfilaments by experimental alterations in shear stress", Arteriosclerosis (1989)9: 439.

99. Kiya, M, Arie, M "Viscous shear flow past small bluff bodies attached to a plane wall", J. of Fluid Mechanics (1975) 69(4): 803-823.

100. Kishino, A, Yanagida, A "Force measurements by micro manipulation of a single actin filament by glass needles", Nature (1988) 334: 74-76.

101. Kolodney, MS, Wysolmerski, RB "Isometric contraction by fibroblasts and endothelial cells in tissue culture: A quantitative study", Journal of Cell Biology (1992) 117: 73-82.

102. Kreis, TE, Birchmeier, W "Stress fibers sarcomeres of fibroblasts are contractile", Cell (1980) 22: 555.

103. Ku, DN, Giddens, DP "Pulsatile flow in a model carotid bifurcation", Arteriosclerosis (1983) 3: 31.

104. Ku, DN, Giddens, DP, Zarins, CK, Glagov, S "Pulsatile flow and arteriosclerosis in human carotid bifurcation: positive correlation between plauque location and low and oscillating shear stress", Arteriosclerosis (1985) 5: 293.

105. Ku, DN, Liepsch, D "The effects of non-Newtonian viscoelasticity and wall elasticity on flow at a 90° bifurcation", Biorheology (1986) 23: 359-70.

106. Kupfer, A, Demert, G, Singer, SJ, Proc. Natl. Acad. Sci., USA (1983) 80: 7224-28.

107. Laemmli, UK, Nature (London) (1970) 227: 680-685.

108. Langille, BL, Benedeck, MP, Keeley, FW "Adaptions of carotid arteries of young and mature rabbits to reduced carotid blood flow", Am. J. Physiol. (1989) 256: H931-H939.

109. Langille, BL, Graham, JJK, Kim, D, Gotlieb, AI "Dynamics of shear-induced redistribution of F-actin in endothelial cells *in vivo*", Artersclerosis and Thrombosis (1991)11(6): 1814.

110. Langille, BL, O'Donnell, F "Reductions in arterial diameter produced by chronic decreases in blood flow are endothelium dependent", Science (1986) 231: 405-7.

111. Langille, BL, Reidy, MA, Kline, RL "Injury and repair of endothelium at sites of flow disturbances near abdominal aortic coarctations in rabbits", Arteriosclerosis (1986)6: 146-154.

112. Levesque, MJ, Liepsch, D, Moranec, S, Nerem, RM "Correlation of endothelial cell shape and wall shear stress in a stenosed dog aorta", Arteriosclerosis (1986) 6: 220-229.

113. Lewis, WH, Lewis, MR "Behavior of cells in tissue cultures", in General Cytology, Condy, EV, ed., Univ. of Chicago Press, Chicago (1924) 385-447.

114. Ling, SC, Atabeck, HB, Fry, DL, Patel, DJ, Janick, JS. Circulation Research (1968)23: 789.

115. Lipton, BH, Bensch, KG, Karasek, MA "Microvessel endothelial cell transdifferentiation: phenotypic characterization", Differentiation (1991) 46: 117-133.

116. Lowry, OH, Rosebrough, NJ, Far, AL, Randall, RJ, Journal of Biological Chemistry (1951) 193: 265-75.

117. Luna, EJ, Hitt, AL "Cytoskeletal-plasma membrane interactions", Science (1992) 258: 955-64.

118. Lux, SE, Nature (1979) 281: 426.

119. Lyne, WH "Unsteady viscous flow over a wavy wall", J. of Fluid Mechanics (1971) 50(1): 33-48.

120. Maday, Y, Patera, AT "Spectral element methods for the incompressible Navier-Stokes equations", State of the Art Surveys on Computational Mechanics, eds: Noor, AK, Oden, JT, (1989) 71-143.

121. Matsudaira, P "Modular organization of actin crosslinking proteins", TIBS (1991) 16: 87-92.

122. McIntire, LV, Diamond, SL, Shanefkin, JD, Eskin, SG "Regulation of gene expression in endothelial cells exposed to shear stress: Implications for thrombosis, atherosclerosis, and intimal hyperplasia", (abstract) First World

Congress of Biomechanics (1990) vol. II: 314.

123. McKenna, NM, Wang, Y-L "Possible translocation of actin and alpha-actinin along stress fibers", Exptl. Cell Res. (1986)167: 95-105.

124. Molony, L, Armstrong, L "Cytoskeletal reorganizations in human umbilical vein endothelial cells as a result of cytokine exposure", Exptl. Cell. Res. (1991) 196: 40-48.

125. Montenegro, MR, Eggen, DA "Topolography of atherosclerosis in the coronary arteries", Laboratory Investigation (1968) 18: 586-593.

126. Nerem, RM, Girard, PR "Hemodynamic influences on vascular endothelial biology", Toxic. Path. (1990) 18: 572-582.

127. Nerem, RM, Levesque, MJ, Cornhill, JF "Vascular endothelial morphology as an indicator of blood flow", ASME J. Biomech. Eng. (1981) 103: 172-176.

128. Nerem, RM, Seed, WA "An *in vivo* study of aortic flow disturbances", Cardiovasc. Res. (1972) 6: 1-14.

129. Olesen, S-P, Clapham, DE, Davies, PF "Haemodynamic shear stress activates a K^+ current in vascular endothelial cells", Nature (1988)221: 168-170.

130. Oosawa, F "Actin-actin bond strength and the conformational change of F-actin", Biorheology (1977) 14: 11-19.

131. Pollard, TD, Journal of Cell. Biochem. (1986) 31: 87-95.

132. Reidy, MA, Langille, BL "The effect of local blood flow patterns on endothelial cell morphology", Exp. Mol. Path. (1980)32: 276-289.

133. Ronquist, EM, Patera, AT "Spectral element multigrid. I. Formulation and numerical results", J. Sci. Comput. (1987) 2 (4): 389-406.

134. Ross, R "The pathogenesis of atherosclerosis-an update", New England Journal of Medecine (1986) 314: 488-99.

135. Ross, R Glumset, JA "The pathogenesis of atherosclerosis", New England Journal of Medicine (1976) 295: 369-77, 420-25.

136. Sachs, F "Mechanical transduction in biological systems", Crit. Rev. Biomed. Eng. (1988) 16: 146-69.

137. Sachs, F in "Cell Shape: Determinants, Regulation and Regulatory Role", eds: Stein, WD, Bronner, F (1989) Academic, San Diego, CA: 63-92.

138. Satcher, RL, Bussolari, SR, Gimbrone, MA, Dewey, CF "The distribution of fluid forces on model arterial endothelium using computational fluid dynamics", J. Biomech. Eng. (1992) 114: 309-16.

139. Sato, M, Levesque, MJ, Nerem, RM "Micropipette aspiration of cultured bovine aortic endothelial cells exposed to shear stress", Arteriosclerosis (1987) 7(3): 276-286.

140. Sato, M, Theret, DP, Wheeler, LT, Ohshima, N, Nerem, RM "Application of the micropipette technique to the measurement of cultured porcine aortic endothelial cell viscoelastic properties", J. Biomech. Eng. (1990) 112: 263-68.

141. Sato, M, Schwartz, WH, Pollard, TD "Dependence of the mechanical properties of actin/α-actinin gels on deformation rate", Nature (1989) 325: 828-30.

142. Schliwa, M, van Blerkam, J, Porter, K "Stabilization of the cytoplasmic ground substance in detergent opened cells and a structural and biochemical analysis of its composition", Proc. Natl. Acad. Sci., USA (1981) 80: 5417-20.

143. Schnittler, H, Franke, R-P, Drenckhahn, D "Role of the endothelial actin filament cytoskeleton in rheology and permeability", Z. Kardiologie (1989) Supl. 78(6): 1-4.

144. Schwartz, CJ, Mitchell, JR "Observations on localizations of arterial plaques", Cir. Res. (1972) 11: 63-73.

145. Sdougos, HP, Bussolari, SR, Dewey, CF Jr "Secondary flow and turbulence in a cone-and-plate device", J. of Fluid Mechanics (1984) 138: 379-404.

146. Shen, J "Signal transduction by fluid shear stres in vascular endothelium", Ph.D. Thesis, MIT (1992).

147. Shen, J, Luscinskas, FW, Gimbrone, MA Jr, Dewey, CF Jr "Flow modulates cytosolic calcium response of vascular endothelial cells to adenine nucleotides", Am. J. of Physiology (1991) 262: C384-C390.

148. Shen, J, Luscinskas, FW, Connolly, A, Dewey, CF Jr, Gimbrone, MA Jr "Fluid shear stress modulates cytosolic free calcium concentration in vascular endothelial cells", Am J. Physiol. (1992) in press.

149. Silkworth, JB, Stehbens, WE "The shape of endothelial cells in *en face* preparations of rabbit blood vessels", Angiology (1975) 26: 474-487.

150. Simionescu, M, Simionescu, N, Silbert, JF, Palade, GE "Different microdomains on the luminal surface of the capillary endothelium I: preferential

distribution of anionic sites", Journal of Cell Biology (1981) 90: 605-13.

151. Slot, J, Genze H "A new method of preparing gold probes for multiple-labeling cytochemistry", Eur. J. Cell. Biol. (1985) 38: 87-93.

152. Spain, DM "Atherosclerosis", Scientific American (1966) 215: 48-56.

153. Stehbens, WE "Turbulence of blood flow", Q. J. Exp. Physiol. (1959)44: 111-117.

154. Stossel, TP "The actin system and the rheology of peripheral cytoplasm", Biorheology (1986) 23: 621-31.

155. Stossel, TP "The mechanical responses of white blood cells", Inflammation: Basic principles and Clinical correlates, Gallin, JI, Goldstein, IM, Synderon, R, eds. (1988) Raven Press, New York: 325-42.

156. Suzuki, A, Yamazaki, M, Ito, T "Osmoelastic coupling in biological structures: formation of parallel bundles of actin filaments in a crystalline-like sturcture caused by osmotic stress", Biochemistry (1989) 28: 6513-18.

157. Taniguchi, M, Kamiya, Y "Morphological changes and crystal structure of skeletal muscle actin", Nuclear Instruments and Methods (1983) 208: 541-44.

158. Theret, DP, Levesque, MJ, Sato, M, Nerem, RM, Wheeler, LT "The application of a homogeneous half-space model in the analysis of endothelial cell micropipette measurements", J. Biomech. Eng. (1988) 110: 190-99.

159. Virchow, R "Phlogose und thrombose ingefassytem, gesammelte abhandlungen zur wissen schaft lichen medicin", Franfurt-am-main, Germany: Meidinger Sohn (1856) 458.

160. von Rokitansky, C; A Manual of Pathologic Anatomy, Day, GE, ed., trans. London: Sydenham Society, vol 4. (1852) 261.

161. Wechezak, AR, Wight, TN, Viggers, RF, Sauvage, LR "Endothelial adherence under shear stress is dependent upon microfilament reorganization", Journal of Cell Physiology (1989) 139: 136-149.

162. Weinbaum, S, Tzehgai, G, Ganatos, P, Pfeffer, R, Chien, S "Effect of cell turnover and leaky junctions on arterial macromolecular transport", Am. J. Physiology, Heart & Circulation Physiology (1985)248: H945-H960.

163. Weskler, BB, Jaffe, EA "Prostacyclin and the endothelium", in Vascular Endothelium in Hemostasis and Thrombosis (Chapter 3), Gimbrone, MA ed., Churchill Livingstone, Edinburgh (1986) 40-56.

164. White, GE, Fujiwara, K "Expression and intracellular distribution of stress fibers in aortic endotheilium", Journal of Cell Biology (1986)103: 63-70.

165. White, GE, Gimbrone, MA Jr, Fujiwara, K "Factors influencing the expression of stress fibers in vascular endothelial cells *in situ*", Journal of Cell Biology (1983) 97: 416.

166. Wissler, RM "Relationship of atherosclereosis in young men to serum lipoprotein cholesterol concentrations and smoking", J. Am. Med. Assoc. (1990) 264: 3018-24.

167. Wong, AJ, Pollard, TD "Actin filament stress fibers in vascular endothelial cells *in vivo*", Science (1983)219: 867-869.

168. Wong, AJ, Pollard, TD, Herman, IM "Actin filament stress fibers in vascular endothelial cells *in vivo*", Science (1983) 219: 867-69.

169. Yoshizumi, M, Kurihana, H, Sugiyama, T, Takaku, F, Yanagisana, m, Masaki, T, Yasaki, Y "Hemodynamic shear stress stimulates endothelin production by cultured endothelial cells", Biochem. Biophys. Res. Commun. (1989) 161: 859-64.

170. Zand, T, Nunnari, JJ, Hoffman, AH, Savilonis, BJ, MacWilliams, B, Majno, G, Joris, I "Endothelial adaptions in aortic stenosis: correlation with flow parameters", Am. J. Pathology (1988)133: 407-418.

171. Zarins, CK, Zatina, MA, Giddens, DP, Ku, DN, Glagov, S "Shear stress regulation of arterial lumen diameter in experimental atherogenesis", J. Vasc., Surg. (1987) 5: 413-420.

APPENDIX: LINEAR FLOW OVER A WAVY WALL

The governing Navier-Stokes equations and boundary conditions are given in Eqs. (1) and (2), and two paragraphs following them. For the Reynolds number Re approaching zero, the equations reduce to those of Stokes with boundary conditions appropriate to linear shear flow:

$$\frac{\partial u}{\partial x} + \frac{\partial v}{\partial y} + \frac{\partial w}{\partial z} = 0 \tag{a-1}$$

$$\frac{\partial^2 u}{\partial x^2} + \frac{\partial^2 u}{\partial y^2} + \frac{\partial^2 u}{\partial z^2} = \frac{1}{\mu}\frac{\partial P}{\partial x} \tag{a-2}$$

$$\frac{\partial^2 v}{\partial x^2} + \frac{\partial^2 v}{\partial y^2} + \frac{\partial^2 v}{\partial z^2} = \frac{1}{\mu}\frac{\partial P}{\partial y} \tag{a-3}$$

$$\frac{\partial^2 w}{\partial x^2} + \frac{\partial^2 w}{\partial y^2} + \frac{\partial^2 w}{\partial z^2} = \frac{1}{\mu}\frac{\partial P}{\partial z} \tag{a-4}$$

$$\text{for} \quad y \to \infty, \; u = \sigma y, \quad \text{and} \quad (v, w) = 0 \tag{a-5}$$

where σ is the shear rate. The boundary condition at the surface requires (u, v, w) to vanish.

A linearized solution is sought: that is, the velocity field is described by the solution to the problem of linear shear flow over a flat wall (Couette flow) plus a small perturbation caused by wall waviness. The velocity perturbation must vanish at infinity, recovering Eq. (a-5), and the sum of the velocity perturbations and the linear shear flow must be zero at the perturbed wall surface.

Linearization of the Equations

The wavy wall can be expressed in analytical form by the equation:

$$y = \eta \equiv \hat{\eta}\, e^{i(\alpha x + \beta z)} \tag{a-6}$$

Only the real part of Eq. (a-6) is taken to have physical significance. Equation (a-6) defines a surface with waviness in both the x and z directions with amplitude $\hat{\eta}$ and wavenumbers α and β, respectively. To facilitate manipulation of the

equations, the symbol η will be used to indicate the surface, implying the right-hand side of Eq. (a-6).

The form assumed for the velocities and pressure are as follows:

$$u = U + \hat{u}(y)e^{i(\alpha x + \beta z)} \tag{a-7}$$

$$v = \hat{v}(y)e^{i(\alpha x + \beta z)} \tag{a-8}$$

$$w = \hat{w}(y)e^{i(\alpha x + \beta z)} \tag{a-9}$$

$$P = \hat{P}(y)e^{i(\alpha x + \beta z)} \tag{a-10}$$

$U = \sigma y$ is the Couette flow solution. The form of the pressure and velocity perturbations are the product of: 1) an unknown function of y alone; and 2) a periodic function of x and z that matches the form of the boundary η. The boundary conditions on the velocities are:

at the surface, $y = \eta$:

$$\hat{u}(\eta) + \sigma\eta = 0 \tag{a-11}$$

$$\hat{v}(\eta) = 0 \tag{a-12}$$

$$\hat{w}(\eta) = 0 \tag{a-13}$$

and, for $y \to \infty$:

$$\hat{u}(\infty) = \hat{w}(\infty) = \hat{v}(\infty) = 0 \tag{a-14}$$

$$\hat{u}'(\infty) = \hat{v}'(\infty) = \hat{w}'(\infty) = 0 \tag{a-15}$$

where primes denote differentiation with respect to y.

When the velocities and pressure given by Eqs. (a-7) - (a-11) are substituted in Eqs. (a-1) - (a-4), the following results:

$$i\alpha\hat{u} + \hat{v}' + i\beta\hat{w} = 0 \tag{a-16}$$

$$\hat{u}'' - K^2\hat{u} = \frac{1}{\mu}\, i\alpha\hat{P} \tag{a-17}$$

$$\hat{v}'' - K^2\hat{v} = \frac{1}{\mu}\, i\alpha\hat{P}' \tag{a-18}$$

$$\hat{w}'' - K^2\hat{w} = \frac{1}{\mu}\, i\beta\hat{P} \tag{a-19}$$

where

$$K^2 = \alpha^2 + \beta^2 \tag{a-20}$$

By some algebraic manipulation, Eqs. (a-16) through (a-19) can be combined to produce the following single fourth-order differential equation in terms of K:

$$\hat{v}'' - K^2\hat{v} = \frac{1}{K^2}\,(\hat{v}'''' - K^2\hat{v}'') \tag{a-21}$$

Linearization of the Boundary Conditions

If the amplitude of the waviness $\hat{\eta}$ is small and the wavelengths in both the x and z directions are long, the lower boundary condition can be linearized to the following form:

$$\hat{u}(0) = -\sigma\hat{\eta}\ ;\ \hat{v}(0) = \hat{w}(0) = 0 \tag{a-22}$$

The form of the continuity equation (Eq. a-16) provides a second constraint on $\hat{v}$ at $y = 0$:

$$\hat{v}'(0) = i\alpha\hat{\eta}\sigma \tag{a-23}$$

Transformation of Variables

It is convenient to transform to a new variable ψ:

$$\psi = (\hat{v}'' - K^2\hat{v}) \tag{a-24}$$

The transformed form of Eq. (a-21) is

$$\psi'' - K^2\psi = 0 \tag{a-25}$$

which has a general solution

$$\psi = Ae^{Ky} + Be^{-Ky} \tag{a-26}$$

Substituting Eq. (a-26) into Eq. (a-24) and solving for $\hat{v}$ yields

$$\hat{v} = \left[\frac{2AKy + 4CK^2 - A}{4K^2}\right] e^{Ky} - \left[\frac{2BKy - 4DK^2 + B}{4K^2}\right] e^{-Ky} \tag{a-27}$$

[where A, B, C, and D are arbitrary constants to be determined by the boundary conditions Eqs. (a-14), (a-15) and (a-22)]. Application of Eq. (a-22) results in the following:

$$C - \frac{A}{4K^2} + D - \frac{B}{4K^2} = 0 \tag{a-28}$$

The constraints on $\hat{v}$ and its y-derivative at $y = \infty$ produce

$$\hat{v}(\infty) = \lim_{y\to\infty}\left[\frac{2AKy + 4CK^2 - A}{4K^2}\, e^{Ky}\right] \tag{a-29}$$

$$\hat{v}'(\infty) = \lim_{y\to\infty}\left[\frac{-A + 2KAy + 4CK^2}{4K}\, e^{Ky}\right] \tag{a-30}$$

Equations (a-14) and (a-15) imply $A = C = 0$. Substituting Eq. (a-27) into (a-23) yields

$$\hat{v}'(0) = \frac{-A + 4CK^2}{4K} - \frac{B + 4DK^2}{4K} = i\alpha\hat{\eta}\sigma \tag{a-31}$$

Using $A = C = 0$, and Eqs. (a-28) and (a-31), the constants B and D can be solved for:

$$B = -2i\,\alpha\hat{\eta}\sigma K \;\; ; \;\; D = -i\,\alpha\hat{\eta}\sigma/2K \tag{a-32}$$

Therefore the expression for $\hat{v}$ that satisfies the boundary conditions is

$$\hat{v}(y) = i\,\alpha\hat{\eta}\sigma y \;\; e^{-Ky} \tag{a-33}$$

Using similar techniques, the functions $\hat{u}$ and $\hat{w}$ may be determined; the results are summarized as follows:

$$\hat{u}(y) = \frac{\alpha^2\hat{\eta}\sigma}{K} \;\; y\, e^{-Ky} - \sigma\hat{\eta}e^{-Ky} = \left[\frac{\alpha^2}{K}\, y - 1\right] \sigma\hat{\eta}e^{-Ky} \tag{a-34}$$

$$\hat{w}(y) = \left[\frac{\alpha K}{\beta} - \frac{\alpha^3}{BK}\right]\hat{\eta}\sigma\, y\; e^{-Ky} \tag{a-35}$$

Final Solution for Velocity, Pressure and Shear Stress

Using the solutions reported in Eqs. (a-33) through (a-35), the final form of the velocities and pressure can be written as the real part of Eqs. (a-7) through (a-10):

$$u = \left[\frac{\alpha}{K}\; y - 1\right]\hat{\eta}\sigma e^{-Ky} \;\; \cos\;(\alpha x + \beta z) + \sigma y \tag{a-36}$$

$$v = -\alpha\hat{\eta}\sigma y e^{-Ky} \;\; \sin\;(\alpha x + \beta z) \tag{a-37}$$

$$w = \frac{\beta\alpha\hat{\eta}\sigma}{K} \;\; y\; e^{-Ky} \;\; \sin\,(\alpha x + \beta z) \tag{a-38}$$

$$P = -2\mu\alpha\hat{\eta}\sigma e^{-Ky} \;\; \sin\;(\alpha x + \beta z) \tag{a-39}$$

The shear stress imposed by the fluid on the wavy surface may be calculated with the following formulae:

$$\tau_{yx} = \mu \left[\frac{\partial u}{\partial y} + \frac{\partial v}{\partial x}\right] \tag{a-40}$$

$$\tau_{yz} = \mu \left[\frac{\partial v}{\partial z} + \frac{\partial w}{\partial y} \right] \tag{a-41}$$

The direction of each of the two surface shear stresses is shown in Figure 1 and their values are given below:

$$\tau_{yx} = \mu\sigma \left[\frac{\alpha^2 + K^2}{K} \hat{\eta} - 2\alpha^2 \hat{\eta} y \right] e^{-Ky} \cos(\alpha x + \beta z) + \mu\sigma \tag{a-42}$$

$$\tau_{yz} = \mu\sigma \left[\frac{\beta\alpha\hat{\eta}}{K} - 2\beta\alpha\hat{\eta} y \right] e^{-Ky} \cos(\alpha x + \beta z) \tag{a-43}$$

At the cell surface ($y = 0$ in the linearized solution), the shear stresses are

$$\tau_{yx} \mid_{y=0} = \mu\sigma + \frac{\mu\sigma(\alpha^2 + K^2)\ \hat{\eta}}{K} \cos(\alpha x + \beta z) \tag{a-44}$$

$$\tau_{yz} \mid_{y=0} = \mu\sigma \frac{\beta\alpha\hat{\eta}}{K} \cos(\alpha x + \beta z) \tag{a-45}$$